

EPA-600/2-76-249a
September 1976

Environmental Protection Technology Series

CHARGED DROPLET SCRUBBER FOR FINE PARTICLE CONTROL: Laboratory Study



**Industrial Environmental Research Laboratory
Office of Research and Development
U.S. Environmental Protection Agency
Research Triangle Park, North Carolina 27711**

RESEARCH REPORTING SERIES

Research reports of the Office of Research and Development, U.S. Environmental Protection Agency, have been grouped into five series. These five broad categories were established to facilitate further development and application of environmental technology. Elimination of traditional grouping was consciously planned to foster technology transfer and a maximum interface in related fields. The five series are:

1. Environmental Health Effects Research
2. Environmental Protection Technology
3. Ecological Research
4. Environmental Monitoring
5. Socioeconomic Environmental Studies

This report has been assigned to the ENVIRONMENTAL PROTECTION TECHNOLOGY series. This series describes research performed to develop and demonstrate instrumentation, equipment, and methodology to repair or prevent environmental degradation from point and non-point sources of pollution. This work provides the new or improved technology required for the control and treatment of pollution sources to meet environmental quality standards.

EPA REVIEW NOTICE

This report has been reviewed by the U.S. Environmental Protection Agency, and approved for publication. Approval does not signify that the contents necessarily reflect the views and policy of the Agency, nor does mention of trade names or commercial products constitute endorsement or recommendation for use.

This document is available to the public through the National Technical Information Service, Springfield, Virginia 22161.

EPA-600/2-76-249a

September 1976

CHARGED DROPLET SCRUBBER
FOR FINE PARTICLE CONTROL:
LABORATORY STUDY

by

C.W. Lear

TRW Systems Group
One Space Park
Redondo Beach, California 90278

Contract No. 68-02-1345
ROAP No. 21ADL-043
Program Element No. 1AB012

EPA Project Officer: Dale L. Harmon

Industrial Environmental Research Laboratory
Office of Energy, Minerals, and Industry
Research Triangle Park, NC 27711

Prepared for

U.S. ENVIRONMENTAL PROTECTION AGENCY
Office of Research and Development
Washington, DC 20460

CONTENTS

	<u>Page</u>
NOMENCLATURE	xi
1. INTRODUCTION	1-1
1.1 Charged Droplet Scrubbing Devices	1-2
1.2 The TRW Charged Droplet Scrubber	1-5
1.3 Particulate Removal Mechanisms	1-12
1.4 Charged Droplet Scrubbing Efficiencies	1-19
2. EXPERIMENTAL DESIGN	2-1
2.1 Program Objectives	2-1
2.2 Research Scale Scrubber	2-3
2.3 Bench Scale Scrubber	2-5
3. TEST PROCEDURES	3-1
3.1 Collector Current Measurements	3-1
3.2 Droplet Formation Photography	3-1
3.3 Laser Velocimeter	3-5
3.4 Particulate Removal Efficiencies	3-7
4. RESULTS	4-1
4.1 Basic Mechanism Studies	4-1
4.2 Research Scrubber Measurements	4-42
4.3 Bench Scale Scrubber Measurements	4-75
4.4 Scrubber Performance	4-85
4.5 Performance Comparisons	4-90
5. CONCLUSIONS	5-1
6. RECOMMENDATIONS	6-1
7. REFERENCES	7-1
APPENDIX A	A-1

FIGURES

<u>Number</u>		<u>Page</u>
1-1	TRW Systems charged droplet scrubber operating principle	1-6
1-2	Schematic diagram of TRW 3000 SCFM charged droplet scrubber	1-9
1-3	TRW 3000 SCFM charged droplet scrubber installed on process simulator	1-10
1-4	Droplet-particle interaction model	1-22
1-5	Nomogram for fractional efficiencies of charged droplet scrubbers	1-30
2-1	Experimental scrubber unit	2-4
2-2	Water flow rate vs. pressure calibration	2-6
2-3	TRW charged droplet scrubber bench scale unit	2-8
2-4	Schematic of electric arc zinc rod	2-9
2-5	Bench-scale scrubber electrode assembly	2-10
2-6	Bench-scale CDS with auxiliary equipment	2-11
2-7	Flow distributing vanes	2-13
2-8	Blower unit and flow straightener	2-13
3-1	(a) End view cross section of segmented current collector used to monitor axial current distribution in research scrubber	3-2
3-1	(b) Side view of segmented current collector showing collector electrode plates	3-3
3-1	(c) Current monitor circuit of segmented current collector	3-3
3-2	Modified schlieren photo setup used for high speed photography of droplet formation	3-4

FIGURES (cont.)

<u>Number</u>		<u>Page</u>
3-3	Schematic diagram of laser velocimeter experiment	3-5
3-4	Interference fringe pattern	3-6
3-5	Laser velocimeter experiment	3-8
3-6	(a) Zinc oxide particulate under a scanning electron microscope, sample No. 1; magnification, 10,000X	3-9
3-6	(b) Zinc oxide particulate under a scanning electron microscope, sample No. 2; magnification, 3000X	3-10
3-7	Distributions of light and heavy density zinc fume from test 4/14/74-1	3-11
3-8	Data-fitted and hypothetical fume mass distribution function from Andersen sampler data	3-14
4-1	Limits of surface charge densities on water droplets (rayleigh limit) and columnar segments of water	4-4
4-2	Surface field limits	4-6
4-3	Water droplet evaporation lifetimes, temperature of 20°C	4-11
4-4	Water droplet evaporation lifetimes, temperature of 100°C	4-12
4-5	Vapor pressure of a singly charged droplet	4-13
4-6	Water droplet vapor pressure as given by equation 4-7, for uncharged and singly charged droplets	4-15
4-7	Temperature dependence of nucleation pressures	4-17
4-8	Induced charging geometry, spherical particle	4-18
4-9	Induced charging model, spherical particle with protrusion	4-19
4-10	Induced charging of spherical particles by corona breakdown at the particle. Induced charging occurs under each curve	4-20

FIGURES (cont.)

<u>Number</u>		<u>Page</u>
4-11	Induced charging of irregular particles by corona breakdown at the particle	4-21
4-12	Plot of equation (4-17) related to particle drift time	4-25
4-13	Induced charging impact parameter for the models of equations (4-13) and (4-19). A sequence of drift times is plotted	4-28
4-14	Plot of equation (4-22) to obtain minimum particle size collectible by induced charging	4-29
4-15	Parametric study of collision effectiveness probability for $E_{OD}/E_C = 45.1$	4-36
4-16	Parametric study of collision effectiveness probability for $E_{OD}/E_C = 1.25$	4-37
4-17	Parametric study of collision effectiveness probability for $E_{OD}/E_C = 0.10281$	4-38
4-18	Functional dependence of collision effectiveness probability on impact parameter, A	4-40
4-19	Functional dependence of collision effectiveness probability on particle radius	4-41
4-20	Corona current versus electrode voltage for five-tube electrode	4-43
4-21	(a) Collector current distribution for 18 gauge spray tubes, no air flow, 34.8 ± 10 microamperes total flow current	4-44
4-21	(b) Collector current distribution for 18 gauge spray tubes, 3.6 M/Sec air flow, 38.4 ± 4.2 microamperes total collector current	4-44
4-21	(c) Collector current distribution for 18 gauge spray tubes, no air flow, 40.1 ± 4.1 microamperes total collector current	4-45
4-21	(d) Collector current distribution for 18 gauge spray tubes, 3.6 M/Sec air flow, 37.0 ± 2.9 microamperes total collector current	4-45

FIGURES (cont.)

<u>Number</u>		<u>Page</u>
4-21	(e) Collector current distribution for 18 gauge spray tubes, no air flow, 34.2 ± 1.4 microamperes total collector current	4-46
4-21	(f) Collector current distribution for 18 gauge spray tubes, 3.6 M/Aec air flow, 39.6 ± 0.2 microamperes total collector current	4-46
4-22	(a) Collector current distribution for 22 gauge spray tubes, no air flow, 68.5 microamperes total current	4-47
4-22	(b) Collector current distribution for 22 gauge spray tubes, 3.6M/Sec air flow, 72.6 microamperes total current	4-48
4-22	(c) Collector current distribution for 22 gauge spray tubes, no air flow, 34.9 microamperes total current	4-48
4-22	(d) Collector current distribution for 22 gauge spray tubes, 3.6 M/Sec air flow, 41.7 microamperes total current	4-49
4-23	Velocity monitoring locations	4-51
4-24	Velocity profile - 22 gauge spray tube	4-53
4-25	Velocity profile - 18 gauge spray tube	4-53
4-26	High frequency sweep	4-54
4-27	Low frequency sweep	4-54
4-28	Velocity profile for droplets charged to the rayleigh limit	4-57
4-29	End spray tube, 22 gauge, 4 inch water pressure	4-59
4-30	End spray tube, 22 gauge, 10 inch water pressure, 1/15 sec exposure with 70 flashes per second	4-59
4-31	End spray tube, 22 gauge, 12 inch water pressure	4-60
4-32	Second spray tube, 22 gauge, 18 inch water pressure, wetting agent in the water	4-60
4-33	End spray tube, 22 gauge, 8 inch water pressure, 133 droplets counted	4-61

FIGURES (cont.)

<u>Number</u>		<u>Page</u>
4-34	End spray tube, 22 gauge, 14.5 inch water pressure. 159 droplets counted	4-61
4-35	End spray tube, 22 gauge, 14.5 inches water pressure. Grid overlay for counting droplets. 165 counted.	4-62
4-36	Second spray tube, 22 gauge, 18 inch water pressure, wetting agent in the water	4-62
4-37	Center spray tube, 18 gauge, 0.5 inch water pressure	4-65
4-38	Center spray tube, 18 gauge, 0.2 inch water pressure	4-65
4-39	Center spray tube, 18 gauge, 1.5 inch water pressure	4-66
4-40	Center spray tube, 18 gauge, 5 inch water pressure	4-66
4-41	Histogram of the normalized frequency function for droplet radius	4-67
4-42	Percentage number of droplets less than a given radius from the distribution of figure 4-35	4-68
4-43	Percentage number of droplets less than a given radius, from the distribution of figure 4-40	4-69
4-44	Droplet number density distribution for figure 4-35	4-72
6-1	Structural arrangement of recommended 50,000M ³ /hr CDS pilot plant	6-4
6-2	CDS lower section assembly	6-5
6-3	CDS electrode and collector plate assemblies	6-6
6-4	Experimental device for measuring induced charging drift times. The particulate is charged in the spray, then drifts to the walls under the influence of a uniform field	6-8

TABLES

<u>Number</u>		<u>Page</u>
1-1	Modified Melcher classification of scrubber devices	1-3
1-2	Performance summary: Kraft process recovery boiler, CDS pilot installation, soda ash particulate	1-11
1-3	Particle removal mechanisms occurring in charged droplet scrubbers	1-14
4-1	Nominal conditions for collision-effectiveness-probability parameter studies	4-35
4-2	Parameters for 22 gauge spray tube photographs--figures 4-29 through 4-36	4-58
4-3	Parameters for 18 gauge spray tube droplet photographs--figures 4-37 through 4-40	4-64
4-4	Distribution parameters for figures 4-35 and 4-40	4-70
4-5	Distribution parameters for 22 gauge spray tube counts	4-70
4-6	Distribution parameters for 18 gauge spray tube counts	4-71
4-7	Droplet density and flux	4-74
4-8	Various results of the high volume sampler tests, Nos. 4/8-1 through 4/25-4	4-77
4-9	Non-varying parameters for high volume sampler tests 4/23-1 through 4/25-4	4-77
4-10	Performance results of the water entrainment sampling tests, Nos. 4/17-1 through 5/23-1.	4-79
4-11	Constant conditions for the three alcohol impinger tests	4-80
4-12	Results of the alcohol impinger tests	4-81

TABLES (cont.)

<u>Number</u>		<u>Page</u>
4-13	Royco analysis of apparent fractional efficiencies, or number fraction of outlet over inlet	4-82
4-14	Scrubber operating conditions for Andersen sampler tests	4-82
4-15	Andersen sampling test conditions and results	4-83
4-16	Effects of dry charging on Andersen sampler results	4-84
4-17	CDS performance for sub-micron particle removal	4-89
4-18	Performance comparison	4-91
6-1	Design parameters for TRW/CDS	6-3

NOMENCLATURE*

A	Interaction impact parameter	D/S
	Area	m ² or cm ²
	Electrode corona voltage/current function slope	μAMP/(KV) ²
C _D	Aerodynamic drag coefficient	
C _O	Correction constant for thermal lag in droplet evaporation	
C _P	Correction constant for thermal lag in droplet evaporation	
D	Distant of farthest approach for interaction, partial center to droplet surface	microns or meter
	Diffusivity of vapor in a gas	m ² /sec
E	Local electric field in scrubber volume. Usually approximated as V/L	volts/meter
\bar{E}	Reciprocal average electric field. Usually approximated as V/L	$L/\int^L dx/E(x)$ volts/meter
E'	Electric field perturbation	volts/meter
E _b	Local electrical breakdown field in the gas between planar electrodes; for standard air	3 x 10 ⁶ volts/meter
E _C	Droplet characteristic electric field in collision effectiveness probability analysis	V/M
E _O	Surface electric field or local breakdown field on a sphere or cylinder	volts/meter
F	Force	newtons
G(a)	Induced charging function	
H	Condensate heat of vaporization	joules/Kgm

* Undesignated units are dimensionless

NOMENCLATURE, Continued

K	Mobility	meter ² /volt-sec
	Thermal conductivity	joules/sec-m-°K
L	Effective scrubbing volume length	m
M	Mass of particle or droplet	Kg or gm
M _p	Particle mass	Kg or gm
N	Number of electronic charges, or atoms, or molecules	
N _{Re}	Reynolds number	
P _c	Condensate vapor pressure in a gas stream	m bar
P _D	Vapor pressure at a droplet surface	m bar
P _v	Saturation vapor pressure	m bars
Q̇	Volume flowrate	m ³ /sec
R	Radius, usually particle	microns or meters
R _c	Gas constant	joules/kgm-°K
R ¹	Relative humidity	
S	Radius; usually droplet	microns or meters
S _p	Most probable droplet radius	microns or meters
T	Absolute temperature	°K
U	Free-stream droplet - particle relative velocity	m/sec
U _c	Droplet characteristic velocity in collision effectiveness probability analysis	m/sec
U _p	Most probable droplet velocity	m/sec
V	Scrubber electrode voltage	volts
V _o	Electrode corona onset voltage	KV
W	Flue gas velocity in scrubber	m/sec

NOMENCLATURE, Continued

a	Dimensionless variable d/s	area; m^2
b	Upper bound on particle-to-droplet charge ratio	
d	Distance from particle center to droplet surface, a variable of motion	microns or meters
e	Electronic charge	1.602×10^{19} coul.
e_2	Droplet area utilization efficiency	
e_3	Droplet volume utilization efficiency	
erf	Error function	
f	Frequency	sec^{-1}
$f ()$	Size distribution over the parameter in parentheses	m^{-1}
grad	Vector gradient operator	meter^{-1}
h	Scrubber half-width; or particle drift path length	meter
k	Boltzmann constant	1.38×10^{-16} erg/ $^{\circ}\text{K}$
m	Molecular mass	gm
$n ()$	Density distribution over the size parameter in parentheses	m^{-4}
n_o	Average spatial number density	m^{-3}
p	Collection efficiency, or collision effectiveness probability	
q	Droplet or particle charge	coulombs
\bar{r}	Droplet - particle center-to-center vector distance	meter
s	Surface charge density	coul/m^2 or coul/m
t	$(\ln S_s - \ln S_g) / \ln \sigma_g$, Log-normal distribution variable	
	Time variable	sec

NOMENCLATURE, Continued

\bar{u}	Particle or droplet vector velocity	m/sec
u_d	Particle drift velocity	m/sec
\bar{w}	Local gas velocity vector field	m/sec
z^*	Radius of a cylinder containing interacting particulate	microns or meters
β	Electrostatic dipole moment	coul-meter
Δ	Light interference fringe spacing	microns
δ_g	Density of particulate carrier gas	0.00127 gm/cm ³ for air at 20°C
ϵ	Dielectric constant of matter, usually particulate	
ϵ_0	Electrical permittivity of free space	8.854 x 10 ⁻¹² coul/volt-meter
η_M	Mass removal efficiency	
$\eta(R)$	Fractional scrubbing efficiency	
η_c	Collision effectiveness	
θ	Angular coordinate	radians or degrees
λ	Mean-free - path to interaction	m
	Wave length of light	microns
Λ	Scrubber efficiency parameter	
μ	Viscosity of carrier gas	1.82 x 10 ⁻⁵ Kg/m-sec for air at 20°C
ρ	Particulate or droplet true density	Kg/m ³
Σ	Interaction cross-section	m ²
σ	Liquid surface tension	dynes/cm
σ_g	Geometric standard deviation	
σ_u	Log-normal standard deviation	

NOMENCLATURE, Continued

τ_c	Interaction time constant	sec
τ_{df}	Droplet formation time	sec
τ_o	Characteristic particle drift time	sec
τ_r	Effective particle residence time	sec
(r,θ)	Position coordinates in a field calculation	meter, radian
(x,z)	Position coordinates in a field calculation	m

1. INTRODUCTION

Charged droplet scrubbing is similar to conventional scrubbing methods in that it removes particulate and fumes from dirty air by means of interaction of droplets of scrubbing liquor with the particles of dirt or fume. Beyond this, the similarity ends. Because of their unusual electrical interaction mechanisms, which are not yet fully understood, charged droplet scrubbers are still considered as novel and experimental devices in industrial pollution control. In the charged droplet scrubber the electrical interaction mechanisms exist in addition to the normal impact and diffusional scrubbing mechanisms. These are strong in the 0.1 to 1.0 micron particulate size range, where the normal mechanisms lack effectiveness.

As the name "charged droplet scrubbing" implies, the scrubbing droplets, usually water, will generally carry a high electrical charge which is deliberately induced. The droplets may move under the influence of electric fields, either deliberately applied or existing by virtue of the ambient space charge. The particulate may also carry a charge other than its naturally occurring charge. All these conditions may contribute to the electrical interaction aspects of charged droplet scrubbers.

This report describes work done under contract to the Environmental Protection Agency to determine the applicability of charged droplet scrubbing specifically to the control of fine particulate. Throughout this report, the reference to fine particulate will indicate the general range of 0.1 to 1.0 micron in diameter. The program was directed first towards obtaining estimates of the effectiveness of the various charged droplet scrubbing mechanisms. Secondly, but with equal emphasis, the program was directed toward analysis and testing of the TRW Charged-Droplet-Scrubber concept (CDS), which has been shown to give superior performance for many fine particle scrubbing applications. Finally, it was the purpose of this study to derive some basic performance comparisons between charged droplet scrubbers and other conventional types of scrubbers and electrostatic precipitators.

The program was conducted in three basic phases, which are discussed more-or-less separately in this report. Phase one was an analytical study of important basic mechanisms in charged droplet scrubbers, and their overall effects in estimated efficiency. Phase two was a systematic experimental investigation of selected mechanisms to quantify their effects and verify their importance. These experiments were carried out using a small research scale scrubber, also referred to as an experimental unit. The mechanisms investigated during this study were primarily those concerned with droplet-particle collision and charge exchange interaction. These are the predominant mechanisms in the TRW/CDS. The third and final phase of the program was performance

verification testing of an operating CDS utilizing the important interaction mechanisms studied in the first two phases. This testing emphasized the measurement of total and fractional mass utilization efficiency, and the effect on performance of scrubber operating parameters. The device constructed for this testing was capable of delivering up to 1700 m³/hr (1000 CFM) of gas flow through three series CDS stages. It is referred to in this report as the bench scale scrubber.

1.1 CHARGED DROPLET SCRUBBING DEVICES

Charged droplet scrubbing concepts may be broadly classified according to types of devices, as well as according to droplet-particle interaction mechanisms. In this section we discuss a device classification originally introduced by Melcher et al.¹

The particle removal mechanisms which are dominant or significant in a given device depend on the physical state of droplets and particulate and their surroundings in that device. The state of an aggregate of droplets or particles will be statistically distributed, and the state of the ambient surroundings is likely to be statistically distributed throughout the ambient volume also. Furthermore, consideration must be given to the time evolution of the states of individual drops and particles within the aggregate.

The Melcher classification is a partial classification according to state. It is presented in Table 1-1. The classification is made according to charge state of drops and particle, and according to ambient electric field. Other important state variables which should be considered are droplet and particulate size and conductivity, and ambient gas temperature and humidity. Even these new variables leave aside any thermochemical considerations.

In Table 1.1 the Melcher class numbers have been retained, but augmented with sub-classes A and B to indicate if the electric field (if present) is externally imposed or self-induced by space charge. The state of charge on drops and particles is indicated in columns two and three, and the ambient field state is indicated in column four. The terminology is partly due to Melcher, but mainly derived from common usage.

Within each of Melcher's classes there is a dominant interaction mechanism tending to remove particulate from the ambient gas stream. Usually this mechanism is a force between drops and particles. However, the dominant mechanism may change if other physical parameters change, such as droplet and/or particle size, ambient humidity, etc. Also the dominant mechanism may be significantly augmented by one or more secondary mechanisms.

Table 1-1. MODIFIED MELCHER CLASSIFICATION
OF SCRUBBER DEVICES

Class	Drops Charged	Particles Charged	Ambient Electric Field	Terminology
I	No	No	None	Mechanical Scrubbers
II-A -B	Yes	No	Imposed Space-Charge	Electrical Scrubbers
III	Yes	Yes	None	Electrical Agglomerators
IV-A -B	No	Yes	Imposed Space-Charge	Electrical Agglomerators
V-A -B	Yes	Yes	Imposed Space Charge	Hybrid Electrical Scrubbers

Charged droplet scrubbing devices may also vary widely according to methods used to generate the charged droplets. Other than its importance to the effectiveness and quality of the scrubbing droplet distribution obtained, the method of droplet generation does not directly affect the scrubbing efficiency as the physical state within the scrubbing volume does. Droplet generation methods in general have been adequately discussed by Melcher¹ and need not be reviewed here.

The dominant characteristics and mechanisms of each of the Melcher classes will now be briefly summarized. The particulate removal mechanisms referred to here will be defined and discussed in more detail in Section 1.3.

Class I: Mechanical Scrubbers

Here there is no electrical charge present and no electric field, hence no electrical interaction. The interactions are purely mechanical, and appear in most conventional scrubber devices. For larger particulate, collection occurs mainly through inertial impact with the droplet. In order to achieve the necessary inertial forces, a relative velocity between droplets and particulate must be mechanically induced. For smaller particulate, collection through turbulent diffusion and Brownian diffusion tends to dominate. Condensation mechanisms may also be important for fine particulates, depending on scrubber design.

Class II: Electrical Scrubbers

Here the drops are charged, and move under the influence of an ambient field. The scrubbing mechanisms of Class I are still basic. However,

the relative velocity between droplet and particle is now maintained by electrical forces, and the normal hydrodynamic decay will not occur. Electrically induced inertial impact is the dominant mechanism for particulate larger than about one micron. Large, highly charged droplets (100 to 200 microns diameter) are needed to give this process maximum efficiency. Electrostatic dipole forces may exist but will make a difference only for small, highly conducting particles.

Induced charging followed by electrostatic precipitation will be an important mechanism in the fine particle size range, which is too small for impact scrubbing and too large for effective diffusion. Induced charging will also lower the probability of impact capture. It is most effective for highly conducting particulate, where the surface charge on the particulate can re-arrange itself so as to enhance the electric field during the relatively short period of time that the drop and particle are in close proximity. Wake entrainment and molecular and turbulent diffusion play much the same role as in Class I scrubbers. Droplet-evaporation charging will be significant in low humidity gas streams, again only for very fine particulate, evaporation charge release followed by diffusion charging may compete with induced charging for significance.

In the Class II scrubber the droplet charging process will generally release some corona discharge, either deliberately or through inefficiencies. Depending on the design, more or less of this corona may reach particulate and charge it. This could be an important particle removal mechanism.

The TRW/CDS is a member of this class, being an applied field type of electrical scrubber.

Class III: Electrical Agglomerators

In this class, droplets and particles carry opposite charges and no net ambient fields exist. There are, of course, local fields associated with the charge distribution. These fields tend to agglomerate droplets and particulate by virtue of mutual attraction. Relative velocities are small, on the order of drift velocities, unless and until electric forces cause local relative acceleration.

Electrostatic monopole forces are the dominant interactions. Again, the droplets need to be large and highly charged relative to the particulate in order to give good efficiency. Then many particles can be collected before a drop is discharged. Molecular and turbulent diffusion may be significant again for very fine particulate. Also for small, highly conducting particulate an induced charging mechanism may occur which discharges both drop and particle without agglomeration taking place. This leads to a loss of efficiency. For low humidity systems with small droplets, droplet-evaporation charging may have the same effect. In a supersaturated gas stream, on the other hand, nucleation and growth of droplets by condensation may have a significant perhaps even dominant-effect.

Since both droplets and particles are charged, corona charging followed by electrostatic precipitation may be a significant mechanism.

Class IV: Electrical Agglomerators

Droplets are uncharged, particles are charged and there is a dipole-inducing electric field. There is an electrically induced relative velocity due to the action of the field on the particulate. For large highly charged particles the electrically induced impact is the dominant mechanism. For fine particulate, electrostatic dipole-monopole forces become competitive and perhaps dominant. Large, highly conducting droplets enhance this dipole action. As the droplets become charged, they too move under the influence of the field. The relative velocity effect is weakened, and monopole forces will degrade efficiency. For very fine particulate, diffusive processes will be significant. Wake entrainment can occur with moving droplets. Induced charging without agglomeration can degrade the efficiency. Corona charging followed by electrostatic precipitation can be a significant mechanism.

Class V: Hybrid Electrical Scrubbers

These devices are much the same as Class II devices, except the particulate is now charged oppositely from the droplets. The added charge may enhance the droplet-particle interaction. If discharge without agglomeration occurs, the subsequent collection efficiency is weakened. The agglomerating action will itself cause charge neutralization of the droplets and subsequent loss of collection efficiency. Joubert^{2,3} has described a multi-stage device of this type in which successive stages were of opposite polarity. The particulate penetrating one stage would take on the charge of that stage, and would enter the next stage as though it were a Class V device. The efficiency of this mode of operation was less than when the device was operated with all stages at the same (positive) polarity.

1.2 THE TRW CHARGED DROPLET SCRUBBER

The TRW Charged-Droplet-Scrubber is a class II-A electrical scrubbing device (Table 1-1) in which the droplets are relatively large and highly charged, the particulate is generally uncharged, and the ambient electric field is externally imposed. The imposed electric field is used both to form charged droplets electrohydrodynamically and to move them through the scrubbing volume. A high relative velocity through the scrubbing volume is achieved by the droplets by means of the high electric field forces on them. The high relative velocity between droplets and particulates results in a high droplet collection efficiency.

Figure 1-1 is a diagrammatic sketch of the TRW/CDS showing its operating principal. The scrubbing liquor, generally fresh water, is

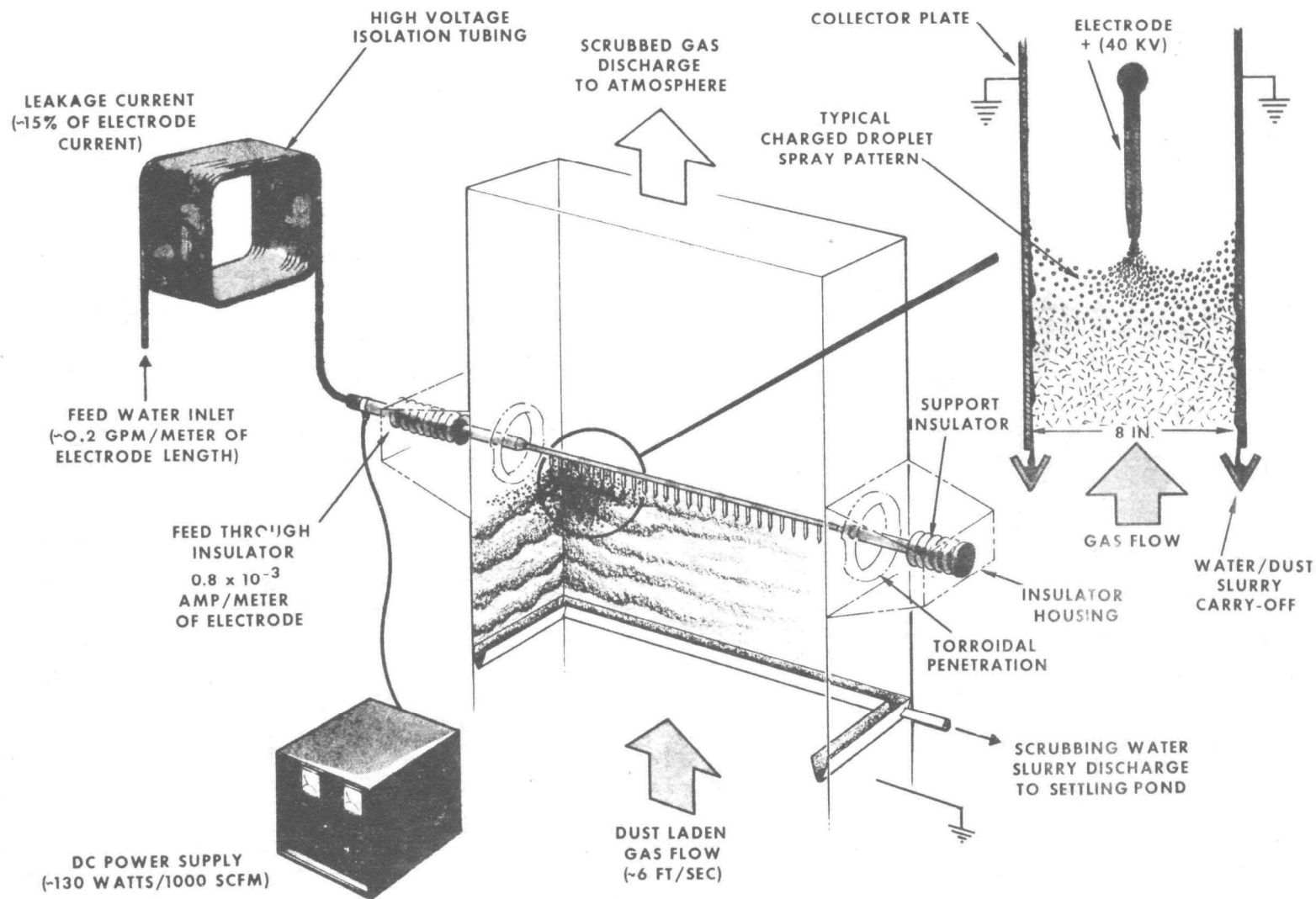


Figure 1-1. TRW SYSTEMS CHARGED DROPLET SCRUBBER OPERATING PRINCIPLE

raised from ground potential to high voltage (about 40 kv) by flowing through a long electrical resistance path in the form of an insulating tubing. Electrical isolation is achieved through the resistance of the water itself. Following the tie-point with the high voltage power supply, the water is allowed to pass through another 6 feet or so of tubing (not shown) which provides an extra isolation between the power supply and the high voltage electrode. The purpose of this resistance is to quench high-current arcing from the electrode. The water is then introduced into a hollow electrode which contains a series of hollow, elongated spray tubes. Emerging at the tips of these spray tubes, the water sees a high electric field force. Droplets are formed here by the joint action of electrical and surface tension forces, in a classical electrohydrodynamic spraying process. The droplets thus formed are highly charged, their surface field being near the local corona limit or Rayleigh stability limit. They move swiftly through the scrubbing volume under the influence of the electric field between the electrode and the collecting walls.

Because of the high droplet velocities (around 30 m/sec) induced by the ambient electric field, there is a large relative motion between droplets and particulate. This large relative motion enables the small particles to overcome aerodynamic forces which would normally sweep them around the droplet with the flow stream. Under inertial forces, they are able to approach the droplet more closely and thus interact. This close approach leads to enhancement of particulate collection by agglomeration and by electrical interaction. The result is an improvement of overall efficiency as compared to conventional scrubbing devices.

The TRW/CDS was chosen for the phase two and phase three testing of this program because it makes use of some of the strongest and most effective of the mechanisms studied on the program. Perhaps its main merit is in the enhancement of collision effectiveness probability realized by high droplet velocities. Before the inception of the present program, the CDS had been subjected to extensive testing for scrubbing efficiencies in the 1 to 100 micron particulate size range. This was done both in laboratory scale experiments and in selected pilot scale field tests. Overall performance was generally better than anticipated, ranging from 60 to 80 percent per stage mass collection efficiency. Good potential for extension of capability into the sub-micron particulate size range was indicated.

Work on electric scrubbing concepts at TRW dates back to 1968. It was pre-dated by TRW efforts in electrostatic spraying processes which were directed towards development of high efficiency, low thrust space engines for satellite stationkeeping⁴⁻⁶. These programs, known collectively as the Colloid Thruster Programs, provided a technology base for studies of electrostatic spraying, as well as incentive to find other potentially useful applications. The TRW/CDS proved to be one such application with good commercial potential. Initial efforts were directed towards

feasibility determination and consisted of scrubbing mechanism analyses, cost analysis and preliminary laboratory experiments⁷. This was followed by controlled pilot-scale engineering development⁸ and in-depth design analysis⁹. All this took place within the confines of TRW facilities.

Concurrently and subsequently, an important phase of pilot scale field testing at selected industrial sites was being carried out. These programs are of interest because they provided the first practical data indicating potential field performance of the CDS. The pilot plant development history will be reviewed here very briefly from this standpoint.

A 1700 m³/hr (1000 SCFM) Charged Droplet Scrubber was designed, built and utilized as a pilot scale unit for preliminary field testing in 1971. The pilot scale unit was installed on a local asphalt plant (Los Angeles) for field testing. The unit consisted of two high voltage electrodes staged in series and mounted in a duct with an 0.2 by 1.2 meters (8 inches by 48 inches) cross section.

The purpose of this test was to confirm laboratory scale results and gain experience under field operating conditions. Approximately 2 months of testing was completed covering a wide variety of asphalt plant nominal and upset operating conditions. Inlet and outlet dust loadings were measured using Joy Manufacturing dust and fume sampling systems. Cleaning efficiencies with this experimental pilot scale unit were consistently in the 96 to 98 percent range and generally substantiated analytical predictions and laboratory scale results.

In the latter part of 1972, a 5000 m³/hr (3000 SCFM) unit was built and tested on a specially designed TRW process simulator. This larger unit was designed to evaluate parallel scrubbing modules. A schematic diagram of the 5000 m³/hr Charged Droplet Scrubber is shown in Figure 1-2 and a photograph of the scrubber is shown in Figure 1-3. From the diagram of Figure 1-2, it can be seen that this unit consisted of three parallel modules each with three high voltage electrodes in series.

With the 5000 m³/hr (3000 SCFM) unit mounted on the TRW process simulator, tests were conducted using asphalt aggregate dust. These tests were made to verify performance prior to a field test program in Hiroshima, Japan. The unit was subsequently shipped to Japan where it was evaluated on a Japanese asphalt plant. The test was successful, and results exceeded the performance obtained on the process simulator.

Two units, built in 1973 for pilot field testing, were rated at 1700 m³/hr (1000 SCFM). These units were designed and built for pilot plant field testing in the United States. The first was tested on a paper mill recovery boiler (Kraft process). Prior to shipment for field test, preliminary tests were made to determine cleaning efficiency as a function of particle size range. Two separate tests were made using size graded talcum powders.

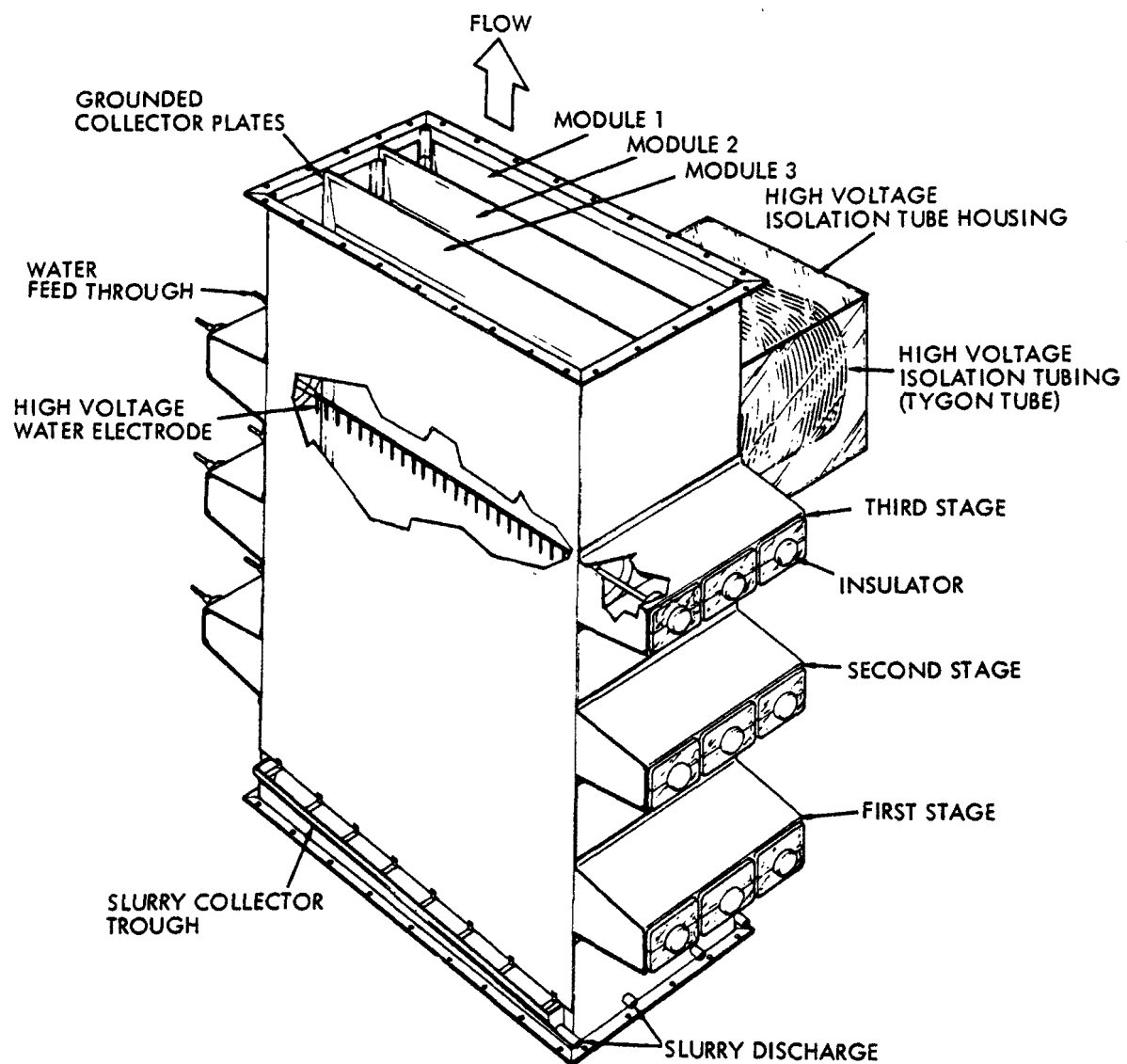


Figure 1-2. SCHEMATIC DIAGRAM OF TRW 3000 SCFM CHARGED DROPLET SCRUBBER

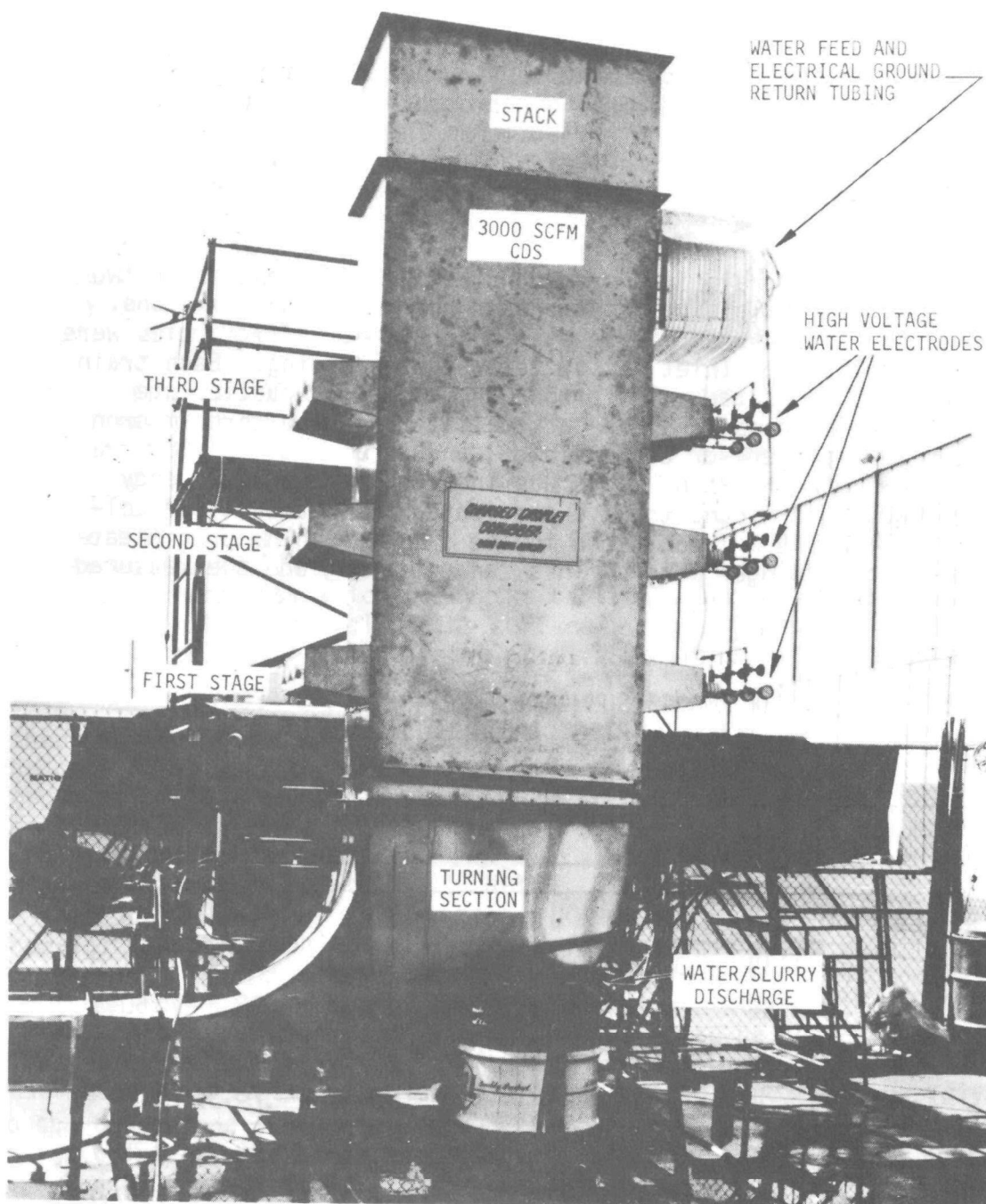


Figure 1-3. TRW 3000 SCFM CHARGED DROPLET SCRUBBER
INSTALLED ON PROCESS SIMULATOR

The Kraft process pilot plant yielded some fairly reliable data on soda ash particulate. The CDS that was used was not optimized, but was configured for low energy and minimum start-up cost. Higher performance would have been achieved with a fine-particle scrubber design having a closer plate spacing.

Table 1-2 shows edited results of the test. The CDS was installed as a secondary unit at the outlet of an electrostatic precipitator controlling emissions from the recovery boiler. The fume at the CDS inlet was, on the average, 15 percent by weight under 3 microns in diameter. The resulting geometric mean size of the number density distribution is about 1.5 microns.

The table shows inlet grain loadings and cleaning efficiencies in two classifications, particle size greater than and less than 3 microns. Results are shown for two and three stage operation. Efficiencies were obtained by simultaneous inlet and outlet weight sampling. Each train consisted of a 10 mm heated inlet probe, a cyclone for particulate larger than three microns, a glass-packed filter for sub-three-micron particulate, an impinger for condensibles, and an aspirative flow inductor. The impinger catch, which was included in the efficiency calculation, was later found to have precipitated small amounts of colloidal sulfur from the H₂S contained in the flue gas. The precipitate was formed in the impinger water. This tended to degrade the measured efficiency.

Table 1-2. PERFORMANCE SUMMARY: KRAFT PROCESS RECOVERY
BOILER, CDS PILOT INSTALLATION, SODA ASH
PARTICULATE

	Inlet Loading (gr/SCF)			Cleaning Efficiency (Weight %)		
	Total	>3 μ	<3 μ	Total	>3 μ	<3 μ
Three Stages	0.0848	0.0631	0.0217	89.9	91.4	85.3
	0.1119	0.0784	0.0335	85.4	95.4	61.8
	0.2156	0.1627	0.0529	85.4	96.2	60.0
	0.7446	0.6302	0.1144	94.9	98.3	76.0
	2.328	0.213	2.115	84.7	78.4	85.4
Two Stages	0.2156	0.1627	0.0529	80.5	93.7	39.7
	0.3297	0.2680	0.0617	88.2	96.5	52.0

1.3 PARTICULATE REMOVAL MECHANISMS

The removal of sub-micron size particulate from a gas stream has proven to be difficult to accomplish. This is due in part to low mobility and unfavorable inertial properties of the small particulate. One basic problem is that of establishing a significant relative velocity between a particle to be removed and the collecting surface (in this case, droplets). For smaller and smaller particulate, this becomes harder and harder to do, and requires more and more energy input to the gas stream, or the collecting surfaces or both.

If a significant relative velocity can be established, the particulate can be made to impinge upon some collecting surface and thereby be removed from the gas stream. Such a collecting surface may be a stationary or moving part of the hardware, as in a precipitator device, or it may be an agitated liquid surface, as in a scrubber.

If one defines a Reynolds number based on some mean particle diameter and the velocity of the particles relative to the collection surface, one finds that for smaller and smaller Reynolds numbers the particles tend to be increasingly dominated by viscous forces in their motion. This will force their motion to follow gas flow streamlines, which never reach collecting surfaces. Only for Reynolds numbers of one or greater do inertial forces play a significant part. Inertial forces are a major mechanism which carry the particles across streamlines, allowing them to reach collecting surfaces. Thus, as particle sizes become smaller, larger relative velocities are required to support this mechanism.

Other mechanisms which play important roles in the transport of mass to the collecting surfaces include molecular and turbulent diffusion forces, thermal gradients, condensation forces and electrical forces. Reserving the latter for our discussion of charged droplet scrubbing mechanisms, consider next the molecular and turbulent diffusion forces (diffusiophoresis).

Inertial impact scrubbing is effective for particle sizes down to about one micron. Particulates above 0.1 micron in size are still too massive to be moved about much by anything except the strongest turbulent forces. Below the 0.1 micron limit, they begin to be increasingly affected by molecular forces, and random Brownian motion will be observed. Very fine particulate may then diffuse freely and rapidly to the collecting surfaces, where hopefully they will adhere. The diffusion constant, and hence the diffusion time to the collecting surface, is a function of particle size¹⁰. The diffusion constant, collector geometry and desired cleaning efficiency are all factors in determining the required residence time in the scrubbing volume, which may be prohibitively long.

The particle size range between about 1.0 and 0.1 micron remains then relatively unaffected by either impact or diffusion mechanisms. Because electrical interactions are effective in this size range, charged droplet scrubbing is of great interest here.

In a sufficiently humid environment, fine particulate may act as nucleation sites for the growth of water droplets, which may more easily be removed from the gas stream once they are large enough. This is the basis for condensation scrubbing, which has been studied in its own right as a primary mechanism for scrubbing fine particulate¹¹. This process may also be important in charged droplet scrubbers, depending on the humidity environment. The remaining mechanism, thermophoresis or forces due to thermal gradients, is generally not significant in charged droplet scrubbers and need not be considered.

The most important classes of interactions in charged droplet scrubbers are naturally electrical. To prepare for our discussion of these interactions and put them in proper perspective with other important interactions, it is convenient to attempt some kind of a fundamental classification. This classification will define forces occurring on particulates which tend to remove them from the gas stream. Force mechanisms such as these may then be analyzed to obtain characteristic interaction times and interaction cross-sections independently of which device they are occurring in.

Table 1-3 presents such a classification in condensed form. The emphasis is on a breakdown of droplet-particulate interaction forces under heading A in the table. However, in many charged droplet devices either droplets or particulate or both may be charged by means of a corona electrode. This may occur deliberately, or as a side effect. Particulate may be field charged in a corona discharge. It is therefore appropriate to consider corona charging as a particulate removal mechanism. Since it is not a droplet-particle type interaction it is given a separate heading B.

Direct Collision and Agglomeration (1.0)

The droplet and particle collide forming an agglomerated particle which is easier to remove than the single particle. The resulting agglomerate is removed from the gas stream by inertial or electrostatic forces. The agglomeration is effected by long range forces such as inertial impact or short range forces such as electrostatic.

Inertial Impact (1.1)

Inertial impact between a droplet and particle will occur if there is sufficient relative velocity difference or momentum difference between the two. The relative velocity difference can be maintained by mechanical, gravitational, or flow forces, in which case the droplet is neutral,

Table 1-3. PARTICLE REMOVAL MECHANISMS OCCURRING
IN CHARGED DROPLET SCRUBBERS

A. Droplet-Particle Interaction Mechanisms

1.0 Direct Collision and Agglomeration

1.1 Inertial Impact

1.1.1 Mechanically Induced Relative Velocity

1.1.2 Electrically Induced Relative Velocity

1.2 Electrostatic Attraction

1.2.1 Monopole-Monopole Forces

1.2.2 Dipole-Monopole Forces

1.3 Wake Entrainment

1.4 Molecular and Turbulent Diffusion

2.0 Induced Charging

3.0 Droplet-Evaporation Charging

4.0 Droplet Condensation

B. Corona Charging

or by electrostatic forces, in which case the droplet is charged. It is assumed that the droplet is larger than the particle in this process and has the large velocity relative to the gas stream.

Mechanically Induced Relative Velocity (1.1.1)

The droplet is introduced into the gas stream with a high relative velocity and is either collected before drag forces reduce the relative velocity to zero or is accelerated to the collector by a flow field in the gas stream. It is assumed that the net acceleration on the droplets is larger than that on the particulate by virtue of their size difference.

Electrically Induced Relative Velocity (1.1.2)

The droplets are introduced into the gas stream as charged particles and are then accelerated through the gas stream by an ambient electric field. The ambient field may be an applied field to obtain the high values necessary for the accelerating forces, or it can result from the presence of space charge due to the droplets.

Electrostatic Attraction (1.2)

Either the droplets or particulate or both are in the gas stream as charged particles. If both are charged, they will have opposite polarity. The droplets and particulate are brought into close proximity as

a result of any relative velocity or Brownian motion. When the two are sufficiently close, electrostatic attraction will cause them to collide and agglomerate. The droplet size for use in this type of removal process is generally small relative to those used in inertial impacting; therefore, net forces producing relative velocity will be small.

In a classical sense, there are two types of electrostatic forces strong enough to be of interest. These arise from the monopole and dipole type charge distribution.

Monopole-Monopole Forces (1.2.1)

These forces are most important when droplet and particle are both charged and with opposite sign. It may happen by inefficiencies in the device that droplet and particle both arrive with the same sign, and this of course is deleterious to the collection efficiency. In general, the oppositely charged droplet and particulate are placed within a volume, given no deliberately induced relative velocity, and are allowed to agglomerate through mutual electrostatic attraction. These forces are effectively short range, since inertial and aerodynamic forces dominate the relative motion for separations greater than several droplet diameters.

The ratio of electrostatic monopole forces to aerodynamic forces can be simply estimated. Let s_1 and s_2 be the droplet and particle radii, with s_2 the smaller. Let u be their relative velocity and r the center-to-center separation. Electrostatic forces may be written:

$$q_1 q_2 / 4\pi \epsilon_0 r^2 \quad (1-1)$$

where $q = 4\pi \epsilon_0 s^2 E_0$

The value of E_0 will generally be governed by the charging field or the breakdown field strength at the surface of an inductively charged droplet. A value of 10^6 volts/meter is typical. Aerodynamic forces are determined by fluid momentum convection, and are given roughly by

$$\delta_g u^2 \pi s_2^2$$

where δ_g is the density of the carrier gas. Substitution gives the ratio

$$\frac{\text{Electrostatic Forces}}{\text{Aerodynamic Forces}} = \frac{4 \epsilon_0 E_0^2 s_1^2}{\delta_g u^2 r^2} \quad (1-2)$$

Upon substituting some appropriate numbers for E_0 and δ_g , this gives a ratio of

$$\left(\frac{1.65}{u} \frac{s_1}{r} \right)^2$$

Dipole-Monopole Forces (1.2.2)

When a perfectly conducting sphere is placed in a uniform electric field, charge will flow and separate to form an induced dipole. This effect is discussed by Melcher⁵ as a field charging mechanism. Field lines will bend toward the sphere (e.g., a conducting droplet) and terminate on the surface charge distribution. The effect for charged particles whose motion is dominated by electric field forces is a factor of three enhancement of the geometric cross section of the droplet, as far as collisions are concerned. The basic interaction here is between dipole and monopole. The electrostatic forces obey an inverse cube distance law, and depend on the relative orientation of the dipole and the monopole position vector.

If a perfectly non-conducting dielectric sphere is placed in a uniform electric field, it will assume a dipole moment whose strength is dependent on the polarizability of the dielectric. In practice, particulates will assume some dipole moment depending on both charge flow and polarization. Such a dipole will interact with a charged droplet, but this interaction will almost always be negligible in comparison with other forces. For larger particles inertial forces dominate. For smaller particles the induced charging mechanism will dominate, but the dipole interaction leads to an enhancement of the induced charging cross section.

The next higher order of electrostatic force is a dipole-dipole interaction. This is truly a second order effect, as will be seen from the discussion of induced charging in Section 4.

Wake Entrainment (1.3)

This mechanism is of importance mainly in the scrubbing of very fine particulate, less than 0.01 micron in diameter. The particulate may become entrained in the wakes of moving droplets, and be carried along by viscous forces. This allows diffusive mechanisms time to operate more effectively.

Molecular and Turbulent Diffusion (1.4)

Again, this mechanism is significant only for very fine particulate. A particle may cross the boundary layer around a moving drop and attach to the drop with a diffusive type motion. Diffusion may have its origins in random molecular collisions (Brownian Motion) or in turbulent eddies in the boundary layer.

Induced Charging (2.0)

In the induced charging process, charge is transferred directly from the droplets to the particulate. In this process, the droplets are charged to near the breakdown limit of the medium or to the Rayleigh stability limit (see Section 4.1 for a discussion of charging limits). As a droplet approaches a particle, there will be field enhancement on the surfaces of both droplet and particle. When the droplet and particle are sufficiently close, the electrostatic field can be high enough to cause either corona breakdown or Rayleigh instability at the droplet surface. The net effect is that charge is transferred to the particle, and the charge density on the particle can be near that of corona breakdown in the surrounding medium. This charge density is higher than that achieved by field charging in a corona and is applied in a shorter time period than by diffusion charging. The particle is removed from the gas stream by an ambient electrostatic field.

This process of particle charging and removal is an extension of the inertial impact process using electrostatic fields. Particulate that would normally be swept out of the path of a moving droplet can still reside close enough to be charged by this process. Agglomeration cannot occur by this process because the particulate will assume the same sign charge as the droplet with a resulting repulsive force.

Droplet Evaporation Charging (3.0)

Charged droplets may lose mass and size and become more highly charged through evaporation of neutral vapor. As evaporation proceeds, a stable limit (usually the Rayleigh limit) is reached rather soon. Continued evaporation will result in release of the droplet charge by instability mechanisms. This charge can be transferred to particulate, and the charged particulate then removed by precipitation in an ambient electrostatic field. The field may be either applied or due to the space charge carried by droplets and particulate.

Although no charge is released directly by evaporation, the instability mechanisms become active through droplet evaporation. The new terminology "droplet evaporation charging" has thus been adopted. This process can proceed only in an environment in which the saturation ratio is below a critical value so that the droplets can evaporate. Once the charge has been released from the droplets, it will accumulate on

the particulate by a diffusion charging process. The ambient field must be low in the system to allow the droplets enough residence time to vaporize; therefore, a field charging will be negligible.

More than one mechanism can contribute to loss of charge from an unstable droplet. These have been explored by Robertson¹². Large, unstable droplets will lose little mass but will spew off streamers of very tiny, very highly charged droplets--almost macromolecular ions. Another mechanism is discharge by electron avalanching initiated by a local, random charge release on the molecular level (e.g., cosmic ray). This will result in almost total discharge. It may occur frequently for volatile droplets, for example, in a high temperature environment, and does not require a full breakdown field strength at the droplet surface.

The process of particulate charging by droplet evaporation charging will accompany the process of electrical agglomeration. It can result in an enhancement of the removal process if the system is designed to accommodate the process of electrostatic precipitation of the particulate. This mechanism can also reduce the effectiveness of the agglomeration process however.

Droplet Condensation (4.0)

Aside from being an interaction mechanism, the nucleation and growth of liquid droplets in a supersaturated atmosphere is a common technique of droplet formation. In the sense that charged or uncharged particulate may act as nuclei for droplet condensation, this process may be thought of as a droplet-particle interaction mechanism. It is a mechanism of practical interest in some types of agglomeration devices. It is also of interest because the same thermodynamic process governs evaporation and condensation.

Corona Charging

In this process, particulate is charged by ions that result from the corona breakdown of the gas surrounding an electrode. The ions attach to the particulate by either field or diffusion charging. An ambient field will exist between the corona electrode and the attractor or collecting electrode. Field lines will terminate on the particulate between the electrodes, which results in the particulate precipitating on to a collector. The charge density of the particulate and the precipitation force is proportional to the field intensity. The quantity of space charge between the electrodes will influence the magnitude of the space-averaged field. The maximum value of averaged field will occur at a particular space charge density. If the density is below this value, the effective electrostatic field can be increased by the addition of droplets which when charged will contribute to the space charge.

The process of diffusion charging is essentially independent of the ambient field, except through its relation to the space charge density. The higher the ion concentration, the faster the charging rate. Diffusion charging is of importance for small particulate only. Droplets can promote the rate of diffusion charging by first being charged in a corona field and then releasing their charge by evaporation within an assemblage of particulate.

1.4 CHARGED DROPLET SCRUBBING EFFICIENCIES

Most types of scrubbing efficiency theories are based upon the classification mean-free-path theory of collisions. Charged droplet scrubbers are no exception. In this section we will give a short derivation of classical efficiency theory, and from it extract parameters which are pertinent to scrubbers in general and charged droplet scrubbers in particular.

The derivation given here has several simplifying assumptions which may not be satisfied in a real scrubber. It is assumed that the droplet and particulate distributions are both homogeneous throughout the scrubbing volume. It is assumed that the time between droplet-particle interactions is long enough to neglect the effects of multiple, simultaneous interactions. Finally it is assumed that the state of a charged droplet is not changed by interaction with a particle, so that it loses no effectiveness in subsequent interactions. The droplet number density distribution is thus not depopulated by interactions with particulate. If enough data were available, these assumptions could be accounted for by spatial variations of droplet number density and collision cross section. These corrections are not made here.

If droplets of radius S are moving through a gas stream containing particulates of radius R , the rate of removal of the particles through collision or other interaction with droplets is given as follows:

$$\frac{d}{dt} n(R) = - \frac{U(S)}{\lambda(R,S)} n(S) \quad (1-3)$$

t = time

$n(R)$ = number density of particles of radius R , m^{-3}

$n(S)$ = number density of droplets of radius S , m^{-3}

$U(S)$ = free stream droplet-particle relative velocity, a function of S

$\lambda(R,S)$ = mean-free-path to interaction, a function of R and S , m

The mean-free-path between droplet interactions may be written in terms of the interaction cross-section.

$$\lambda(R,S) = n(R)/\Sigma(R,S) \quad (1-4)$$

$$\Sigma(R,S) = \text{interaction cross-section, } m^2$$

In a real scrubber, both $n(R)$ and $n(S)$ are distributed over a range of sizes, and these two equations must be combined and integrated over each size range. The resulting integral equation follows.

$$\begin{aligned} \frac{d}{dt} n(R) &= - \int_{S=0}^{\infty} n(R) \Sigma U n(S) dS \\ &= -n(R)/\tau_c \end{aligned} \quad (1-5)$$

τ_c = mean time between collisions for collisional interactions.

In Equation (1-5), $n(R)$ and $n(S)$ are now density distribution functions over R and S , defined so that

$$n(S) = n_{oS} f(S)$$

$$\begin{aligned} n_{oS} &= \text{average spatial number density, } m^{-3} \\ f(S) &= \text{droplet size distribution, } m^{-1} \\ \int_0^{\infty} f(S) dS &= 1 \end{aligned}$$

and similarly for the particulates. Equation (1-5) may then be integrated over time to obtain a fraction number density efficiency $\eta(R)$, which also depends on droplet size distribution parameters embodied in τ_c .

$$\eta(R) = 1 - \exp [-\tau_r/\tau_c] \quad (1-6)$$

τ_r = effective particle residence time

$$= L/W$$

L = length of scrubbing volume

W = flue gas velocity

$$\tau_c = \left[\int_{\Sigma} U n(S) dS \right]^{-1} \uparrow$$

Knowing the fractional efficiency and the particulate size distribution function $f(R)$, one obtains the total mass removal efficiency from an integral:

$$\eta_m = \frac{\int R^3 \eta(R) f(R) dR}{\int R^3 f(R) dR} \quad (1-7)$$

Collection Efficiency

The interaction cross section, Σ , shown in Equation (1-5) may now be derived with particular attention to scrubber mechanisms. The derivation is based on the assumption of a collisional type of interaction, but may be extended to other types of interactions which are non-collisional, but which occur only within a distance-of-farthest-approach, D.

The geometry of the derivation is shown in Figure 1-4. The model assumes that a relatively large droplet is introduced into the carrier gas within which a small particle is at rest. The droplet moves at a drift velocity U which is assumed constant for purposes of the derivation. It may be either mechanically induced or, in the case of a Class II scrubber, electrostatically induced by an ambient electric field. As the droplet moves within the gas, a "wake" flow field is generated which gives rise to accelerations on the particle, and which, if sufficiently strong, can sweep the particle out of the direct path of the droplet.

As the droplet moves through the gas, it sweeps out a volume equal to its path length times its projected area. Particles within this volume which are not swept out by aerodynamic forces as the droplet moves along its trajectory, are collected on the droplet by agglomeration.

Particles within a concentric cylinder of radius $S+D$ may remain within this cylinder as the droplet passes. If a particle passes with its center within a distance D of the droplet surface, it is assumed to have interacted with the droplet strongly enough to be collected, though not necessarily by collision and agglomeration. If the droplet

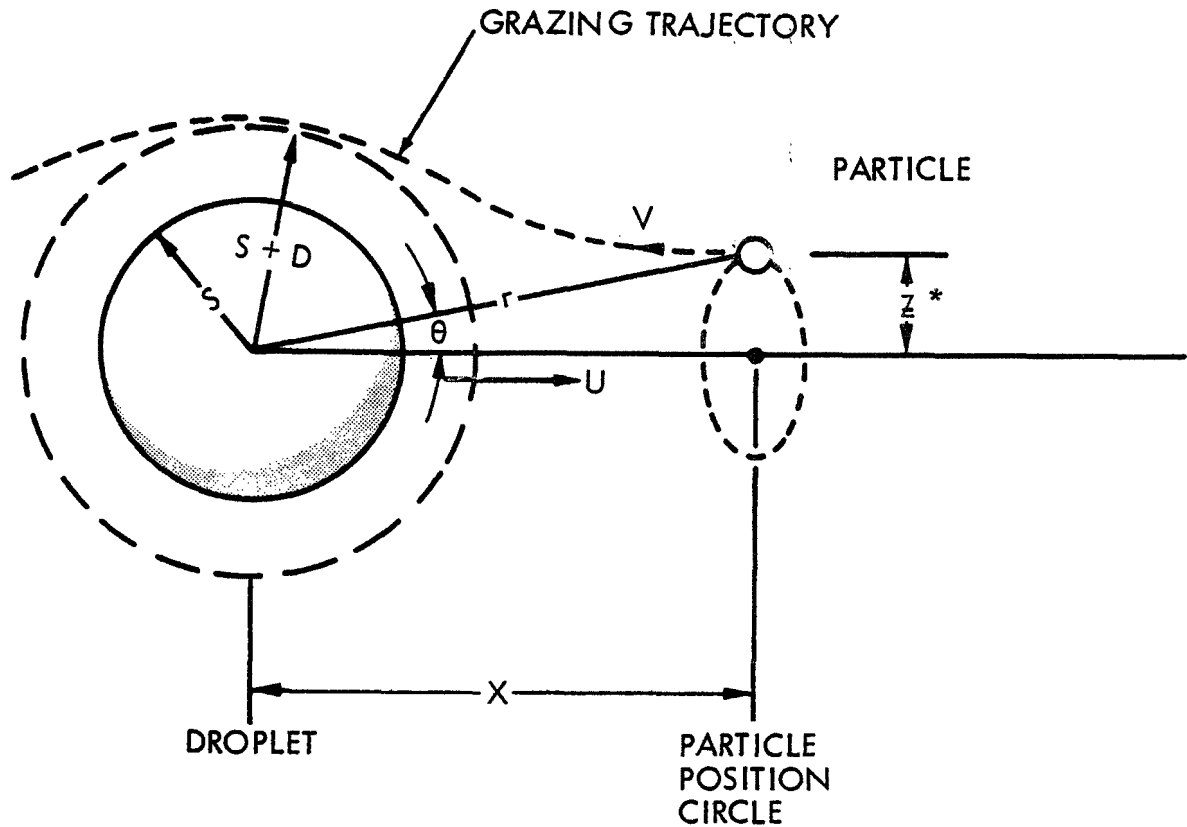


Figure 1-4. DROPLET-PARTICLE INTERACTION MODEL

is charged, a possible interaction mechanism is by charge transfer, or induced charging. This is the major non-collisional interaction phenomenon explored in this program.

Particles originally residing within a third concentric cylinder of radius z^* , as indicated in Figure 1-4, will remain in the interaction cylinder. A particle starting from radius z^* will follow a grazing trajectory as shown in Figure 1-4, and this radius defines an interaction boundary.

A measure of the efficiency of particle collection within this model is given by the following area ratio, the denominator of which is the true geometric coincidence cross section.

$$\eta_c = \left(\frac{z^*}{S+D} \right)^2 \quad (1-8)$$

The first analyses of droplet collision effectiveness were made in terms of this parameter. It was used because in the absence of interactions other than direct impact (i.e., $D = 0$) it is the same as the classically defined droplet collection efficiency¹³, or collision probability. As such, the parameter range is confined between zero and one, and it qualifies as a true efficiency. If, however, D is greater than zero, the possibility exists that η_c can be greater than one. Under these conditions, when electrostatic interactions are included for example, Equation (1-8) does not qualify to be called an efficiency. In order to continue its use, a new name was coined: collision effectiveness. This name quickly degenerated to "collision effectiveness probability," due to the background of its derivation.

The analysis given in the present report is in terms of a collection efficiency which is consistent with common usage. The basis of its definition is the cross section of the complete interaction cylinder.

$$p = \left(\frac{z^*}{S+D} \right)^2 \quad (1-9)$$

This parameter is mathematically equivalent to a probability or an efficiency. It will be equivalently referred to in this report as either collection efficiency or collision effectiveness probability.

The true interaction cross section of Equation (1-5) may now be expressed as follows:

$$\Sigma = \pi z^{*2} = \pi S^2 p (1+A)^2 \quad (1-10)$$

$A = D/S = \text{impact parameter}$

We have here defined a new dimensionless parameter, the impact parameter, which will prove fundamental also in the induced charging analysis.

The collision effectiveness probability is found by solving the complete equations of motion of a particle in the flow field surrounding the droplet. This solution was done numerically and was programmed for the computer. The results are discussed in Section 4.1. It was assumed that the particle was spherical, with motion governed by Stokes' drag law, that the droplet is spherical, and that the velocity distribution in the medium surrounding the droplet is a Stokes' flow field. A classical treatment of this flow field has been given by Happel and Brenner¹⁴. With reference to the nomenclature of Figure 1-4, the velocity distribution is given by the following expressions.

$$w_r = -\frac{1}{2} U \cos \theta \left(\frac{S}{r}\right) \left[\left(\frac{S}{r}\right)^2 - 3\right] \quad (1-11)$$

$$w_\theta = -\frac{1}{4} U \sin \theta \left(\frac{S}{r}\right) \left[\left(\frac{S}{r}\right)^2 + 3\right]$$

w_r, w_θ = components of wake flow field velocity at particle position.

A transformation to rectilinear coordinates gives:

$$w_x = w_r \cos \theta - w_\theta \sin \theta \quad (1-12)$$

$$w_z = w_r \sin \theta - w_\theta \cos \theta$$

The force balance on a particle entering the wake surrounding the droplet is taken to include a Stokes flow drag force and an electrostatic force from the droplet charge. The particle velocity u then obeys the following equations of motion.

$$M_p \frac{du_x}{dt} = 6\pi\mu R (w_x - u_x) - q_d \frac{\partial \phi}{\partial x} \quad (1-13)$$

$$M_p \frac{du_z}{dt} = 6\pi\mu R (w_z - u_z) - q_d \frac{\partial \phi}{\partial z}$$

The particle mass is designated M_p , and the droplet charge is q_d . The components $(w_x - u_x)$ and $(w_z - u_z)$ are the x and z components of the particle velocity relative to the wake around the droplet. The electrostatic forces are calculated from a potential function ϕ which is due to the droplet and particle charge distributions. These charge distributions were calculated to the lowest orders of the parameter (R/S) , and are discussed in Section 4.1. They consist, to the approximation keeping terms to order $(R/S)^3$, of a monopole and dipole component on the particle and a monopole and two dipoles on the droplet.

The leading terms of the potential function ϕ are of order $(R/S)^3$, and higher order terms are neglected. The leading terms consist of the monopole-monopole interaction of the particle charge with the net droplet charge, and the droplet monopole with the particle dipole. The resulting approximation is:

$$\phi = \frac{1}{4\pi\epsilon_0} \left(\frac{q_p}{r} - \frac{\bar{\beta} \cdot \bar{r}}{r^3} \right) \quad (1-14)$$

The values obtained for the particle charge q_p and the induced dipole, β , on the particle will be discussed in Section 4.1.

Induced Charging

The induced charging mechanism will have a direct effect on the efficiency equation, (1-5), through its effect on the impact parameter A and thus on the interaction cross section. Appreciable values of A , apparently one or more, may be achieved through induced charging.

In this mechanism, a charge transfer takes place from droplet to particle by means of field charging or diffusion charging. The name "induced charging" arose because in order for the charge transfer to take place, local electric field lines must terminate on the particle and strengthen the surface field there until local electrical breakdown occurs. Thus the net charge transfer to the particle is not induced, but the precipitating charge distribution on the particle (predominantly dipole) is induced.

Two models for induced charging were studied. The premise of the first model is that the surface electric field on a particle can exceed the local breakdown strength of the medium in which the particle and droplet reside. When breakdown occurs, corona discharge is initiated at the particle surface, and charge is transferred between particle and droplet. The particle will assume charge of the same sign as the droplet.

The field enhancement causing breakdown is due to the dipole-monopole interaction of particle and droplet. The correction by Peek¹⁵ is used to account for the strengthening of the breakdown limit on a curved surface. This is further discussed in Section 4.1.

A second model for induced charging was derived which predicted much larger interaction distances and seemed more capable of fitting observed results. The basis for the model is an assumed electrical breakdown at the surface of the charged droplet, which is charged to the Rayleigh limit (or to the corona breakdown limit). The breakdown occurs because of induced field enhancement between droplet and particle. The resulting released charge migrates to the particle along field lines.

The steps of the analysis are as follows. A dipole moment is induced on the particle, assumed spherical and uncharged, by virtue of its presence in the field of the charged droplet. In this first step, the charged droplet field is assumed unperturbed. The resulting dipole is then imaged into the charged droplet, which is assumed perfectly conducting. The field enhancement due to the dipole-dipole interaction between droplet and particle is then calculated. Next it is assumed that enough net charge is transferred to the particle so that the resulting monopole field will just cancel the dipole-dipole field perturbation at the surface of the droplet. In order for this to be valid, the droplet surface must be charged to a critical limit so that any local field enhancement would cause charge leakage.

When these steps are carried out, it is seen that the particle will experience some charging at an arbitrarily large distance from the droplet. For large enough droplet-particle separations, the induced charge is found to be inversely proportional to the separation. Thus, the question arises as to what constitutes an "effective collision" in terms of the induced charging mechanism.

When the particle becomes charged it acquires a directed drift velocity along ambient field lines. The particle mobility may then be used to calculate its drift time to the collecting walls on the basis of some average electric field value. This drift time is then a practical definition of an "effective collision," if some upper limit is set upon it.

The model thus obtained has limited validity in the sense that the effects of some of the more basic assumptions are not fully known. The assumption most open to question is the sphericity of the particle being collected. Also of an unknown nature is the actual droplet discharge mechanism; its time dependence and its effect upon droplet size and shape have been idealized. Thus, if droplet disintegration occurs through break-up into equal volumes, the model is not valid. The droplet charge is assumed to be at a critical level, and the effects of particle conductivity and electrostatic shielding have been neglected.

The more interesting results of both the induced charging models will be discussed in Section 4.1.

Droplet Area Utilization Efficiency

We may now return to an analysis of the fractional efficiency equation, (1-6). By substituting Equation (1-10) for the cross section, we include collision effectiveness due to both direct impact and induced charging. The exponent may now be written as follows.

$$\tau_r/\tau_c = \pi n_{OS} \tau_r \int_0^S p (1+A)^2 U S^2 f(S) dS \quad (1-15)$$

The droplet distribution function, $f(S)$, has been found to be approximately log-normal. Each of the other quantities under the integral sign are functions of S also. The integral must then be evaluated numerically, or some approximations made. For present purposes, we will assume that some valid approximations can be made in terms of a droplet distribution efficiency, which we shall now derive.

Values of droplet size and velocity will be referenced to distribution parameters in the log normal distribution, $f(S)$. One such parameter is the maximum droplet velocity in the distribution, which is also near the most probable velocity. The most effective scrubbing droplets in the distribution are those with the most probable radius, S_p , of the distribution. This is the "design" droplet radius. These droplets are highly charged, and their surface field is near the local breakdown limit. Smaller droplets may carry the same surface charge density, but are limited in velocity by a smaller total charge. Larger droplets are less efficiently formed and have lower surface charge density, thus lower velocity.

The product $p(1+A)^2$ is a weakly varying function of S , and tends to increase strongly with increasing values of U . Thus it should also reach a maximum value for the maximum, or most probable, droplet velocity. We may thus find the following inequality for the integral in Equation (1-15).

$$\int p(1+A)^2 U S^2 f(S) dS \leq [p(1+A)^2]_{\max} U_p \overline{S^2}$$

The value of $\overline{S^2}$ is an average over the distribution. The value $[p(1+A)^2]_{\max}$ is taken as the value at the most probable droplet parameters, S_p and U_p , and we will henceforth drop the subscript with that understanding.

The above inequality can then be used to define a droplet distribution efficiency, which will be denoted by e_2 and which will be called the area utilization efficiency. The complete set of scrubber efficiency equations now appears as follows:

$$\eta(R) = 1 - \exp(-p(1+A)^2 \Lambda) \quad (1-16)$$

$$\Lambda = \pi \overline{S^2} U_p \tau_r n_{oS} e_2 \quad (1-17)$$

= scrubber efficiency parameter

$$\tau_r = L/W \quad (1-18)$$

$$e_2 = \frac{1}{U_p \overline{s^2}} \int_{s=0}^{\infty} U(s) s^2 f(s) ds \quad (1-19)$$

= area utilization efficiency

There are a total of four independent dimensionless variables which determine scrubber performance by this model. One is the scrubber efficiency parameter Λ , and one is the impact parameter A . Two more will be shown in the results of the collision effectiveness probability analysis discussed in Section 4.1.

The area utilization efficiency in Equation (1-19) is so defined because it is a measure of useful droplet surface area in the droplet distribution. The most effective scrubbers have large geometric cross-section (or equivalently surface area) and move with high velocities. Both these requirements are reflected in Equation (1-19). In addition, e_2 will always be less than one for a log-normal distribution, but will approach one for a distribution with uniform droplet size. Theoretical estimates for e_2 can be made by assuming or measuring velocity and size distributions, but the best estimates are probably obtained directly from efficiency measurements. Some attempt to do this has been made in this program (Section 4.4), but the results must be interpreted with caution. Interactions of particulate with the large-size weakly charged tail of the droplet distribution were not studied extensively, and may contribute importantly to the area utilization efficiency. In addition other mechanisms, such as evaporation and condensation, have been neglected on the basis of analytical studies but have not been firmly rejected by experiment.

The scrubber efficiency parameter may be shown to have the physical significance of a volume ratio as well as a time constant ratio. During a particle residence time period τ_r , the volume of gas cleaned per average scrubbing droplet is

$$\pi \overline{s^2} U_p \tau_r$$

The value of (n_{0se2}) may be taken as the effective number density of scrubbing droplets. The value of Λ is then the ratio of the total volume of gas cleaned during the time τ_r to the total scrubbing volume.

Figure 1-5 is a nomogram of the fractional efficiency as given by Equation (1-15). The variables are collision effectiveness, given by

$$\eta_c = p(1+A)^2$$

and the scrubber efficiency parameter given by Equation (1-17). If collision effectiveness is known, the straight line plots may be used to determine the value of A necessary to obtain a chosen efficiency (one among the seven plotted). If the desired efficiency is not plotted it may be located from the fractional penetration curve. All lines of constant efficiency have the same slope (minus one) on this plot. Their intercepts with the vertical dashed line are given by the ordinate of the fractional penetration curve.

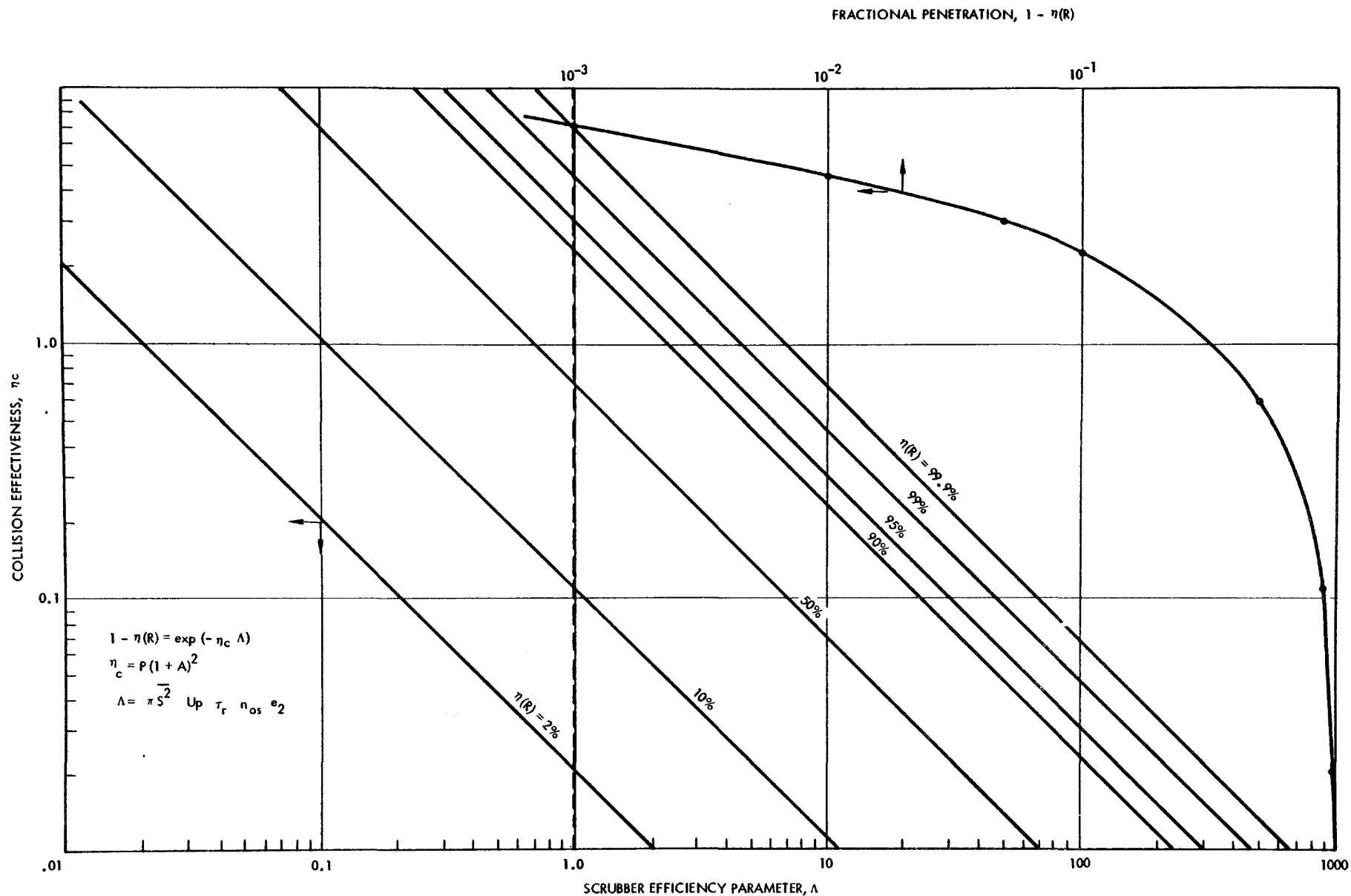


Figure 1-5. NOMOGRAM FOR FRACTIONAL EFFICIENCIES OF CHARGED DROPLET SCRUBBERS

2. EXPERIMENTAL DESIGN

The present program was conducted in three basic phases, which are treated more or less distinctly. The first phase was analytical, and the second and third were experimental. Additional program requirements included the development of design, cost and process recommendations for a pilot demonstration scale Charged Droplet Scrubber.

Phase one was an analytical study of important basic mechanisms in charged droplet scrubbers, and their effects on overall efficiency. The approach to this phase consisted partly of development of new results, and partly of the correlation of prior results for purposes of further analysis and comparison.

Phase two was an experimental program directed toward an investigation of selected scrubbing or interaction mechanisms to quantify their effects and verify their importance. The third phase of the program was also experimental in nature, and consisted of performance verification testing of an operating CDS utilizing the selected scrubbing or interaction mechanisms studied in the first two phases.

In this section we will first review and discuss the overall program objectives. The experimental design of the phase two research scale scrubber and the phase three bench scale scrubber experiments will then be dealt with.

2.1 PROGRAM OBJECTIVES

This program was an exploratory development program, directed toward obtaining estimates of the effectiveness of charged droplet scrubbing for the collection of fine particulates. A variety of charged droplet scrubbing mechanisms were studied to determine contribution to overall performance. Secondly, the program was directed toward analysis and testing of the TRW/CDS concept, which has been shown to have superior performance for a variety of fine particulate control applications. Finally, it was the purpose of this study to derive some basic performance comparisons between charged droplet scrubbers and other types of control equipment.

The program objectives may best be presented in terms of the following task breakdown of the program work plan.

Definition of Basic Mechanisms

The objective of this task was to define and characterize the important mechanisms that remove particulate in charged droplet scrubbers. The task included a study of existing literature.

A further objective of the task was to define the effectiveness of chosen removal (or scrubbing) mechanisms in terms of one or more theoretical charged droplet scrubbing devices. There are two particulate size ranges of interest. These are basically 1.0 to 10.0 and 0.1 to 1.0 micron mass-mean diameters. The primary program interest lies, of course, in the smaller size range. The approach is then to find the effects of performance parameters on device efficiency, and find the contribution to device efficiency of each of the chosen scrubbing mechanisms for each particulate size range.

A further objective of the task was the comparison of performance of the chosen device with a conventional electrostatic precipitator, in each of the particulate size ranges. The basis of this comparison was to be the particulate collection efficiency in the two size ranges of interest, with device performance and operating parameters as variables. These parameters include, for example, specific power consumption, flow pressure drop, equipment sizing, particle resistivity, and specific water usage, if applicable. Interaction times and residence times of particulate are also a valid basis for comparison.

Research Scale Studies

The objective of this task was to experimentally verify the effectiveness of the important scrubbing mechanisms chosen in the first task. This was to be done in a more basic way than from measurements of resultant scrubbing efficiency, and included measurements of basic parameters of the scrubbing droplets themselves.

In order to determine the effectiveness of the particle removal mechanisms of the droplets, it is sufficient to determine the physical state of the droplets themselves. This was the experimental approach taken. The parameters sought were droplet size distribution, number density, velocity and charge distribution. Direct measurements were made of all these except charge distribution, for which the scrubber current distribution was measured instead.

Using this approach, it is not necessary to measure particulate properties directly, as the addition of particulate will not change the state of the droplet distribution significantly except at high loading. The main effect of adding particulate is to alter the scrubber space charge distribution, an effect which can be accounted for.

Bench Scale Studies

The objective of the bench scale studies was to experimentally measure the actual performance of an operating charged droplet scrubber device. The device chosen would be one of the same as was used for the theoretical device studied in tasks one and two. In this case, it was the TRW/CDS.

The basic criterion for performance was particulate fractional collection efficiency in the two size ranges of interest. The effects of important scrubber operational parameters upon the collection efficiency were studied.

Particulate was generated and injected into the flue-gas stream at various loading levels for this test. Both newly dispersed and redispersed aerosols were of interest. This work concentrated on newly dispersed aerosol generation, since this was the best way to guarantee good particulate samples in the smaller size ranges, and ample data is already available for redispersed aerosols.

The purpose of this task was basically to recommend steps for the next stage of scrubber development. It had, as an objective, the basic problem definition for a 10,000 SCFM pilot scale demonstration unit. This unit was designed for field testing on an important industrial source of fine particulate. A basic scrubber design for such a process was presented, and a recommended test plan was developed.

2.2 RESEARCH SCALE SCRUBBER

The research scale unit was a small scrubber, designed for ease of access and modification. All the essential geometry factors for the mechanical and electrical configuration of a full-scale scrubber were maintained as best as possible. Access for visual measurements was provided, and the unit was instrumented for measurement of current density on the collection plates.

Photographs of the research scale scrubber are shown in Figure 2-1. The unit as shown is configured for photographing the droplet formation at the flow tube tips.

The high voltage spray electrode consisted of a support electrode with five (5) spray tubes. Hypodermic needles were used for the spray tubes. The use of hypodermic needles provided a convenient means of changing spray tube size. Both 22 ga and 18 ga tubes were used in the experiments with the research scrubber. The dimension of the tubes are:

0.22 ga - 0.39 mm ID x 0.712 mm OD

0.18 ga - 0.84 mm ID x 1.27 mm OD

The support electrode was a 3/8-inch (0.95 cm) diameter copper tube with five Luerlok fittings soft soldered to the tube, in-line, on 2.5-cm spaced centers. The hypodermic needle spray tubes were attached to these fittings. The spray tube support electrode was suspended and isolated from ground with an insulator machined from a 5-cm diameter teflon rod.

The collector plates were stainless steel sheets, positioned on both sides of the electrode. The collector plates were isolated from ground

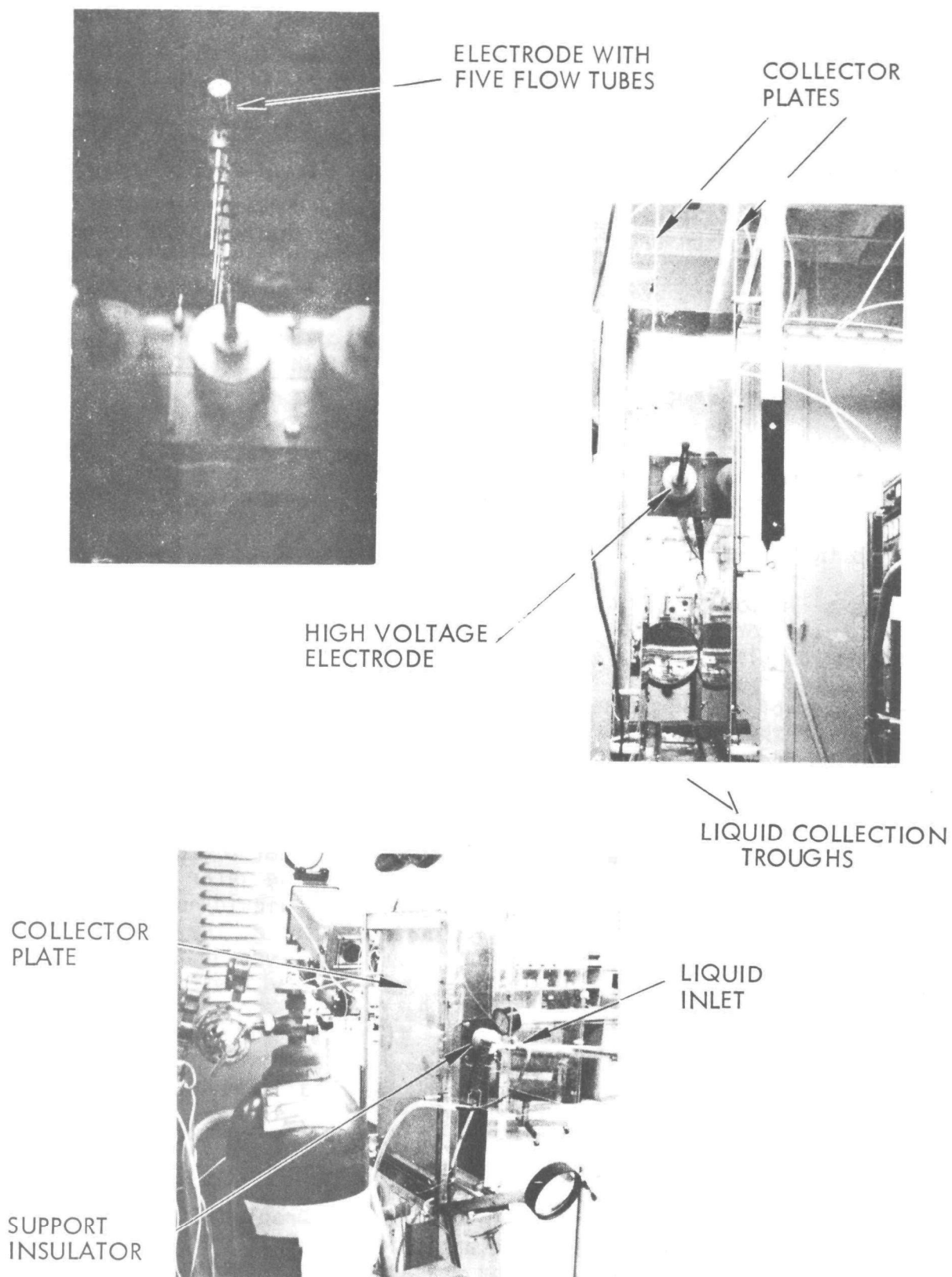


Figure 2-1. EXPERIMENTAL SCRUBBER UNIT

and their separation from the electrode could be varied up to 0.1 meter. This corresponds to a collector spacing of 0.2 meter. During operation, the collector plates could be connected either directly to ground or grounded through a resistor in parallel with a millivolt meter to monitor spray tube current. When the millivolt meter was used, the collectors were connected to ground through a neon bulb and the meter terminals were parallel with a capacitor. This circuit was used to protect the meter in the event of an arc from the spray tubes to the collector.

Water collection troughs were attached to the lower edge of the collector. The sprayed water intercepted by the collector plates emptied into the troughs which were drained through plastic tubing. The plastic tubing was used to maintain electrical isolation of the collector plates.

Air was supplied through the channel between the collector plates with a double squirrel cage blower. A maximum air velocity of 3.5 m/sec with a mean deviation of 0.3 m/sec could be maintained with 0.15 meter collector spacing. Lower velocities were obtained by using reduced voltage to the blower motor.

One of the collector plates contained a removable section in which a segmented collector could be installed. This collector was used to determine axial (longitudinal) current distribution in the scrubber.

The end plates of the scrubber channel were lucite to allow visual observation of the droplet spray. Sections of the lucite were removable to allow undistorted optical measurements of the droplets.

Water was supplied to the high voltage electrode from a container that was isolated from ground. The liquid head was provided by either pressurizing the container or adjusting the elevation of the container relative to the spray tube tips. Pressurization of the water container was used during operation with the 22 ga tubes. The liquid height level head control proved more stable during operation at the low pressure required by the 18 ga tubes. Calibration curves of the water flow rate through an average spray tube at various head pressures are shown in Figure 2-2 for both 22 ga and 18 ga tubes.

A Hipotronics, Model No. 860-40, power supply with a continuously adjustable output voltage of up to 60 kv was used to provide the high voltage.

2.3 BENCH SCALE SCRUBBER

The bench scale unit was a small-scale TRW Charged Droplet Scrubber, fully configured for a real scrubbing application. Only the normal field instrumentation was supplied for the scrubber. Access was provided for inlet and outlet flue gas sampling. The unit was equipped with a 1000 CFM (1700 m³/hr) blower, an aerosol generation section, and a flow turning section equipped with flow distribution vanes.

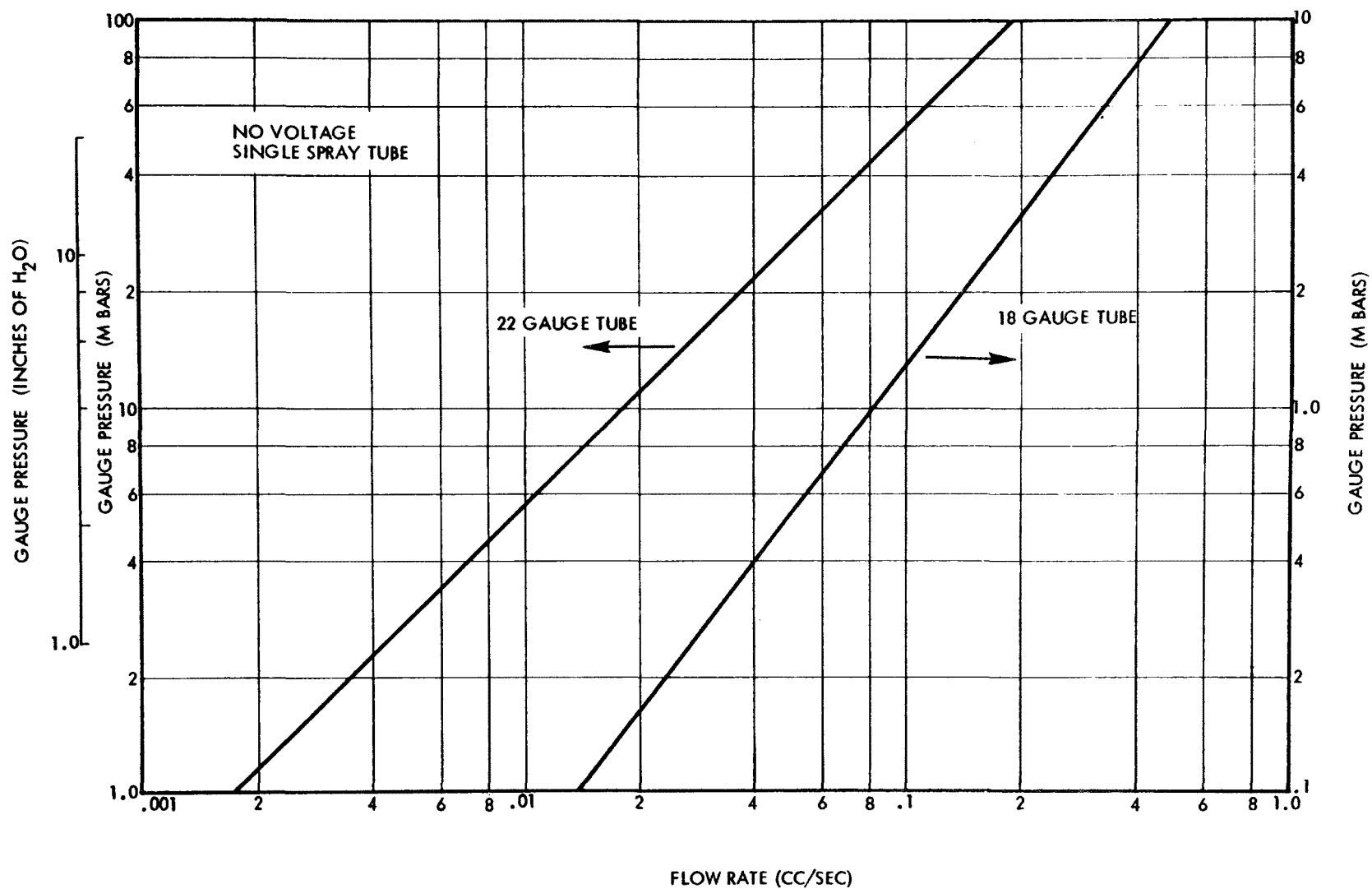


Figure 2-2. WATER FLOW RATE VS. PRESSURE CALIBRATION

Figure 2-3 is a photograph of the bench scale scrubber configured for single stage operation. The blower has a "clover-leaf" damper on the inlet, for flow control. The aerosol generator was an electric arc zinc oxide fume generator, the components of which are seen schematically in Figure 2-4. The flow turning section also acted as a fall-out section for larger particulate. The electrode compartment was designed to minimize field breakdown in the interior. The electrode penetration was a lucite window on the end of the compartment. Another view of the compartment, the electrode and the insulator is seen in Figure 2-5.

The principle of the fume generator was to allow vapor to disperse from a molten pool of zinc which was kept at temperature with the electric arc. The vapor was allowed to disperse and cool in flow of inert nitrogen gas, shielded from the oxidizing flue gas by a flow baffle. When the warm zinc vapor reaches oxygen, it forms a finely dispersed zinc oxide fume. The relative position of the zinc pool and the carbon electrode controls the particle generation rate.

The combined stack and scrubbing volume has a height of 1.52 meters. The collector electrodes, shown broad side in Figure 2-3, were 0.50 by 1.45 meter sheets of stainless steel, set on insulating stand-offs. The collector spacing was adjustable inward from 0.22 meter, depending on the size stand-offs used. Current to the collector plates could be grounded or monitored.

At a 0.2 meter collector spacing, the device handled a flow of 1700 m³/hr at a flue velocity of 4.7 m/sec. This was high for good collection efficiency. At the design velocity of 1.5 m/sec the flue gas rate is 540 m³/hr.

Figure 2-6 shows another view of the scrubber with its auxiliary equipment. A 31.8 meter coil of 1/4 in. (1 cm) ID tygon tubing supplied water resistance of nominally 10 megohms from high voltage to ground. An additional 1.9 meter length acted as an isolation section from high voltage to the electrode. A pressure gauge was attached directly to the end of the electrode. Pressure was read at electrode height. The calibrations in Section 2.2, for water flow, were for pressure at the spray tube tips which were 6 cm lower. A particulate sampling section was included just above the scrubber inlet. The outlet sampler was suspended in the stack and supported from the top of the unit.

A Hipotronics Model 860-40 power supply was used to supply high voltage to the electrode. Its maximum rated voltage is 60 kv and maximum current output is 40 ma. A conventional dc arc welding supply, a Trindl Model 180A, was used to run the fume generator. The supply has a step-wise adjustable output consisting of a series of taps off the transformer secondary. This allowed 16 current settings between 40 amps and 180 amps. The heat load to the zinc melt, and thus the fume generation rate, was adjustable by means of this current setting. The nominal operating current range was around 80 amps.

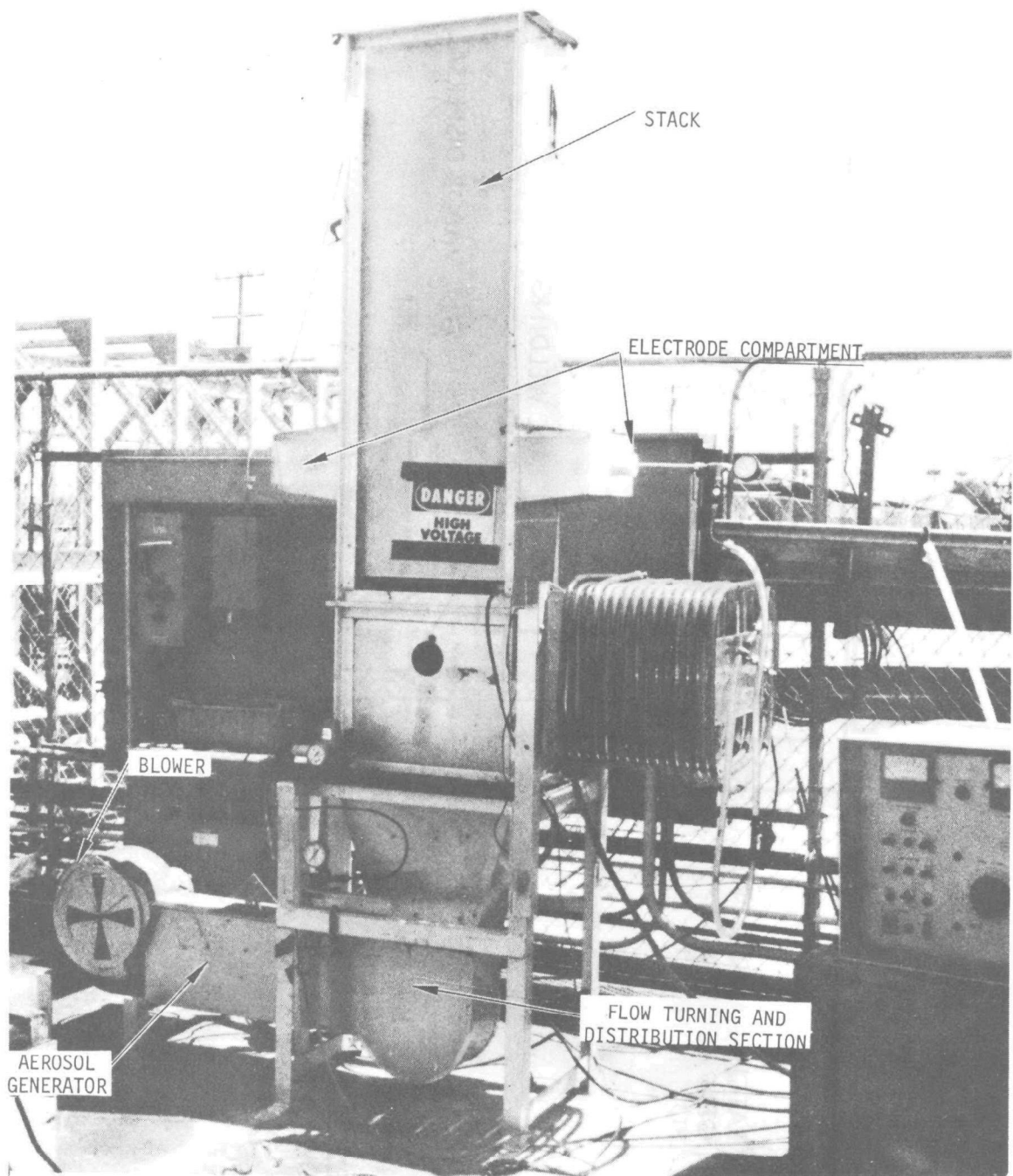


Figure 2-3. TRW CHARGED DROPLET SCRUBBER BENCH SCALE UNIT

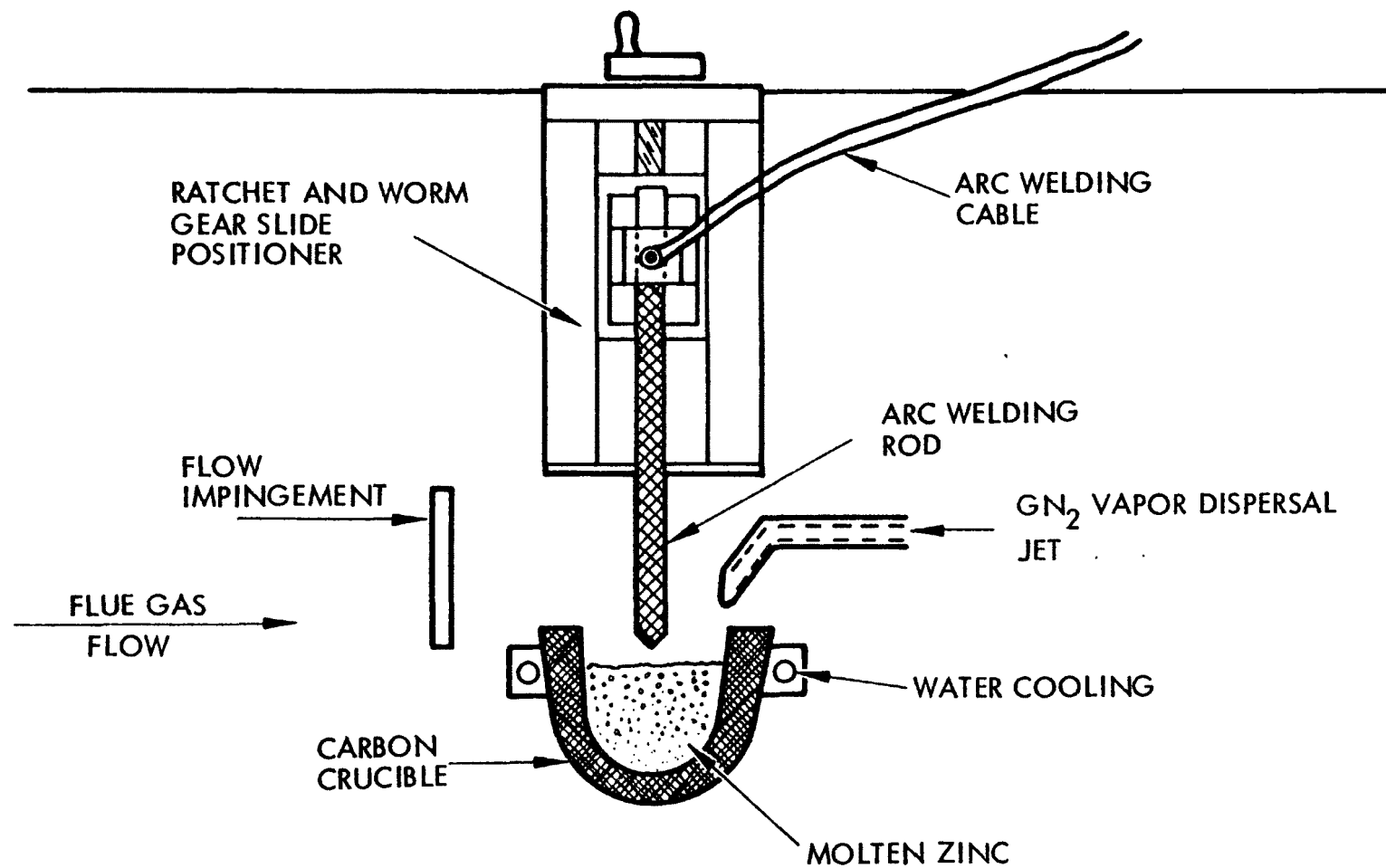


Figure 2-4. SCHEMATIC OF ELECTRIC ARC ZINC ROD

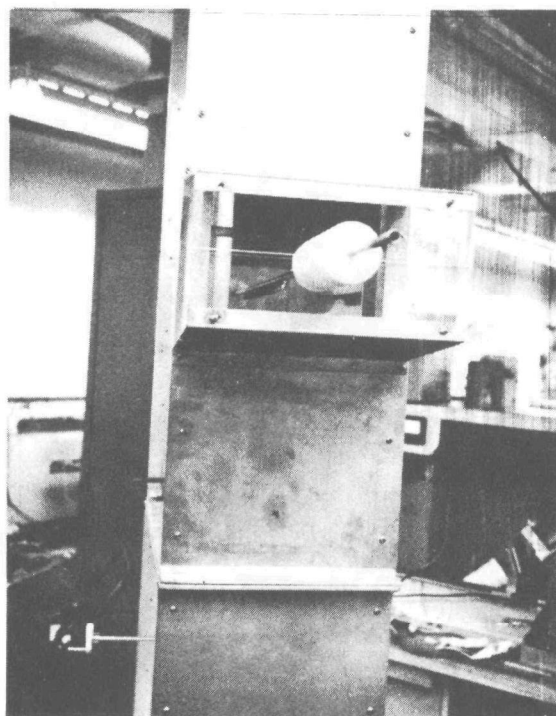


Figure 2-5. BENCH-SCALE SCRUBBER ELECTRODE ASSEMBLY

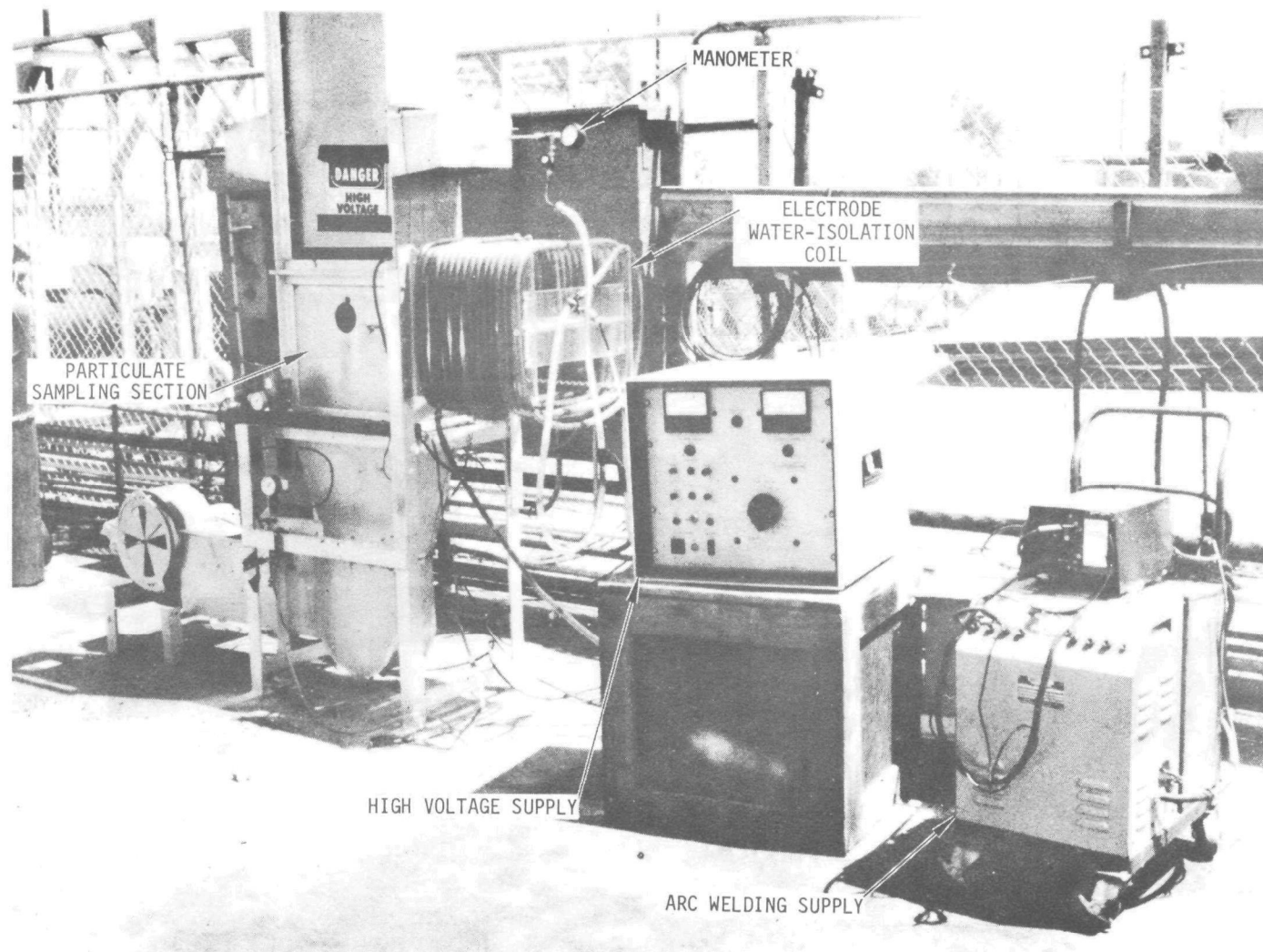


Figure 2-6. BENCH-SCALE CDS WITH AUXILIARY EQUIPMENT

The arc welding electrode was adjusted with a slide and worm gear assembly, which could be operated from outside the enclosure.

The flow distribution across the inlet duct of the scrubber was kept uniform to about 20 percent accuracy with an arrangement of flow turning vanes. These vanes were followed with a flow-straightening honeycomb baffle, which takes out most of the turbulent eddys. These arrangements are shown in Figures 2-7 and 2-8.

The high voltage spray electrode consisted of a support electrode with 15 spray tubes. Both 22 gauge and 18 gauge spray tubes were used. The spray tubes were equipped with Luerlok fittings so that they were easily removable.

The support electrode was a 0.95 cm OD stainless steel tube, with 15 Luerlok fittings silver-soldered into the tube on 2.5 cm spaced centers. The electrode was suspended and isolated from ground with two insulators machined from 2-1/4 in. (5.7 cm) diameter teflon rod, and in turn suspended on the lucite covers on the ends of the electrode compartments.

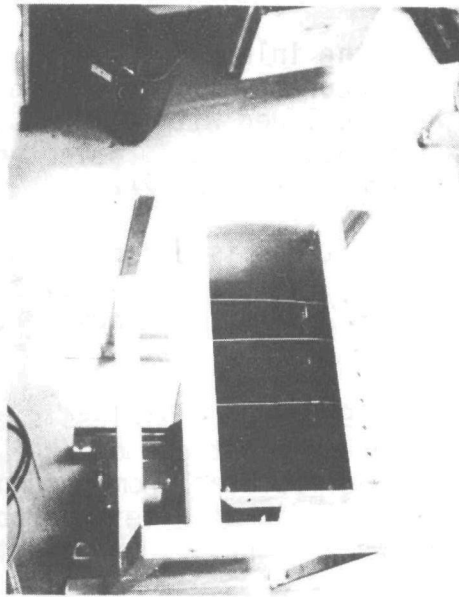


Figure 2-7. FLOW DISTRIBUTING VANES

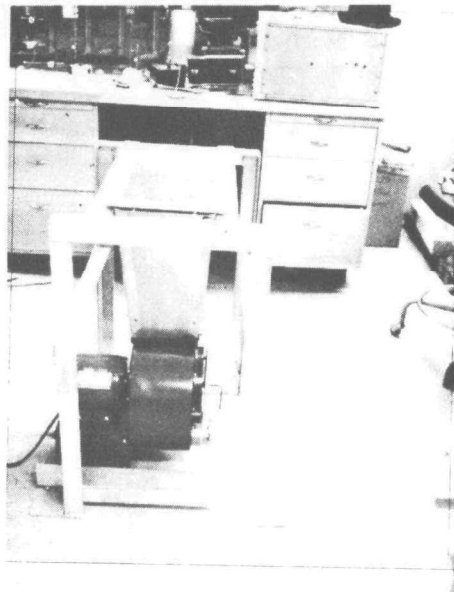


Figure 2-8. BLOWER UNIT AND FLOW STRAIGHTENER

3. TEST PROCEDURES

In this section the test procedures will be described for the basic types of measurements taken during the experimental program. In general, the bench-scale experimentation required only one basic type of measurement. That was scrubbing efficiency. More measurements were taken on the research scale experiments. These included measurements of collector current, high-speed droplet photography and laser velocimeter measurements of droplet velocity.

3.1 COLLECTOR CURRENT MEASUREMENTS

A segmented collector was installed within the collector wall of the research scale scrubber to monitor the axial current distribution from the spray tubes. A schematic diagram of the collector is shown in Figure 3-1. The segmented collector consisted of fifteen collectors, each one inch by two inches. The individual collectors were isolated from each other and from ground. Each of the collectors was shaped so that the collected water would free fall to the collection trough. This prevented shorting between the collector electrodes through liquid columns.

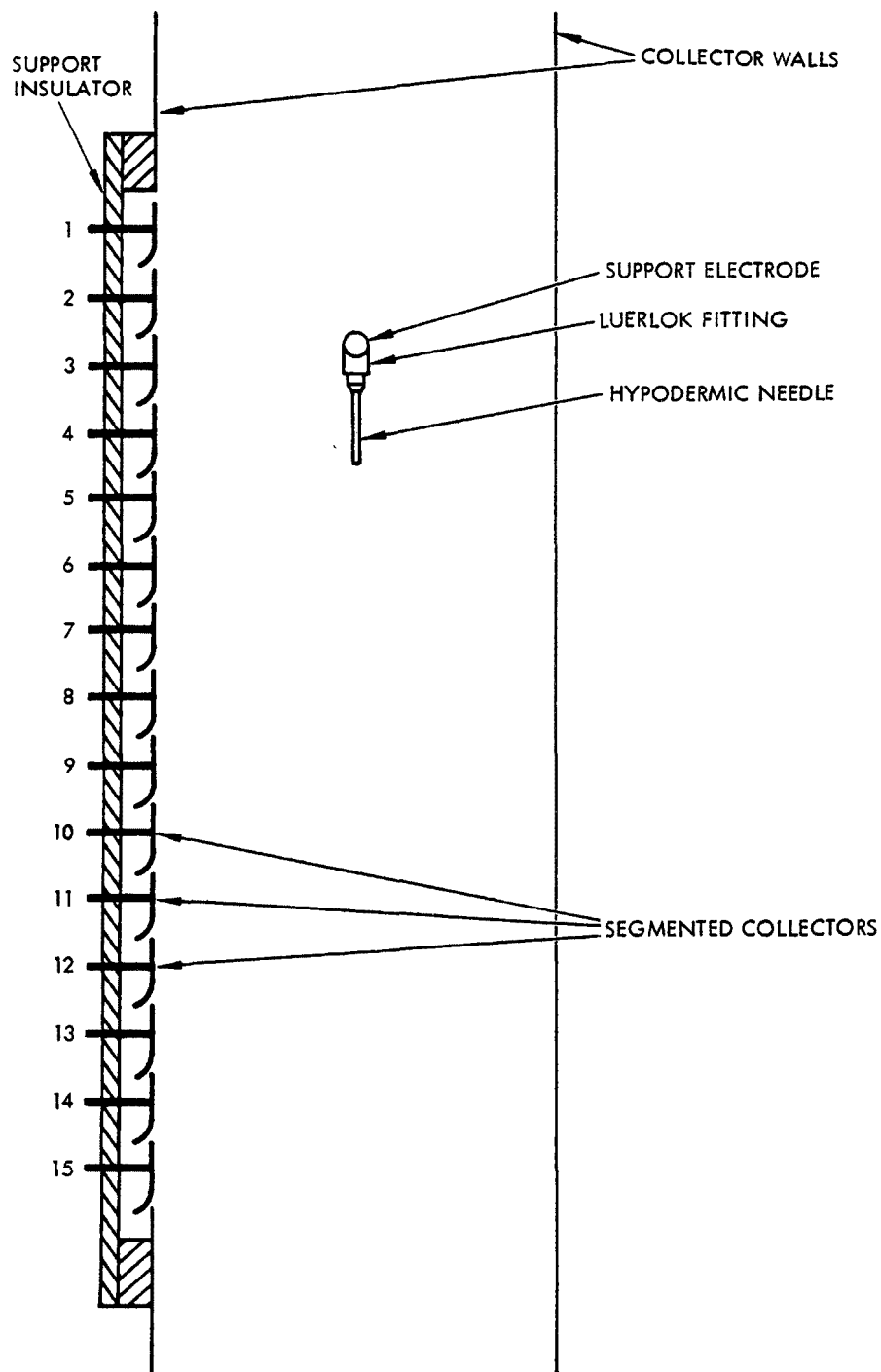
The collector, as shown in Figure 3-1-b, was centered opposite the center spray tube of the five tube array. There were four collectors above the spray tube tips, and eleven below. The entire axial spray pattern was intercepted with this geometry.

The individual collectors were connected to a rotary switch, the output of which was connected to the monitoring circuit shown in Figure 3-1-c. During operation, the collector being monitored would be raised to only a few millivolts above ground. This produced a negligible influence on the current pattern.

3.2 DROPLET FORMATION PHOTOGRAPHY

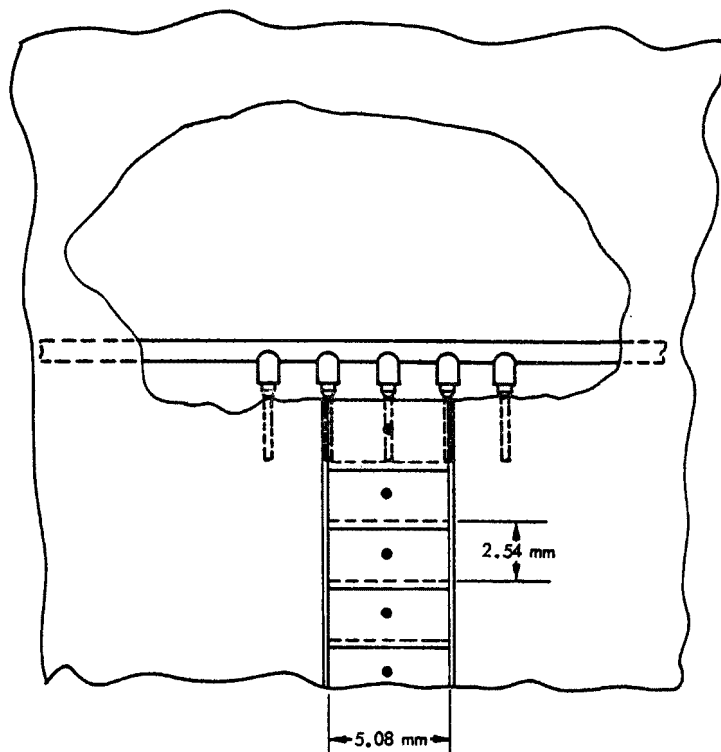
Spray and droplet formation phenomena were photographed using a tripod-mounted 4" by 5" view camera with a special lens arrangement. The camera was mounted to look in the narrow end of the research scale scrubber, so that its view was along the row of spray tubes. Illumination was directed from the opposite end of the electrode. The result was a Schlieren photographic setup, with the droplet images back-lighted. The experimental configuration is shown in Figure 3-2.

Photographs were taken on 5000 speed Polaroid film, with a magnification factor of three. The Polaroid is generally assumed to have a resolution power of about 40 lines per millimeter, so the overall resolution would be about 10 microns in droplet diameter. In practice, nothing under about 60 microns in diameter was seen.

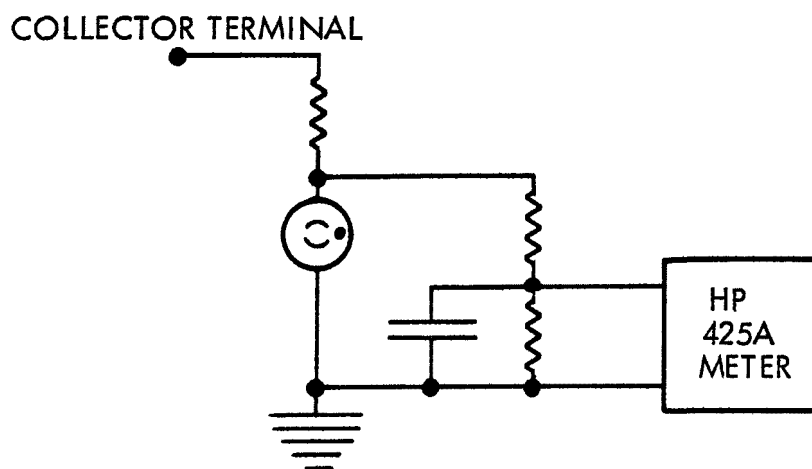


(a) End View Cross Section

Figure 3-1. SEGMENTED CURRENT COLLECTOR
Used to monitor axial current distribution in research scrubber



(b) Side View. Showing collector electrode plates



(c) Current Monitor Circuit

Figure 3-1. SEGMENTED CURRENT COLLECTOR (Continued)
Used to monitor axial current distribution in research scrubber

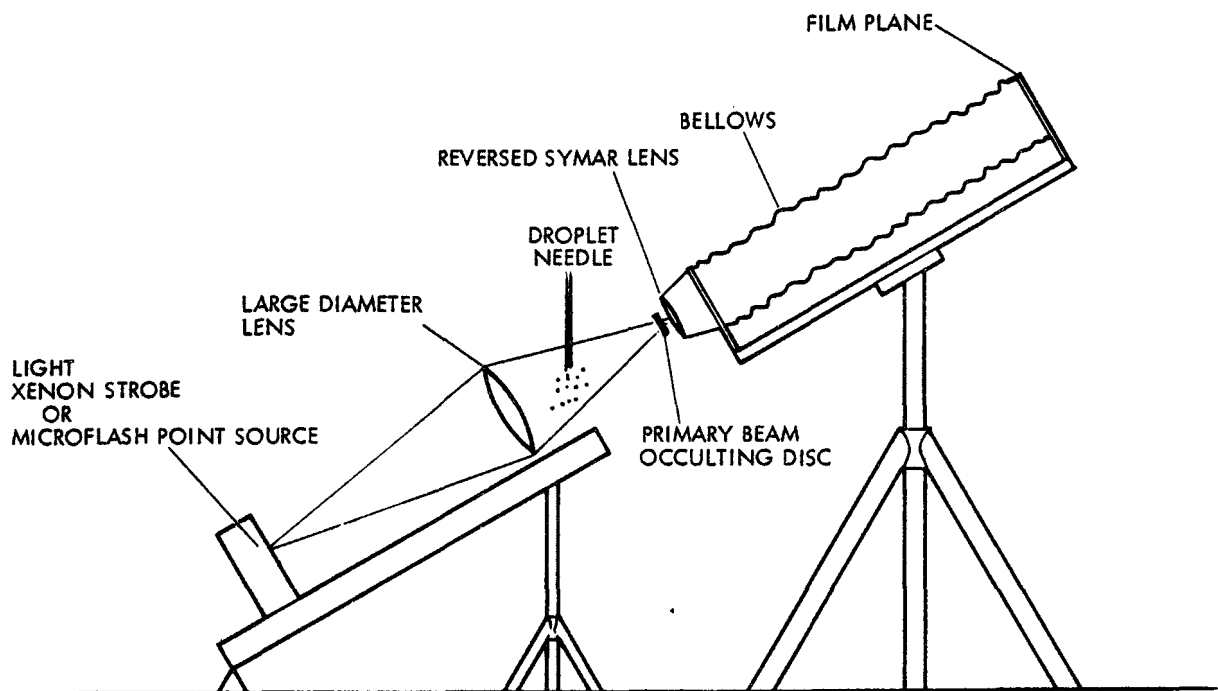


Figure 3-2. MODIFIED SCHLIEREN PHOTO SETUP USED FOR HIGH SPEED PHOTOGRAPHY OF DROPLET FORMATION

Illumination was accomplished with a flash lamp which could be either strobe driven or singly fired. The length of the flash pulse was adjustable between a millisecond and a microsecond. In practice, the exposure time could not have been over a few microseconds. This is based on the fact that no velocity blurring was ever observed, and that the expected droplet velocities within the exposure volume were much greater than would be necessary to cause blurring for the longer time intervals.

A reversed Symar lens was used with the camera. An occulting disc intercepted the primary beam between the flashlamp and the camera. The camera was set at $f/8$ with a 370 mm aperture. The camera objective was about 54 cm from the spray tube tip being photographed. The depth-of-field of the camera lens under these conditions was calculated to be 1.25 cm.

Most of the pictures were focussed on the closest spray tube of the five-tube array. Several photographs were taken of the second spray tube in. These were used to verify that the droplet size and number density distributions were virtually the same in either case. The main end effect is a distortion of current density and droplet trajectories.

3.3 LASER VELOCIMETER

A laser velocimeter experiment similar to one described by Farmer¹⁶ was assembled to measure droplet velocities and direction of motion between the scrubber electrodes. A schematic of the experiment is shown in Figure 3-3. Light from a helium-neon laser is first passed through a beam splitter, producing two orthogonal light beams of nearly equal intensity. One beam, parallel to the original, is allowed to pass into the test region. The second beam is deflected with a mirror so that it crosses the first beam. An interference fringe pattern is established in the region where the beams cross. The pattern consists of parallel planar regions of constructive or destructing light interference.

As a droplet passes through the fringe pattern, light is scattered from the droplet as it enters each reinforced light fringe. The frequency of the scattered light, i.e., the rate at which the fringes are being passed, is proportional to the droplet velocity. The fringe planes were normally parallel to the collector wall, and could be rotated along an axis in the horizontal, parallel to the collector. The rotation was accomplished by rotating the laser, beam splitter and converging mirror about the axis of the laser beam. This rotation allowed for measurement of the droplet direction in a vertical plane normal to the collector.

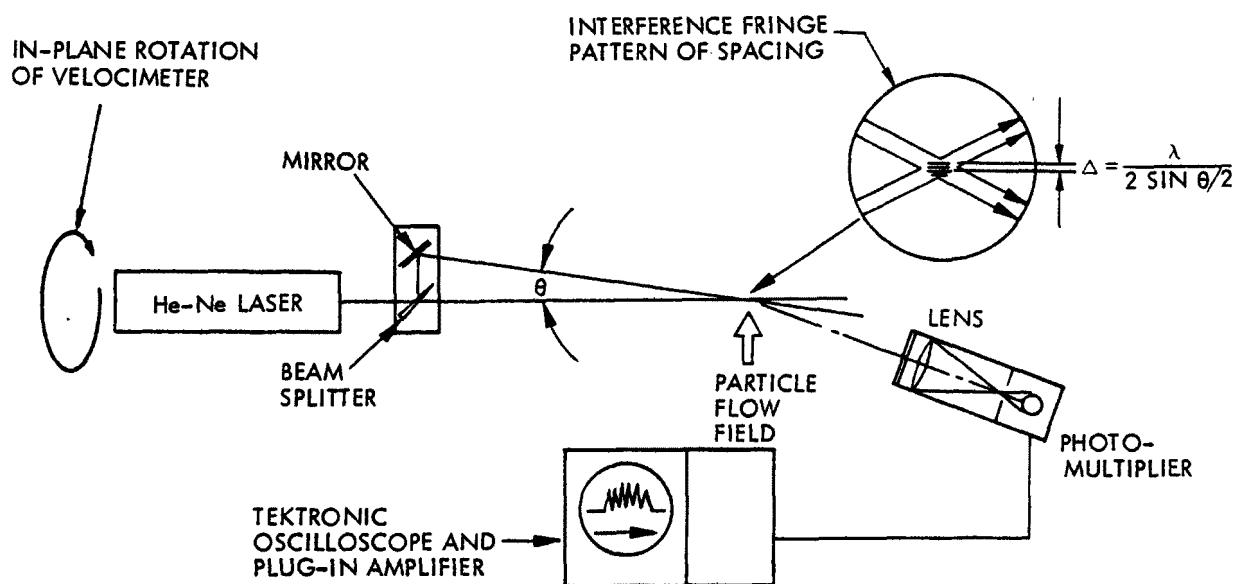


Figure 3-3. SCHEMATIC DIAGRAM OF LASER VELOCIMETER EXPERIMENT. The velocimeter may be rotated around the axis of the laser

The laser used in the experiment was a 15 milliwatt output Spectra-Physics 124A helium-neon laser with a wavelength of 6328 Angstroms. The angle of convergence of the split beam was 0.8953 degrees. From the relationship:

$$\Delta = \frac{\lambda}{2\sin(\theta/2)} \quad (3-1)$$

where Δ = fringe spacing
 λ = laser wavelength
 θ = convergence angle of the beam

the fringe spacing was 40.5 microns. A photograph of the interference fringe pattern is shown in Figure 3-4. The velocity of a droplet passing normal to the grating is then:

$$U = 4.05 \times 10^{-5} f \text{ (meters/sec)}$$

where f is the frequency of the scattered light intensity signal.

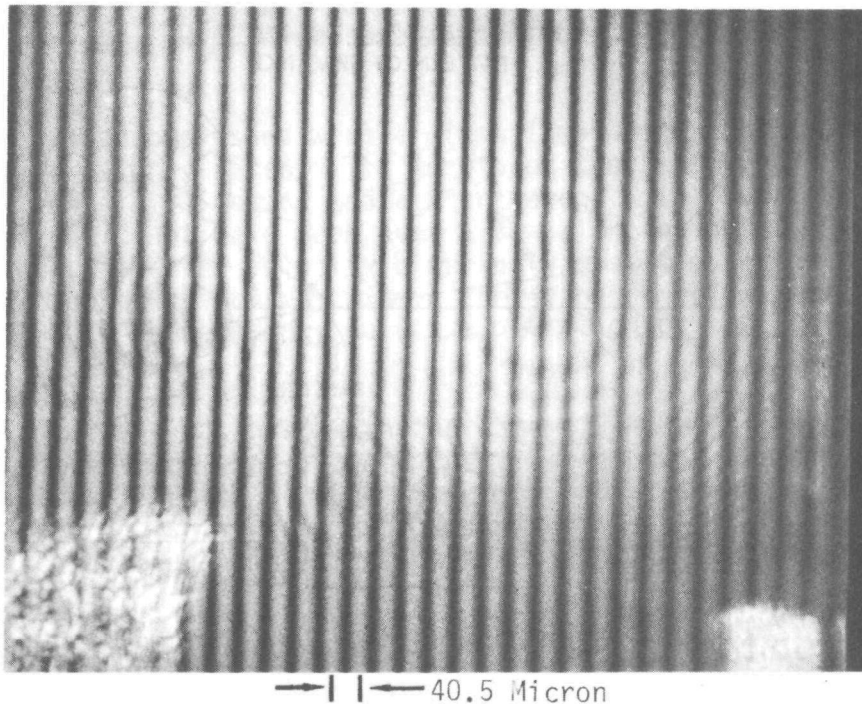


Figure 3-4. INTERFERENCE FRINGE PATTERN

The scattered light was viewed at an angle of approximately 10 degrees from the forward. This allowed for maximum scattered intensity without interference from the direct beam. The light was collected on a 5-inch diameter lense with a 10-inch focal length and focussed on the sensor of an EMI 9558B photomultiplier tube. The output of the tube was recorded on an oscilloscope. A frequency analyzer was used first in the monitoring circuit; however, the droplet flux through the grating was too low to obtain the required event density for the analyzer. The data were recorded by observing individual droplets crossing the grating on a memory scope.

A photograph of the laser velocimeter experiment is shown in Figure 3-5. In order to sample the velocity at various locations in the scrubber, the scrubber was moved relative to the velocimeter assembly. This technique precluded realignment of the optics at each location.

3.4 PARTICULATE REMOVAL EFFICIENCIES

Comprehensive test programs have been conducted to measure scrubbing efficiency of the TRW/CDS on a laboratory and pilot scale, and under controlled conditions and field conditions. Tests have been conducted for both redispersed and newly dispersed aerosols, in many size ranges down to 0.1 micron.

Experimental work on this program was concerned mainly with sub-micron particulate. Particulate removal efficiencies were measured using a zinc oxide fume from the electric arc fume generator. Industrial grade metallic zinc was used for the cathode and the melt. The anode was an electrode from a carbon arc lamp. The fume was white in color, and its deposit was sooty to the touch. Occasionally, when low grade carbon was used at the cathode, the fume would grow black with carbon soot. This was corrected both by obtaining harder carbon rods, and by purging the melt area with gaseous nitrogen. Water cooling was provided for the anode crucible, but was not needed, as ultimately the arc welder current setting provided sufficient temperature control. Some difficulty was experienced with ash build-up around the melt. This was diminished by adding the nitrogen purge.

The fume size was measured by allowing some of the fume to settle gravitationally on glass slides, and then viewing it with a scanning electron microscope. Two samples are shown in Figure 3-6. The size scale indicates a most-probable-value particulate size of about 0.1 micron. The mass-mean diameter will normally be two to three times larger. There is some question as to whether the fume particulate had already agglomerated in transit. Perry's handbook¹⁷ indicates a nominal fume particle size of 0.05 micron for zinc oxide, but this is probably a function of the source. The fume tended to agglomerate somewhat in liquids, as is illustrated in Figure 3-7. The figure also indicates a possible variability in fume size due to poor control of the oxidation process. The two runs presented different appearances in fume color and

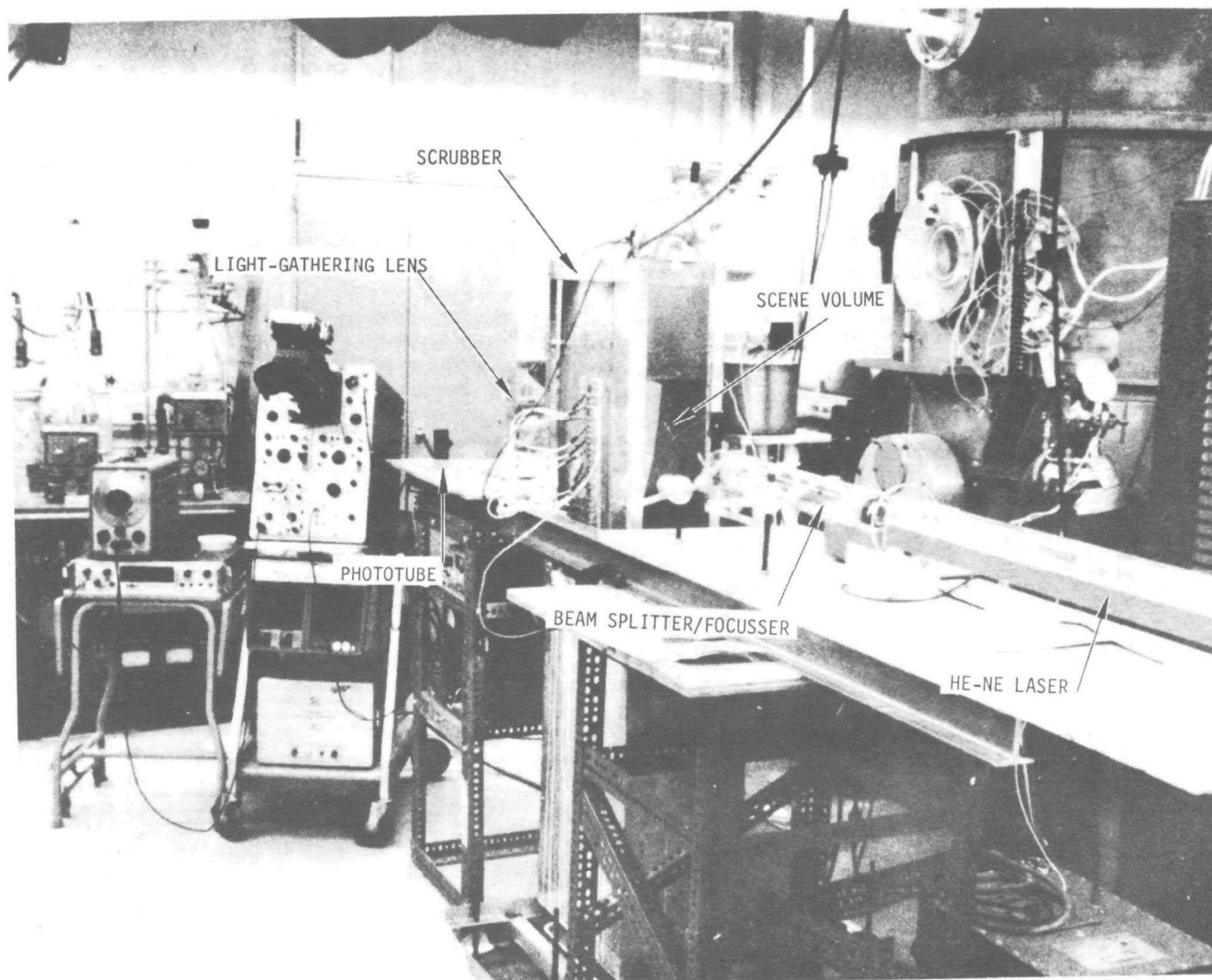


Figure 3-5. LASER VELOCIMETER EXPERIMENT

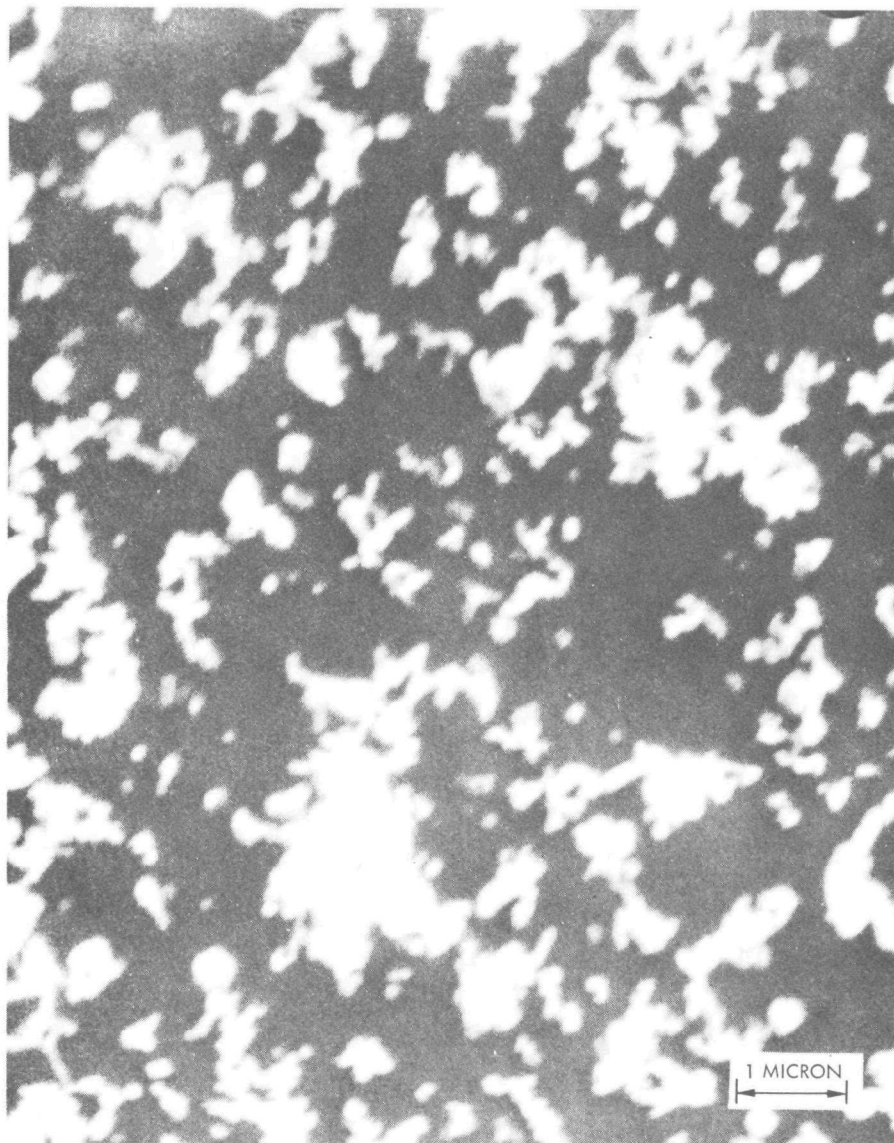


Figure 3-6. ZINC OXIDE PARTICULATE UNDER A
SCANNING ELECTRON MICROSCOPE

a. Sample No. 1; Magnification, 10,000X

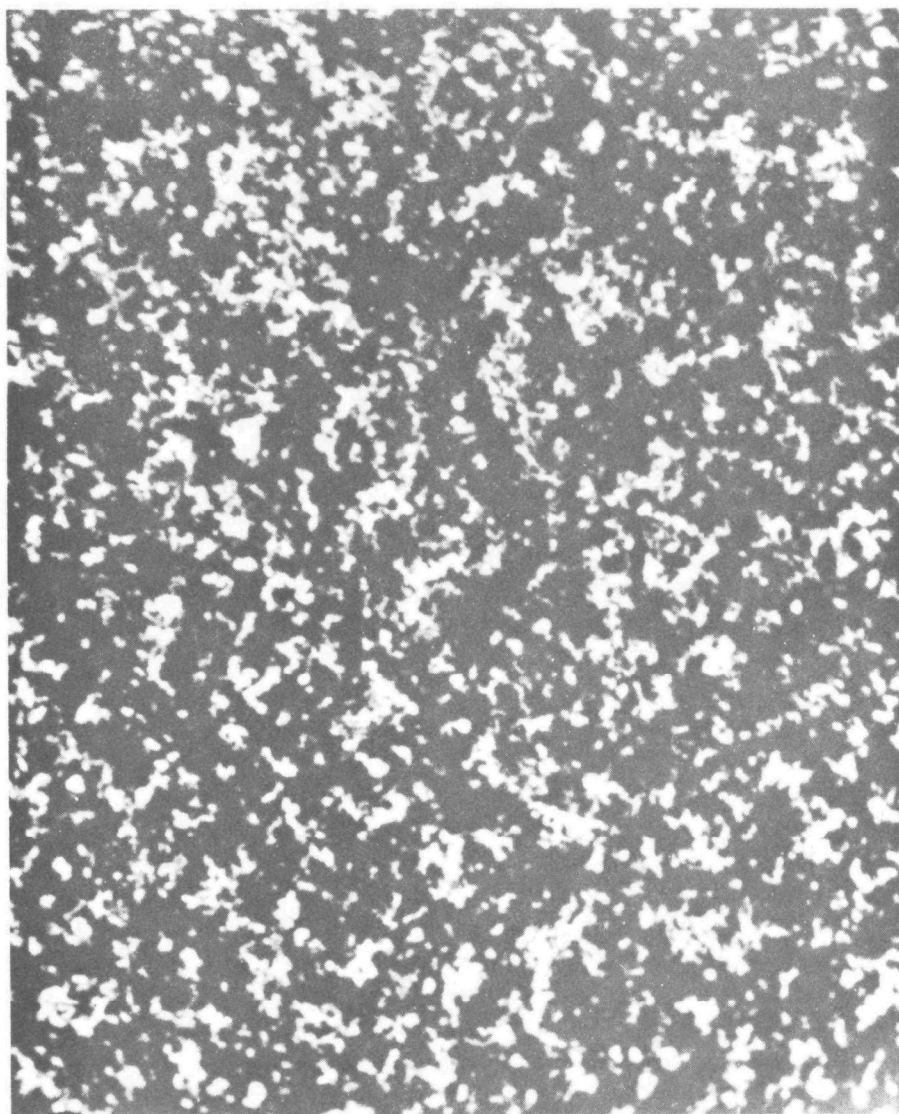


Figure 3-6. ZINC OXIDE PARTICULATE UNDER A
SCANNING ELECTRON MICROSCOPE

b. Sample No. 2; Magnification, 3000X

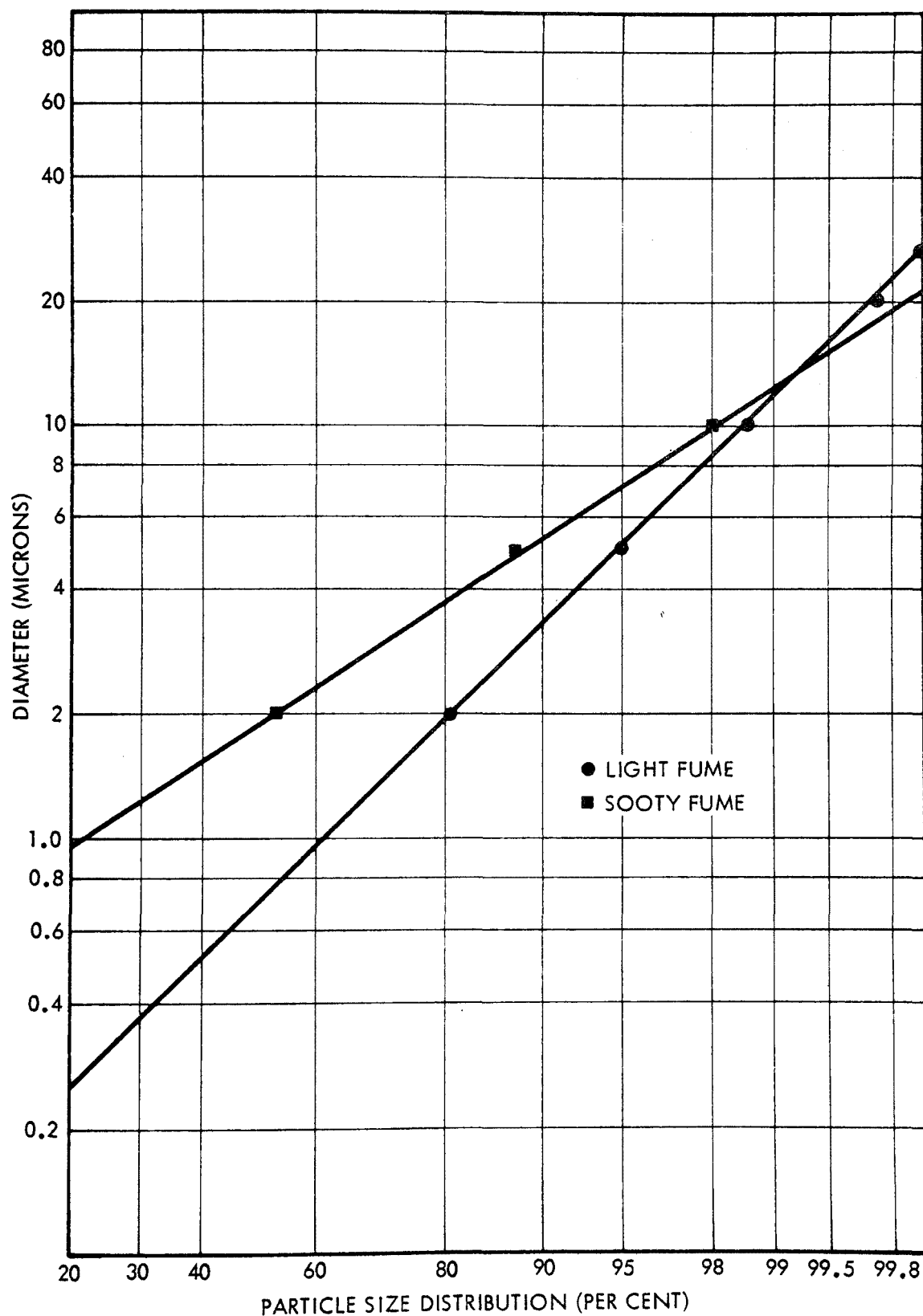


Figure 3-7. DISTRIBUTIONS OF LIGHT AND HEAVY DENSITY ZINC FUME FROM TEST 4/17/74-1

opacity, one being almost pure white and the other being mixed with carbon soot.

Collection efficiency measurements were made by simultaneously sampling the inlet and outlet of the scrubber to determine the average weight or particle number density loading. In most cases, the collected weights were measured directly to obtain total or fractional collection efficiencies. In other cases, a particulate number count was obtained.

Before each sample was collected, the flue outlet velocity was set and measured with a Gelman-Wallace thermo-anemometer. Temperature measurements were made with the same unit, or with a thermocouple wire. Water pressure was set and read at electrode height with a pressure gauge which read 35 inches of water (87 mbar) full scale. The total current to both collecting walls was read, during operation, with a Weston milliammeter of range zero to one amp.

Four sampling methods were used. The first was a pair of Staplex (Model TF1A) high-volume air samplers. Maximum rated flow with these samplers is 70 CFM (120 m³/hr). Their nominal sampling point was at 15 to 20 m³/hr. The sampler inlet duct was 8.25 cm in diameter. The lower sampler had to be equipped for protection from dripping water. Sampling was super-isokinetic, so that the larger portions of the particle size distribution (over about 50 microns) escaped. Flow rate was read directly from the sampler flow meter, and averaged over the sampling time to get total sample volume. The filters were 10 cm diameter fiber filters, staplex type TFA #41, with good capture efficiency claimed down to 0.01 micron. Filter weights were corrected for ambient humidity by noting the weight increment on a standard control filter. The average filter weight was 0.675 gm. Weight measurements were made on a Mettler balance, Model BH26, with an accuracy of 0.1 milligram.

A second series of filter tests was run using an aerosol open-type sampler in conjunction with a Gelman Accupore filter of 47 mm diameter and 0.2 micron nominal pore size. The filters were Teflon. Each sampler was used in conjunction with a dry gas meter and an aspirator vacuum pump. The sampler inlet openings were calibrated for 10 liter/min flow rate. They were also operated slightly super-isokinetically. Typical sample volumes drawn were in the range of 0.04 to 0.06 cubic meters. After the test was complete, the test filters were washed in clean water. The particulate suspension thus obtained was run through a Royco size analyzer with five size classifications; less than 2, 2-5, 5-15, 15-25 and 25-50 microns. After counting, the sample was re-filtered, dried and weighed.

A third method used was a Dreshal type impinger bottle, using isopropyl alcohol for a washing liquid. Again, samples were taken both at the inlet and the outlet of the scrubber. The impinger bottle had a 30 cm long tube with a 2.5 mm diameter nozzle placed 4 mm from the bottom of the bottle. This gives a high velocity impingement in order to create

more complete washing effects. The impinger fluid volume was 275 ml. The gas volume rate was adjusted to obtain near-isokinetic sampling conditions.

The dust sample thus entrained in the isopropyl alcohol was given a Royco particle size analysis as described before. The particle size distribution in isopropyl alcohol showed no appreciable change from that measured in water.

The fourth method used to obtain fractional efficiency measurements was the use of a pair of Andersen stack sampling trains. These are eight-stage aerodynamic particle size samplers, each equipped with an MSA fiberglass back-up filter, type CT-75428. The stages were run bare, with no overlays. Both units were operated isokinetically within about 10 percent.

Three tests were conducted representing three different module operating conditions. A preliminary velocity and temperature traverse was made to select a point of ideal velocity for sampling. The sampling time for each run was 30 minutes. Each sampler was opened and inspected at the end of each run to assure that enough, but not too much, material had been collected. A dry gas meter and a vacuum pump were used to draw the gas sample through the Andersen sampler.

The final and initial weights of each plate and filter were recorded under identical laboratory control conditions.

The inlet fume size distribution as measured by the Andersen sampler has been plotted and analyzed. Figure 3-8 shows data for the mass distribution function versus particle diameter. In all three tests, seventy percent or more of the mass resides in particulate of under 0.25 micron diameter. The figure shows a good straight-line fit to the data, indicating that the distribution has a log-normal tail. If the straight-line fit is extrapolated to smaller diameters, however, it indicates a fifty-percent-mass-diameter of about 0.04 micron, and a corresponding number density diameter of less than the size of a molecule.

As noted in the discussion of Figure 3-6, a microscopic examination of the fume indicates a most-probable particle diameter of around 0.1 micron, by visual estimate, with very little distributed below that size. The inference to be drawn from these facts is that while the distribution has a logarithmic tail, it is actually non-logarithmic and must extrapolate somewhat as shown by the hypothetical dashed line portion of the curve in Figure 3-8. If the shape of the extrapolation is correct, then the small-diameter portion of the distribution can be characterized as highly monodisperse.

There are a number of physical models which would possibly explain this type of behavior. One of them, which is consistent both with the Andersen data and the microscope data, is that there really is in-stream agglomeration taking place, but it is incomplete. The fume initially forms as single crystals which are fairly uniform in size, and grows to about 0.1 micron before the growth reaction stops. By attraction and collision, these tend then to agglomerate while still in-stream. The agglomerate thus formed is the large-diameter log-normal portion of the distribution.

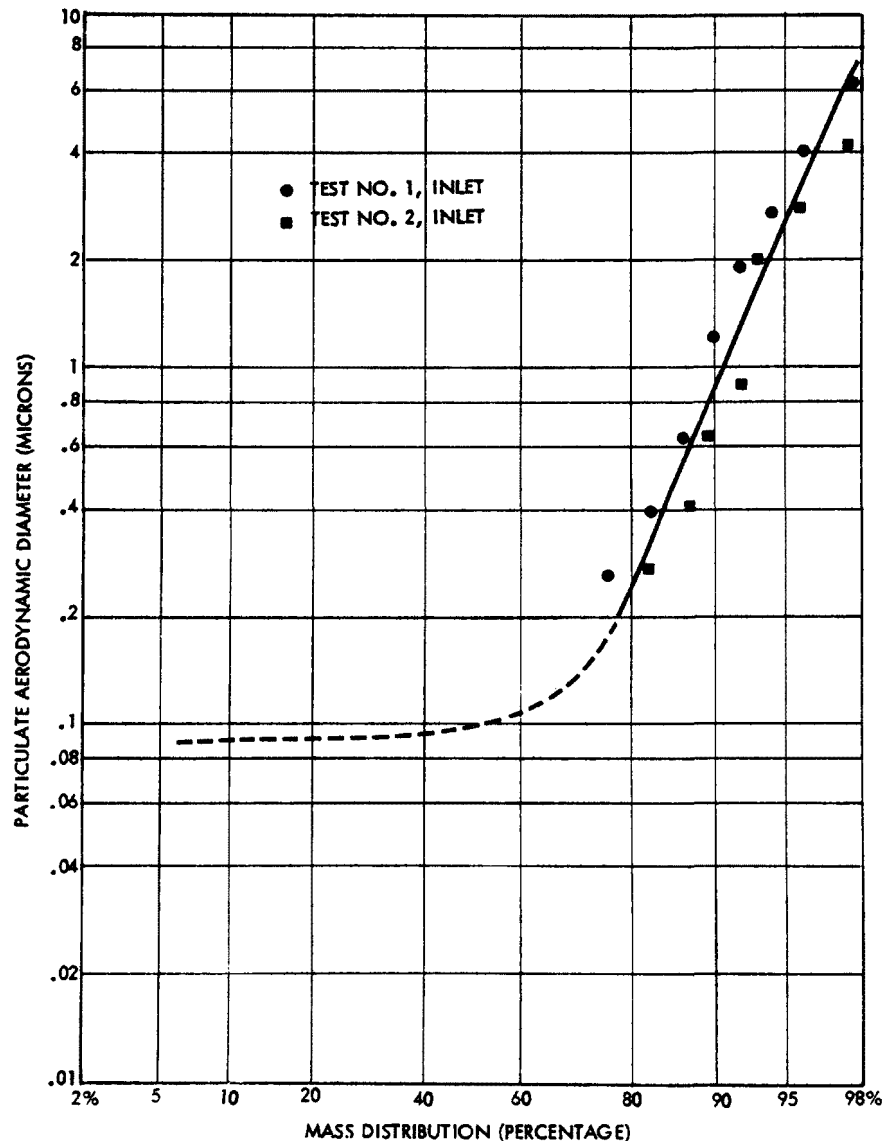


Figure 3-8. DATA-FITTED AND HYPOTHETICAL FUME MASS DISTRIBUTION FUNCTION FROM ANDERSEN SAMPLER DATA

4. RESULTS

There are three significant results of this program which need highlighting. The first of these is an increased knowledge of basic mechanisms and processes in charged droplet scrubbing, and of the parameters that govern them. Second is a better understanding of droplet formation processes and of the physical state of droplets in a CDS, which come out of the research scale work. Third is the more specific fact that the actual scrubbing efficiency, as measured during the bench scale work, is somewhat better than that predicted by the theory of charged droplet scrubbing alone. This will be elaborated in the following Section 4.4 on scrubber performance.

The first three subsections to follow deal specifically with results from the three program phases defined in Section 2; namely, the basic mechanism studies, the research scale experiments and the bench scale experiments. Finally, in Section 4.5, performance comparisons will be made between the TRW/CDS and various other types of control equipment, including conventional electrostatic precipitators and electrical agglomerators.

4.1 BASIC MECHANISM STUDIES

4.1.1 Droplet Charging

The droplets in the Charged Droplet Scrubber (CDS) are formed by electrohydrodynamic spraying. With this method of droplet formation, a high electrostatic field is required at the water spray tube tip. This high field exerts a force on the water issuing from the spray tube and pulls it into long streamers or liquid columns. As water flows into a column from the spray tube and the column increases in length, new surface area is created. Electrostatic field lines terminate on the streamer, inducing a surface charge on the liquid. The rate of formation of new surface multiplied by the surface charge density is then proportional to the current flowing in the liquid column. This is also proportional to the droplet current from the flow tube.

The electrostatic field acting on the liquid column is distorted due to the presence of streamers and droplets issuing from the spray tube. The distortion causes the streamers to vary their direction of motion, thus forming bends in the liquid column. These bends form regions of surface field enhancement. The streamer will "kink" at these points, and the Rayleigh limit for the liquid is exceeded. A section of the liquid column will then break free. This free column is highly charged and will start to pinch, or kink, at regular intervals throughout most of its length. As the pinched sections form, the force increases and causes a catastrophic decrease in local column diameter. The liquid column will then break into a series of small sections which assume the spherical droplet shape. The presence of the severed column and

resulting droplets alters the local field. This causes the liquid column attached to the spray tube to move off in a different direction. This sequence of events can be seen in the droplet photographs shown in Section 4.2.

The size of the droplets formed by electrohydrodynamic spraying, in the absence of forces other than electrostatic, is determined from the size of the liquid streamers issuing from the spray tube. The size of the liquid column comprising a streamer is a function of:

- Spray tube size
- Local field
- Liquid flow rate
- Liquid surface tension
- Liquid resistivity
- Liquid viscosity
- Liquid density

The diameter of the spray tube determines both the magnitude of the electrostatic field near the liquid column and the diameter of the liquid column base. As the column is accelerated under the influence of the local field, the rate at which the column is elongated depends on the strength of the local field. The liquid flow rate will influence the diameter of the liquid streamer as it is elongated at a constant rate.

The other parameters determining the streamer size are properties of the liquid. The surface tension of the liquid determines the rate at which new surface can be created with the available electrostatic field distribution. The liquid resistivity determines the voltage drop along the liquid column while new surface is being created and charged. This voltage drop will influence the charge density, and consequently the electrostatic force extending the liquid column.

The viscosity and density of the liquid determine the viscous and inertial forces resisting the extension of the liquid column.

Once the column has formed and separated from the spray tube, it will separate into droplets. The nominal size of the droplet formed is a function of the column diameter and can be determined from the Rayleigh criterion for liquid column instability. This criterion indicates that the nominal length that a column fragments into is 4.508 times its diameter. The droplet diameter will, therefore, be 1.891 times the liquid column diameter.

If it is assumed that charge is conserved, then the surface charge on each column fragment will become the surface charge on each spherical droplet. The maximum surface charge on the column can be determined from the corona breakdown strength of a cylindrical electrode in the gas medium.

Peek¹⁵ has derived an empirical expression for the enhancement of the corona breakdown field on a regularly curved surface. The form of the enhanced breakdown field is

$$E_o = E_b \delta \left[1 + \frac{C_p}{\sqrt{\delta S}} \right] \quad (4-1)$$

where E_b = normal breakdown strength for the medium at standard conditions

= 3×10^6 volts/meter for normal air

δ = gas density relative to standard conditions

S = electrode radius, meter

C_p = an empirical constant, depending on geometry

= $0.0308 \text{ m}^{1/2}$ for cylindrical geometry

= $0.054 \text{ m}^{1/2}$ for spherical geometry

The surface charge density on a liquid column is now given as follows:

$$s = 2\pi S E_o \epsilon_o \quad (4-2)$$

where s = surface charge per unit length

The total charge q on a column fragment of the critical size is:

$$q = 18.03 \pi S^2 E_o \epsilon_o \quad (4-3)$$

This corresponds to a resulting surface charge density, s' , on the spherical droplet of

$$s' = 1.2607 E_o \epsilon_o \quad (4-4)$$

A curve of the surface charge density for columnar formation of droplets, as given by Equations 4-4 and 4-1, is shown in Figure 4-1, as a function of droplet size. The droplet is water and the surrounding

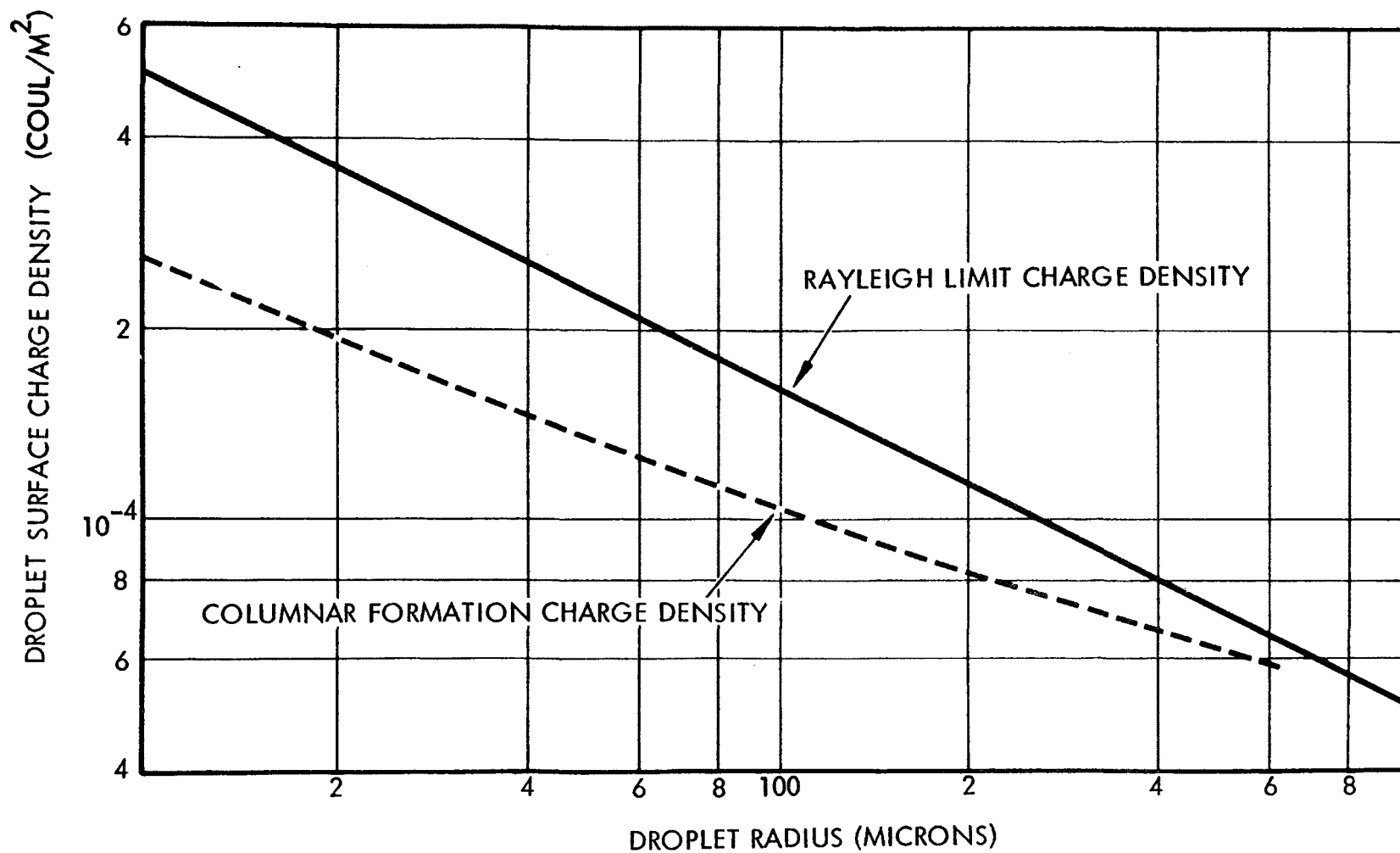


Figure 4-1. LIMITS OF SURFACE CHARGE DENSITIES ON WATER DROPLETS (RAYLEIGH LIMIT) AND COLUMNAR SEGMENTS OF WATER

medium is air at standard conditions.

Another interesting feature of droplets formed in an ambient gas environment is the actual surface field that they can sustain. The Rayleigh limit surface field that can be sustained on a spherical droplet can be expressed as:

$$E'_0 = 2 \left(\frac{\sigma}{S\epsilon_0} \right)^{1/2} \quad (4-5)$$

where E'_0 = surface electrostatic field
 σ = liquid surface tension
 ϵ_0 = permittivity of the surrounding medium
 S = droplet radius

Equation 4-5 can be easily derived from consideration of a critical balance between surface tension forces and electrostatic forces at the droplet surface. The droplet surface charge density resulting in the Rayleigh limit field is also shown in Figure 4-1. These data indicate that the droplets are charged to a value below their Rayleigh limit at formation. The droplets will approach the Rayleigh limit as they evaporate. The fact that droplets are formed with surface charge densities just below the Rayleigh limit would account for the droplet size stability noted in the CDS.

The surface electrostatic field on a droplet that is charged to the Rayleigh limit is large, as can be seen in Figure 4-2. The range of values for the surface field is considerably in excess of that for planar breakdown in normal air (3×10^6 volts/meter). The breakdown field in air is, as shown by Equation 4-1, a function of the source geometry as demonstrated by Peek.

Curves of the surface breakdown field for the spherical geometry case for several values of δ are also shown in Figure 4-2. As can be seen in the figure, the surface field on a water droplet charged to the Rayleigh limit will exceed the Peek's corrected corona field in air at normal density at radii below approximately 34 microns. This would indicate that once a droplet reached this radius, excess surface charge due to a reduction in droplet size would be lost by a corona process. The surface charge density on the droplet would be maintained at a level below the Rayleigh limit. Therefore, an evaporating droplet whose size is below the cross over point of the Peek's field and the

NOTES:
 --- BREAK DOWN FIELD IN AIR ON A SPHERICAL ELECTRODE
 RAYLEIGH LIMIT SURFACE FIELD ON A WATER DROPLET
 $\delta = (\text{AIR DENSITY}) \div (\text{AIR DENSITY AT 1 ATM AND 298°K})$

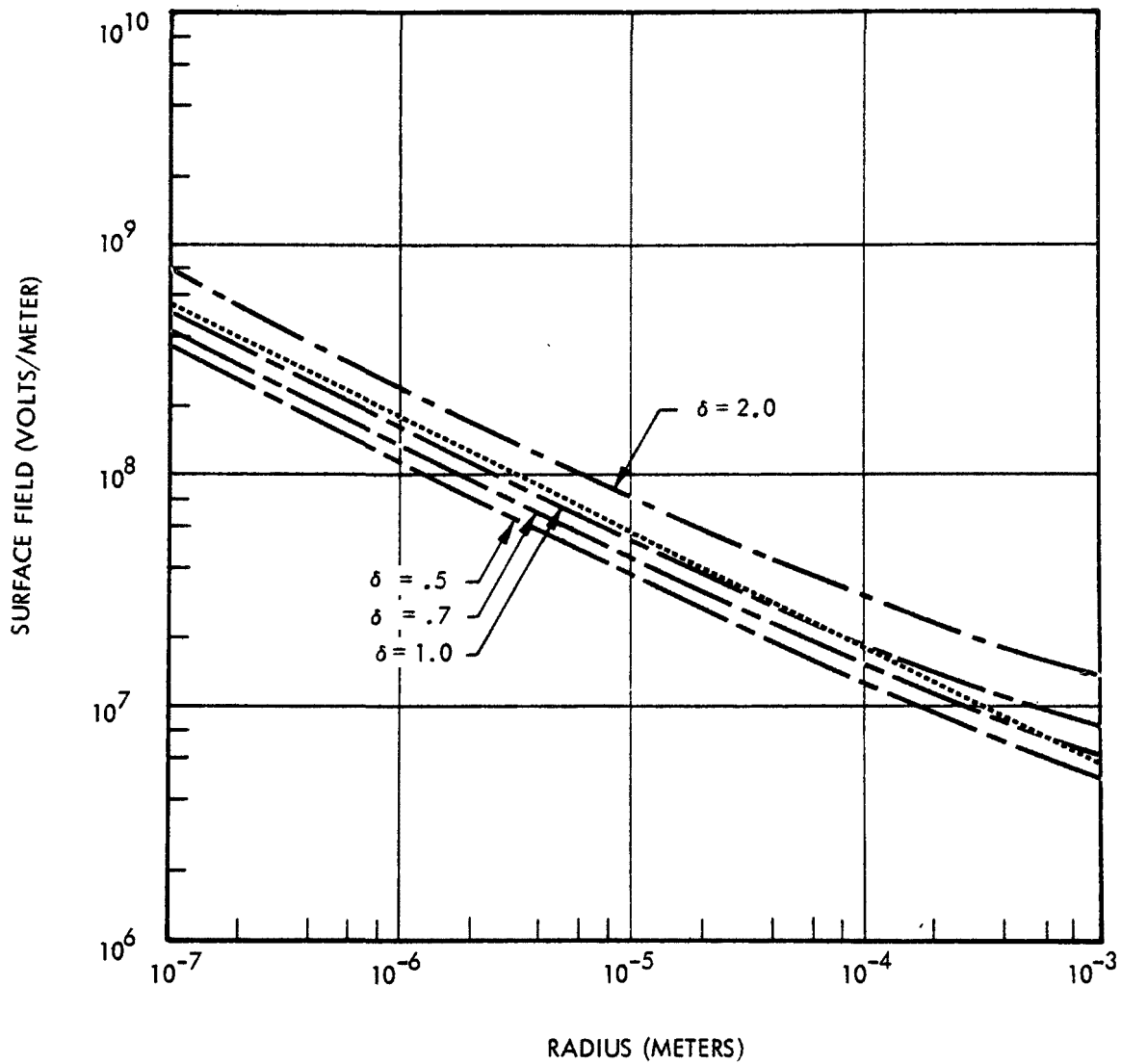


Figure 4-2. SURFACE FIELD LIMITS

Rayleigh limit should not fragment and would lose charge by corona. These results indicate that water droplets formed in the range of 34 to 60 microns radius would break apart, at most only once during their lifetime.

An experiment was performed to determine the applicability of Peek's correction to charged particles in the size range of interest. Cylindrical geometry was used in which the central electrode was 38 microns in diameter. The breakdown field corresponded to a value of C of 0.031 which appears to verify the validity of the Peek's correction.

As a droplet loses mass by evaporation, the surface charge will concentrate, and the surface field increases until it reaches a limiting value shown in Figure 4-2. The surface field goes as

$$E_0 \sim S^{-2} \quad (4-6)$$

where S is the decreasing droplet radius. The evaporation paths defined by Equation 4-6 will form straight lines in Figure 4-2, with slope of negative two.

4.1.2 Droplet Evaporation

The lifetime of a droplet is an important parameter for determining its effectiveness for particulate removal. In most particle removal applications, the medium surrounding the droplets and particles will be sub-saturated or only slightly super-saturated with the vapor phase condensate from which the droplets are formed. The droplets, by virtue of their radius of curvature and charge, will exert a vapor pressure equal to or in excess of the normal condensate vapor pressure. Therefore, under most conditions evaporation of the droplets will occur. The droplet will diminish in size until it becomes either one or a series of singly charged clusters of condensate molecules. These clusters will behave as ions generated in a corona with the ambient gas having a comparable concentration of condensate.

The vapor pressure exerted by a droplet, from Reference¹⁸ is:

$$\ln P_D/P_V = \frac{m_c}{\rho_c kT} \left[\frac{2\sigma}{S} - \frac{(Ne)^2}{32\pi^2 S^4 \epsilon_0} \left(1 - \frac{1}{\epsilon} \right) \right] \quad (4-7)$$

where P_D = vapor pressure of the droplet
 P_V = normal saturated vapor pressure of the condensate
 m_C = condensate molecular mass
 ρ_C = liquid phase condensate density
 T = absolute temperature
 k = Boltzmann constant
 σ = surface tension
 e = electronic charge
 N = number of charges on a droplet
 S = droplet radius
 ϵ_0 = permittivity of the ambient gas
 ϵ = dielectric constant of the condensate

The first term in the bracket of Equation (4-7) is the pressure correction term due to the radius of curvature of the droplet and is a function of the droplet radius and surface tension of the droplet material. The second term in the bracket results from the electrostatic repulsion forces originating from the surface charge on a droplet. The Rayleigh limit of a charged droplet is reached when these two terms are equal.

The rate at which a charged droplet decreases in size will depend on the manner in which the droplet breaks up when the Rayleigh limit is reached and exceeded. The easiest case to analyze and the one that will result in the longest droplet lifetime is that in which the excess charge on an evaporating droplet is lost in a continuous manner and each lost charge is attached to a small cluster of condensate molecules. In this case, the vapor pressure exerted by the droplet will be essentially constant and equal to the condensate vapor pressure. The degree of saturation of the gas stream relative to that of the droplet is then:

$$R' = P_C/P_V \quad (4-8)$$

where P_C = condensate pressure in the gas stream.

The term, R' , is the relative humidity of the gas stream for the conditions assumed.

With the assumption of continuous charge removal¹⁹, the rate of decrease in the size of a droplet can be approximated by

$$\frac{SdS}{dt} = \frac{D\delta_c}{\rho_c C_o} \left(\frac{R' - 1}{R'} \right) \quad (4-9)$$

where D = diffusivity of the condensate vapor in the ambient gas

δ_c = condensate saturation vapor density

C_o = correction term for the thermal lag between droplet and gas stream.

The correction term, C_o , can be expressed, in the absence of convection, as:

$$C_o = \left[1 + \frac{DH^2\delta_c}{R_c T^2 K} \right] \quad (4-10)$$

where H = condensate heat of vaporization

R_c = condensate gas constant

K = thermal conductivity of the ambient gas

The absence of convection will result in the longest droplet lifetime.

At constant temperature and relative humidity, the lifetime of a droplet, τ_D , is:

$$\tau_D = \frac{S_o^2 \rho_c C_o R'}{2D\delta_c(1-R')} \quad (4-11)$$

where S_o = initial droplet size

Typical lifetimes of various size water droplets existing in different saturation environments are shown in Figures 4-3 and 4-4. The data in the figures represent the maximum lifetimes for the droplets by virtue of the charge loss mode assumed. The charged droplets, above the size defined in the previous sub-section, will decrease in size by evaporation until the Rayleigh limit is exceeded. When at this condition, the droplets will separate into multi-charged fragments and charged molecular clusters under the action of the Rayleigh instability.

It was assumed in the lifetime analysis that the droplets lose identity when they reach the molecular cluster stage. In the evaporation process, a multi-charged water droplet will be transformed into vapor phase material and hydrated ions. The existence and most probable size of the hydrated ions or charged molecular clusters can be predicted by Equation (4-7). A curve of Equation (4-7) is plotted in Figure 4-5 in the region of droplet radius less than the critical radius for singly charged water droplets. In this region, the pressure ratio of the droplet pressure to normal vapor pressure is an increasing function of droplet radius. The most probable size or number of molecules in an ion cluster that exists in a gas stream can be determined from Figure 4-5 by using the ambient relative humidity as the ordinate. The number of molecules per cluster, shown in the figure, was determined from the equation:

$$N = \frac{4\pi S^3 \delta_c}{3m_c}$$

where N = number of water molecules per cluster

S = cluster radius

m_c = molecular mass of water

δ_c = water density

The number of molecules per cluster at the various relative humidities, determined from the above equation, correspond to the most frequently observed values reported in Reference²⁰.

The analysis indicates that unless the droplets reside in a high relative humidity and/or the droplets are large, there is only a short time period for a direct interaction between a water droplet and a particle. Once the droplet starts to break-up, the major removal mechanism will be the result of particle charging by the relatively low mobility hydrated ions originating from the droplet.

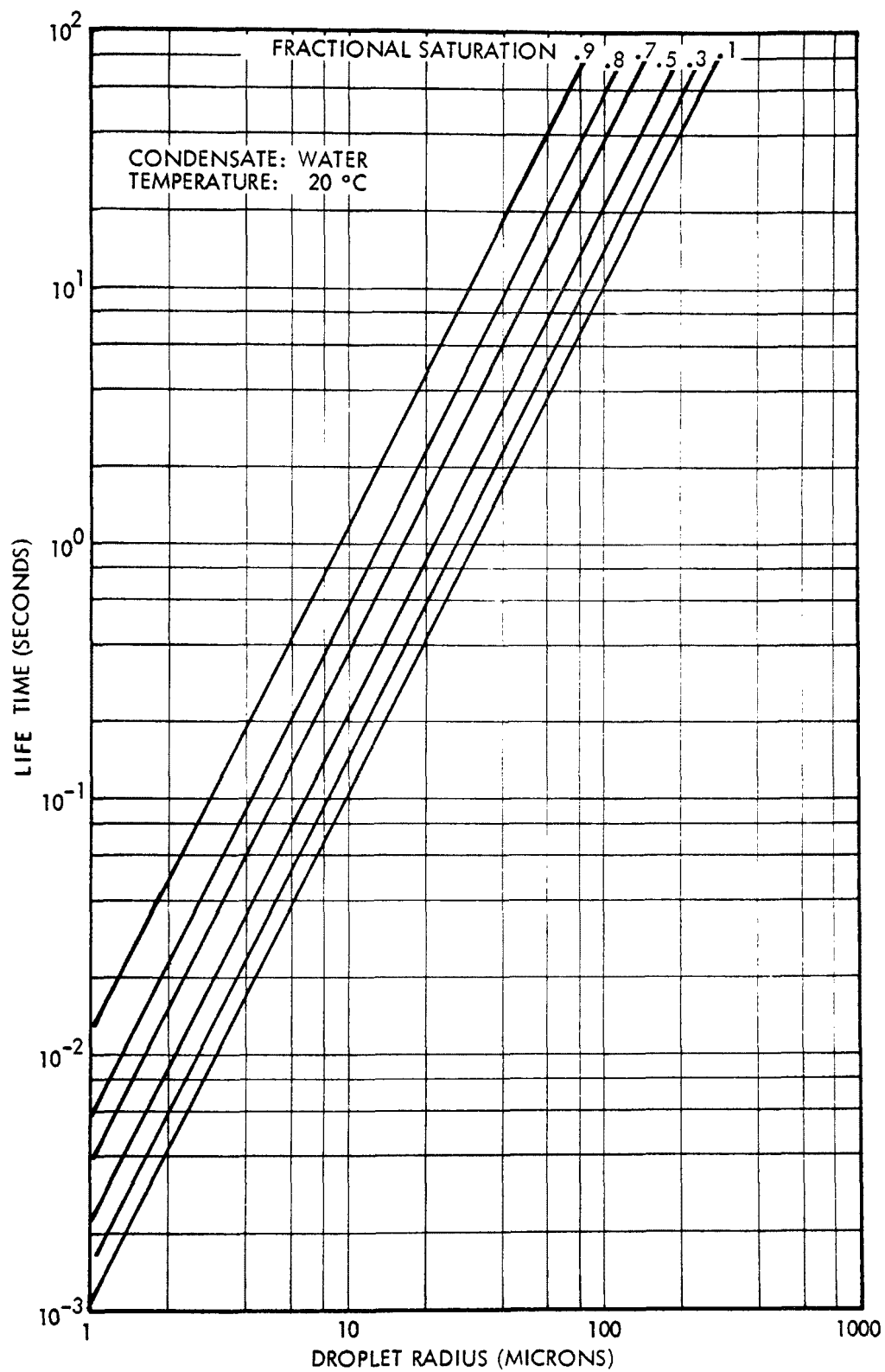


Figure 4-3. WATER DROPLET EVAPORATION LIFETIMES
Temperature of 20°C

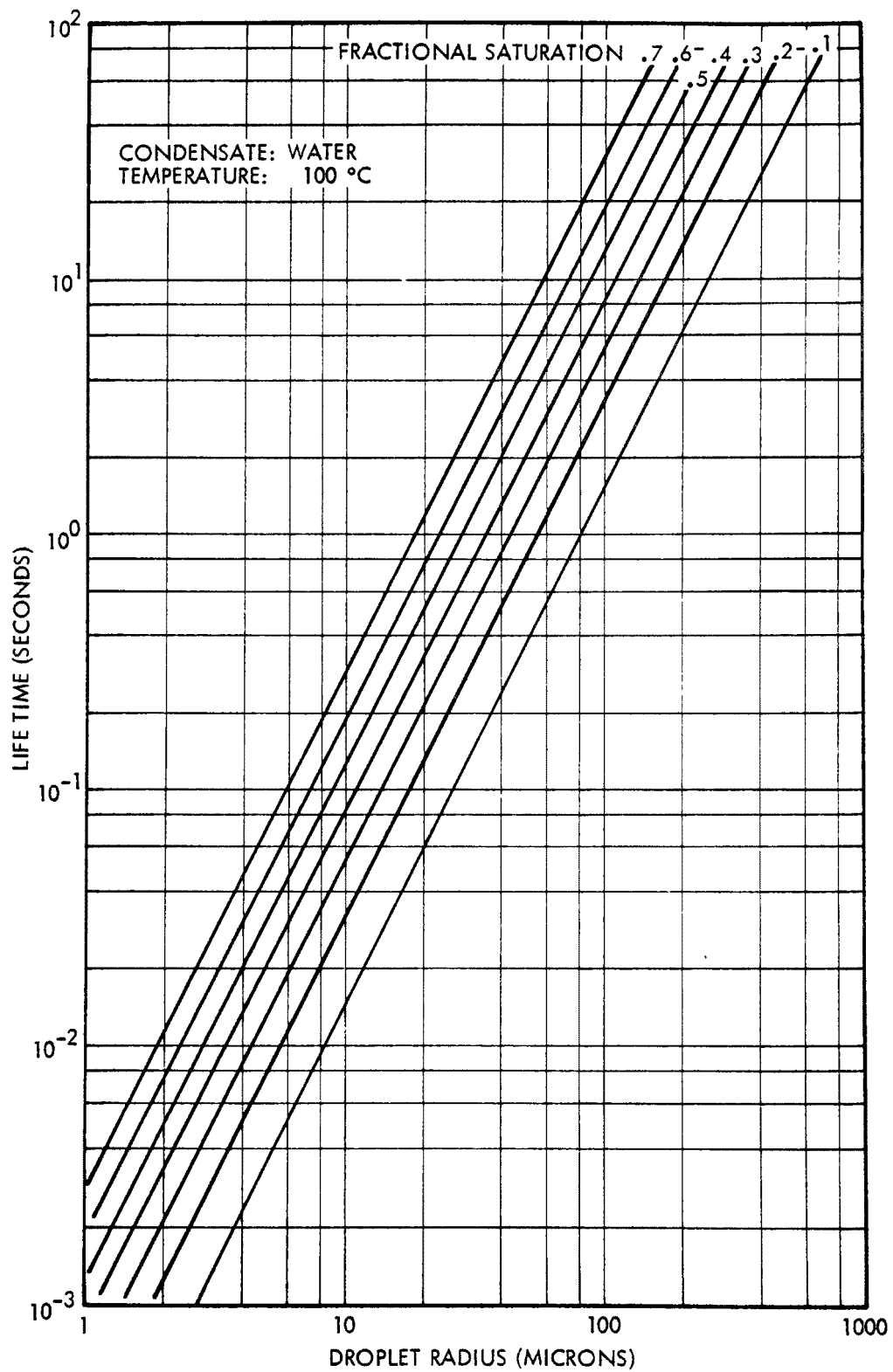


Figure 4-4. WATER DROPLET EVAPORATION LIFETIMES
Temperature of 100°C

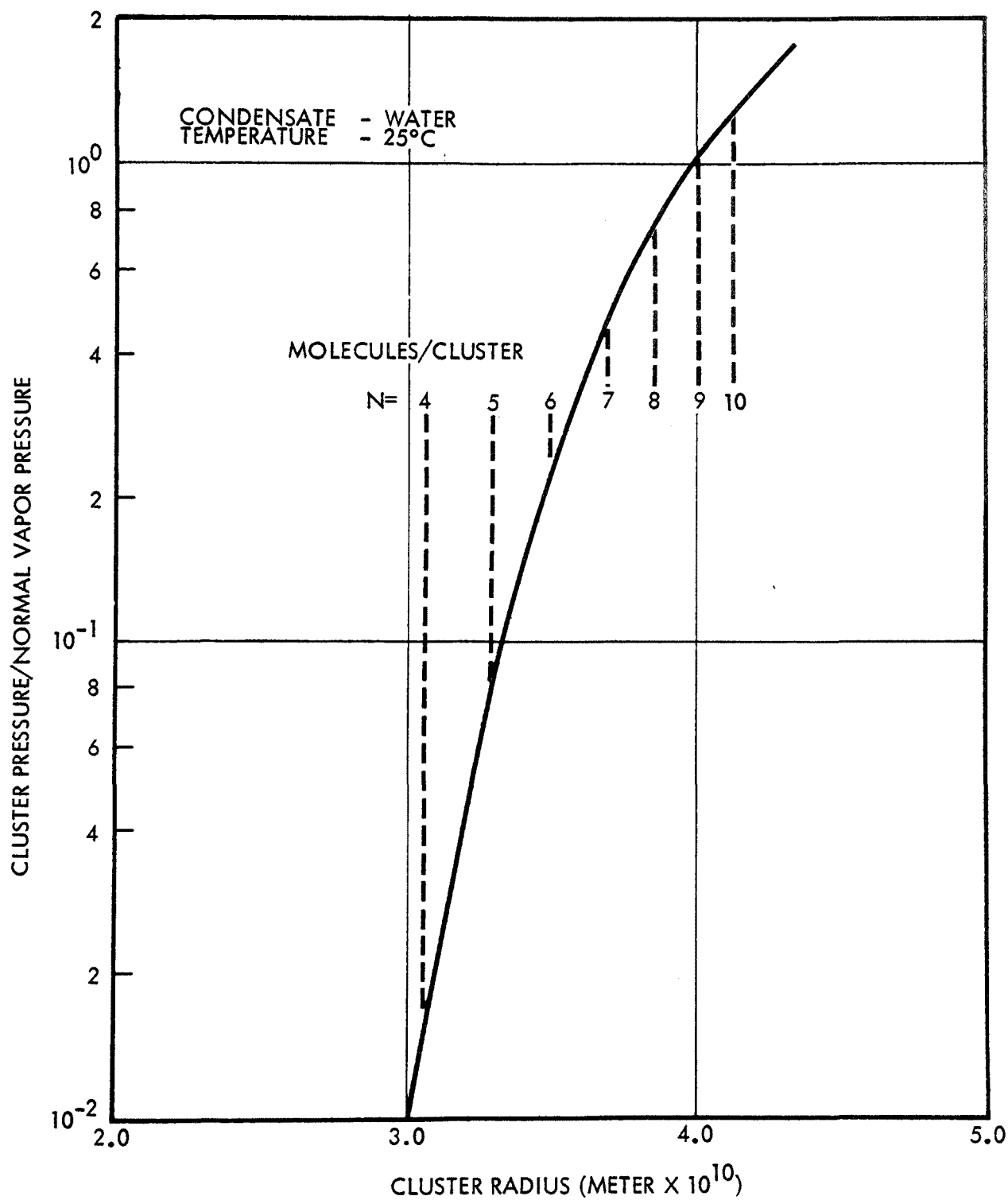


Figure 4-5. VAPOR PRESSURE OF A SINGLY CHARGED DROPLET

Typical droplet velocities in the Charged Droplet Scrubber (CDS) are in the range of 20 to 40 m/sec. The spacing between the spray electrode and collecting electrode is in the range of 0.05 to 0.1 meter. Therefore, typical transient time for droplets in the CDS are in the range of 1.2 to 5.0 msec. These times are short relative to the lifetime of droplets in excess of 10 micron radius.

Equation (4-11) can be rewritten to express the size of a droplet as a function of time. The expression is:

$$S = S_0^2 - \frac{2D\delta_c(1-R')t}{\rho_c C_0 R'} \quad (4-12)$$

where S = droplet radius

t = time

The change in mass and surface area of droplets can be determined from this equation. As an example, the fraction mass loss, $\Delta M/M_0$, and the fraction area loss $\Delta A/A_0$, for a typical droplet in the CDS can be determined. Droplets of the following size and in the following environment were considered:

Droplet size, $S_0 = 6 \times 10^{-5}$ microns

Relative humidity, $R' = 0.1$

Temperature = 25°C

Time = 5 msec

they will have a mass loss and area change corresponding to:

$$\Delta M/M_0 = 2.01 \times 10^{-3}$$

$$\Delta A/A_0 = 1.34 \times 10^{-3}$$

At an ambient temperature of 100°C, the corresponding changes are:

$$\Delta M/M_0 = 1.38 \times 10^{-2}$$

$$\Delta A/A_0 = 9.18 \times 10^{-3}$$

These changes in droplet properties are negligible. Although it is statistically possible, the probability of a droplet fragmenting in the CDS is extremely small. There is a high probability in the presence of particles that excess charge on a droplet due to surface area reduction would be lost through ion leakage. In addition, once a droplet collides with a particle its surface area will increase. The actual surface

area of a droplet in the CDS will increase due to multiple collisions during operation.

In space charge type particle removal devices, the drift rate of the droplets is slow and volumes are large. Therefore, there is a high probability that droplets will lose their identity before impinging on a collecting surface. The droplet charge will be transferred to the particles by field and diffusion charging through ions liberated from the droplets.

The reverse process of evaporation is droplet nucleation and condensation. In a supersaturated gas stream, droplet nucleation on charged particulate, and subsequent condensation growth, may be an important collection mechanism. A gas stream may become supersaturated with scrubbing liquor through abrupt changes in flow temperature or pressure.

Equation (4-7) also describes the necessary conditions on condensate vapor pressure to cause condensation growth of droplets. Figure 4-6 is a plot of this equation for a sample temperature-pressure combination, for uncharged and singly charged droplets. The curve shows the depression of droplet vapor pressure by the addition of charge. The curve for $N = 1$ peaks at the critical radius and critical droplet vapor pressure. If the supersaturated condensate vapor pressure is above this value, singly charged nucleation sites will grow from any size.

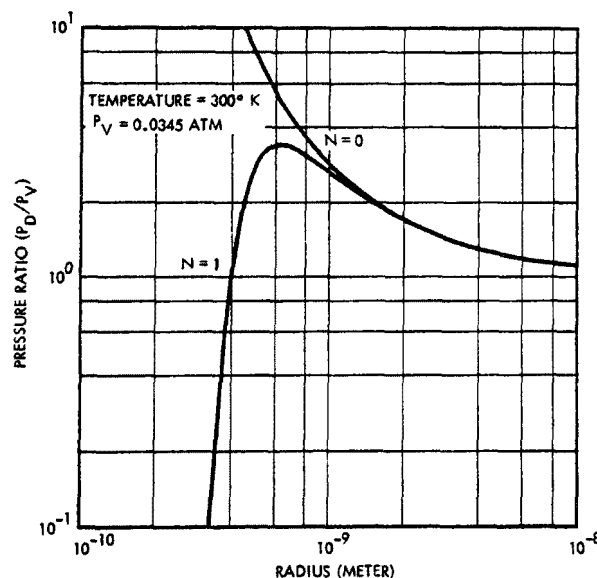


Figure 4-6. WATER DROPLET VAPOR PRESSURE AS GIVEN BY EQUATION 4-7, FOR UNCHARGED AND SINGLY CHARGED DROPLETS

In a supersaturated vapor, molecules of condensate collide often enough to form aggregates. If the vapor pressure is high enough, a sufficient number of these aggregates will reach a critical radius to nucleate spontaneously and without charge. The critical radius is the same for charged and uncharged nucleation, and the spontaneous nucleation pressure is found from the curve for $N = 0$ at the critical radius. As the charge on a nucleation site increases, the critical point moves down and to the right in Figure 4-6. The critical radius is given by

$$S_c^3 = \frac{N^2 e^2}{16\pi^2 \sigma \epsilon_0} \left(1 - \frac{1}{\epsilon}\right)$$

Figure 4-7 shows the variation of water vapor pressure, singly charged site nucleation pressure and spontaneous nucleation pressure as a function of temperature.

4.1.3 Induced Charging

Induced charging, as discussed in Section 1, refers to any mechanism whereby a high enough electric field strength is induced at the surface of a particle or a droplet to cause local electrical breakdown. It is thus a charge transfer mechanism which does not result in agglomeration of droplet and particle. The two induced charging models discussed in Section 1 were for electric breakdown of air at the surface of the particle, and at the surface of the droplet.

Figure 4-8 shows the basic geometry for both models, assuming both droplet and particle are spherical. The equations are written in terms of the particle and droplet radii, and the separation d of the particle center from the droplet surface. The actual surface-to-surface distance, $d-R$, is the active distance of the induced field. The ratio R/d will usually be small enough to neglect, compared to unity.

The first induced charging model to be investigated was that for corona breakdown at the particle surface. The breakdown field strength used was modified with Peek's correction for curvature. The unperturbed field at the droplet surface, E_0 , may then be reduced by the inverse square of the distance. Assuming the particle sees an approximately uniform electric field perturbation from the droplet, the maximum field strength at its surface can be found from the solution of a classical problem in dielectrics²¹. The resulting conditions for induced charging of spherical particulate is as follows:

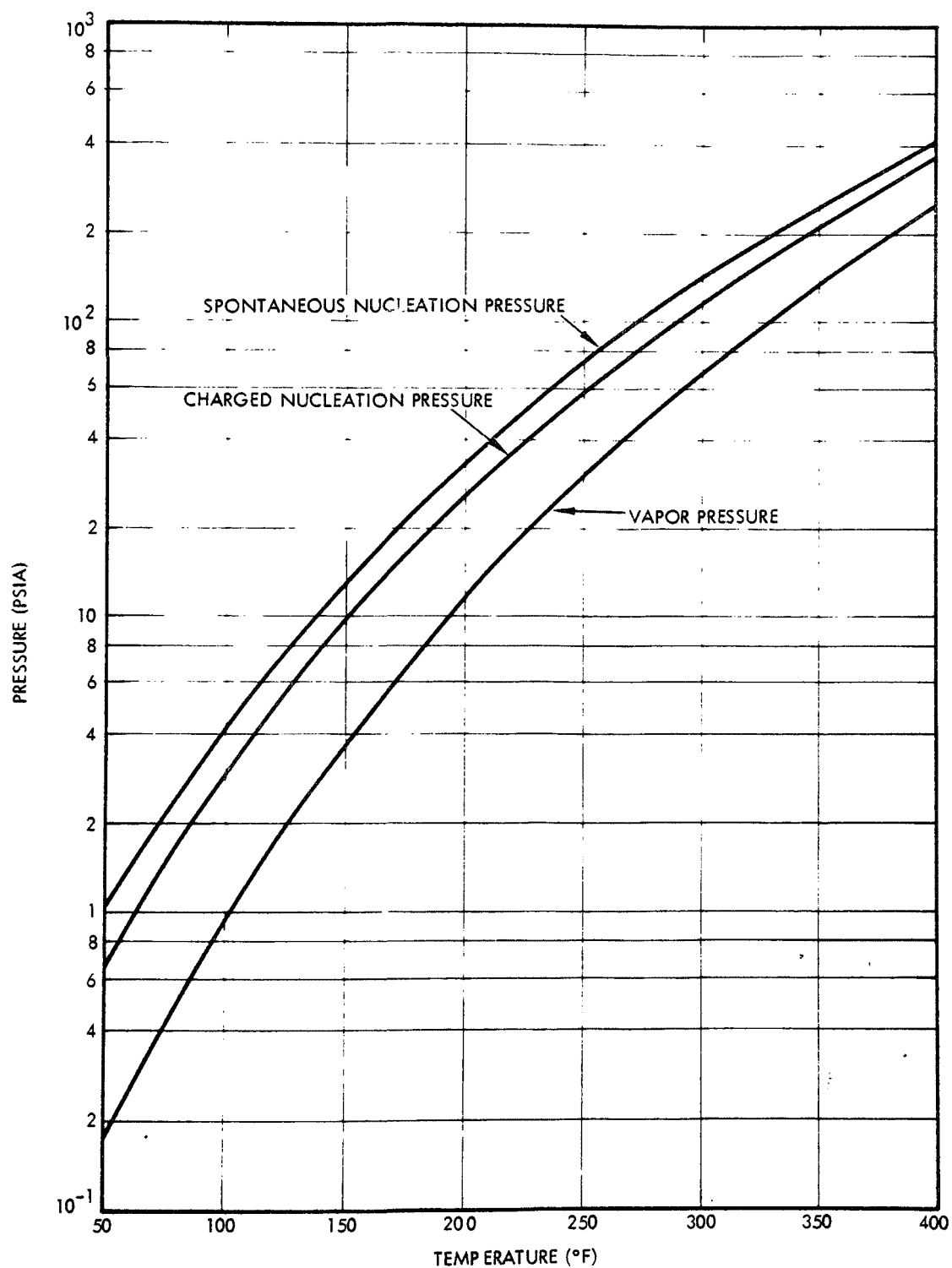


Figure 4-7. TEMPERATURE DEPENDENCE OF NUCLEATION PRESSURES

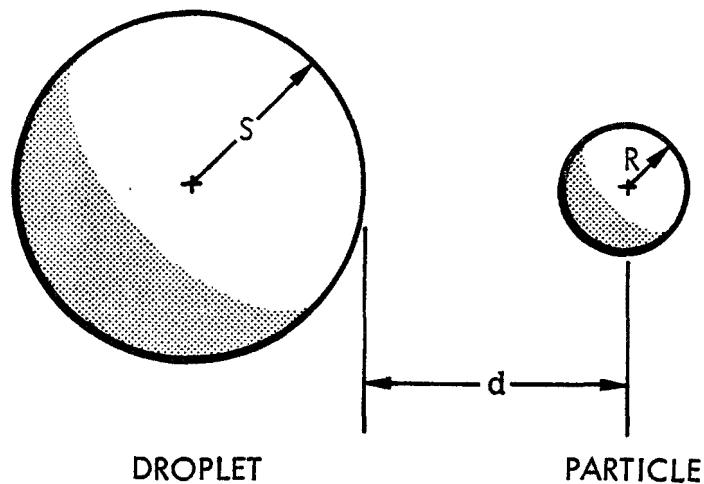


Figure 4-8. INDUCED CHARGING GEOMETRY, SPHERICAL PARTICLE

$$E_{op} = \left(\frac{3\epsilon}{\epsilon+2} \right) E_{oD} \left(\frac{S}{S+d} \right)^2 \geq E_B \left(1 + \frac{C_p}{\sqrt{R}} \right) \quad (4-13)$$

E_{op} = surface field on particle

E_{oD} = surface field droplet

ϵ = dielectric constant of particle material

E_B = breakdown strength of the medium for planar electrodes

C_p = Peek's correction constant,

= $0.054 \text{ m}^{1/2}$ for spherical electrodes

Most particulate will be irregular in shape. Surface irregularities will cause local enhancement of the surface field on a particle, and corona breakdown may occur with a lower ambient field. A field enhancement effect may be derived for a spherical particle containing a spherical protrusion, as shown in Figure 4-9. The enhancement factor is derived from simple potential field considerations. A factor of R/R'

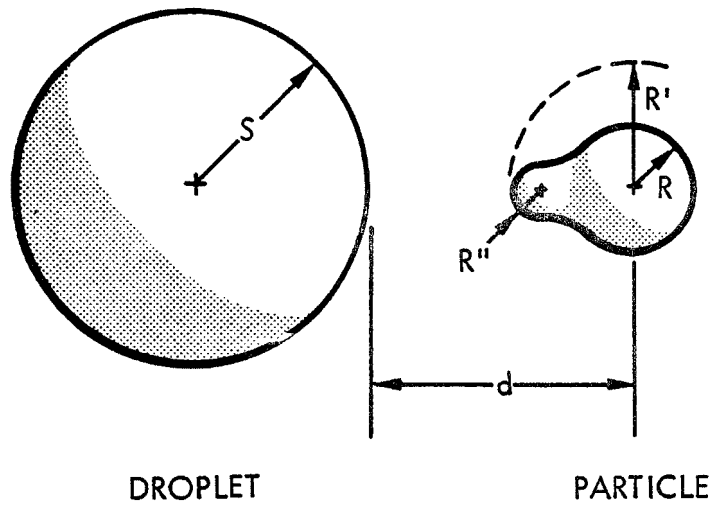


Figure 4-9. INDUCED CHARGING MODEL, SPHERICAL PARTICLE WITH PROTRUSION

accounts for a reduction in average potential from that on the sphere R to the tip of the protrusion. The factor R/R'' gives the field enhancement at the reduced potential due to the increased surface curvature. The equation describing the breakdown limit is then given as:

$$E_{op} = \left(\frac{3\epsilon}{2+\epsilon}\right) E_{oD} \left(\frac{S}{S+d}\right)^2 \frac{R^2}{R'R''} \geq E_B \left(1 + \frac{C_p}{\sqrt{R''}}\right) \quad (4-14)$$

A set of solutions to Equation (4-14) is shown in Figure 4-10. It was assumed in the analysis that the droplet field, E_{oD} , was Rayleigh limited and that the dielectric constant of the particle material, ϵ , was 5.0. For each curve, the region where induced charging occurs is in the area under the curve. The approach distance on the curve is the maximum value of $D-R$ at which charge exchange can occur by this method. The values on the curve to the right of the peak are only approximate because of the deviation from uniform applied field at the particle resulting from geometric effects. The curves will decay to zero at a faster rate in this region if this effect is added.

At the nominal droplet radius of 60 microns, the induced charging effect for spherical particles below one micron in radius does not exist. Experimentally, however, it is known that droplet-particle collisions alone do not explain the observed fractional efficiencies

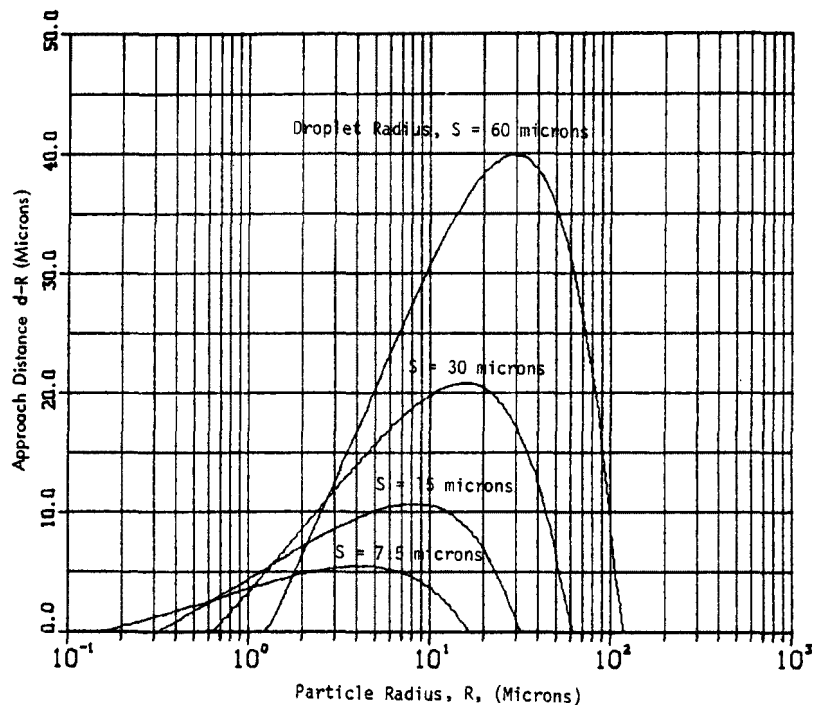


Figure 4-10. INDUCED CHARGING OF SPHERICAL PARTICLES BY CORONA BREAKDOWN AT THE PARTICLE. INDUCED CHARGING OCCURS UNDER EACH CURVE.

for fine particles. If induced charging is an important mechanism, then this spherical particle model does not explain it. The irregular particle model of Equation (4-14) is somewhat more successful.

Solutions to this equation are shown in Figure 4-11. In this analysis, the ratios $R/R'' = 10$ and $R'/R = 1.2$ were assumed. Here, induced charging is effective into the fine particulate range and induced charging by this mechanism can account, with limited success, for enhanced droplet collection efficiency.

A second model for induced charging was derived which assumes charge transfer by electrical breakdown at the surface of the droplet. The nature of the breakdown is unimportant, but it can generally be thought of as a Rayleigh instability since the droplet surface is charged to the Rayleigh limit. An alternative breakdown method is corona discharge. The breakdown occurs because of induced field enhancement

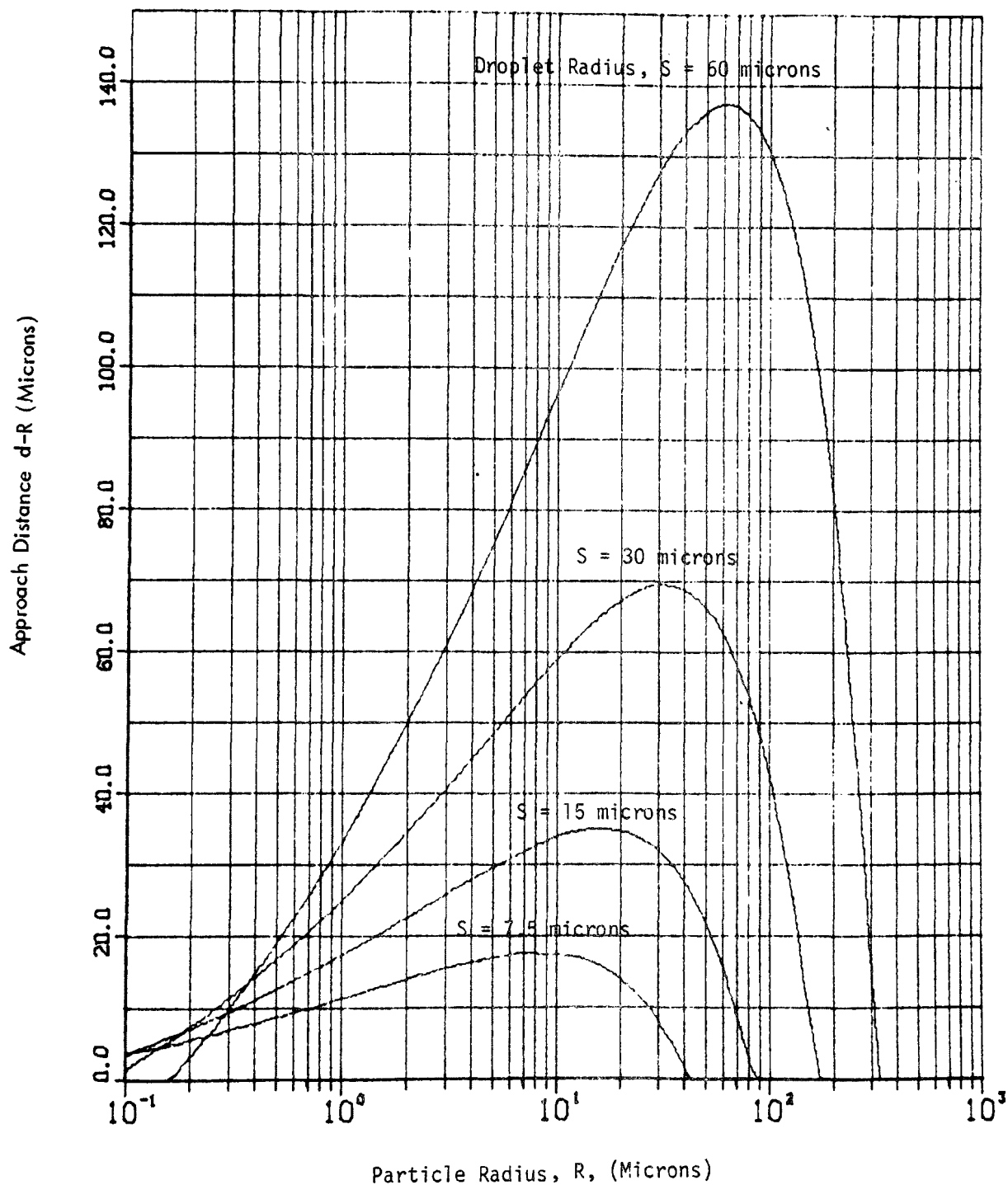


Figure 4-11. INDUCED CHARGING OF IRREGULAR PARTICLES BY CORONA BREAKDOWN AT THE PARTICLE

between droplet and particle. The resulting released charge migrates to the particle along field lines.

This model predicts much larger interaction distance than the first, and is more capable of explaining observed results. It can also be used to predict the amount of charge transferred from droplet to particle. This quantity of charge can then be used as a criterion for effective induced charging. Care must be taken in the interpretation of these quantities, however, because the assumed method of charge transfer is highly idealized. What is assumed is a reversible charge transfer process with no gaseous impedance and no electron cascade charge release effects. What could happen is that once charge transfer is initiated, cascade charge release will become important. If, in fact, it becomes dominant, the droplet may completely discharge itself to its surroundings¹². Surrounding particulate will pick up a good deal of this charge. This enhances the induced charging effect for single events, but renders the droplet practically useless for succeeding events.

The more interesting results of this analysis will now be discussed, following the steps outlined in Section 1.3. The geometry and notation used here are the same as shown in Figure 4-8, and introduced in Section 1.3.

The first result obtained is the dipole moment of the particle, and the method of calculation is based on the same assumptions made in the first induced charging model. The result is:

$$\beta = 4\pi\epsilon_0 \frac{\epsilon-1}{\epsilon+2} R^3 \left(\frac{S}{S+d} \right)^2 E_{0D} \quad (4-15)$$

d = separation, droplet surface to particle center

The dipole moment induced in a perfectly conducting particle is given by the same expression with ϵ set to infinity. The dipole moment induced in a dielectric cylindrical rod of radius R and length αR and axially aligned with the local field is

$$\beta_c = 4\pi\epsilon_0 \left[\frac{\alpha}{4} (\epsilon-1) \right] R^3 \left(\frac{S}{S+d} \right)^2 E_{0D}$$

Thus, in Equation (4-15) the factor $(\epsilon-1)/(\epsilon+2)$ may be regarded as a "properties factor" which leaves the general form valid for a variety of shapes and electrical properties.

The particle dipole will induce an image quadrupole, which closely approximates a dipole, interior to the spherical, conducting droplet. This dipole has the same form as Equation (4-15) but reduced by a factor of $S^3/(S+d)^3$. If this line of treatment were continued, the latter droplet dipole would again induce a second quadrupole in the particle, and so on, thus leading to an infinite converging multipole series describing the induced charge separation. For the present purpose, the series is truncated at the first droplet dipole. Potential field and charge distribution calculations are made to the leading orders of R/S , and terms of order $(R/S)^2$ and higher are neglected compared to one.

The electric field perturbation at the droplet surface is then calculated from this charge distribution.

$$E' = \frac{\beta}{2\pi\epsilon_0} \left(\frac{1}{(S+d)^3} + \frac{1}{d^3} \right) \quad (4-16)$$

Then a charge q_p is placed at the center of the particle, and the image of q_p in the droplet is found. Since the net charge in the droplet remains unchanged, the imaging results in a new dipole in the droplet. The field due to the addition of q_p and its image must then cancel E' . Thus the electric field strength at the surface of the droplet is just neutralized to its equilibrium, critical value. The resulting charge may be expressed in terms of a function $G(a)$ as follows:

$$q_p = 4\pi\epsilon_0 \frac{\epsilon-1}{\epsilon+2} \frac{R^3}{SG(a)} E_{0D} \quad (4-17)$$

$$G(a) = \frac{a(1+a)^4 \left(1 + \frac{3}{2}a\right)}{a^3 + (1+a)^3}$$

$$a = d/S$$

The characteristic charge, q_c , defined by

$$q_c = \frac{\epsilon-1}{\epsilon+2} \left(\frac{R}{S}\right)^3 q_D = q_p/G(a) \quad (4-18)$$

is an important quantity which will re-appear as a parameter in the collision effectiveness probability analysis.

We next seek a definition of an "effective collision" in terms of the drift velocity or drift time to the collecting walls of a particle bearing charge given by Equation (4-17). The mobility of such a particle under the influence of Stokes Law drag may be found from Equation (1-12), and may be expressed in terms of a characteristic mobility.

$$K_p = \frac{q_p}{6\pi\mu R} = K_c/G(a)$$

The average drift velocity can then be calculated as

$$\mu_D = \frac{h}{\tau_D} = K_c \bar{E}/G(a) \quad (4-19)$$

$$K_c = \frac{2}{3} \frac{\epsilon_0}{\mu} \frac{\epsilon-1}{\epsilon+2} \frac{R^2}{S} E_{oD}$$

$$\bar{E} = \left[\frac{1}{h} \int_0^h \frac{dx}{E(x)} \right]^{-1}$$

= a reciprocal average field over the drift path

h = length of drift path (generally taken as scrubber half-width)

Equation (4-19) relates the drift time or the drift velocity with the dimensionless variable a. Figure 4-12 is a plot of the function G(a).

A quadratic approximation for G(a) is good for small values of a.

$$G(a) \cong a + 2.5a^2 \quad a \ll 1 \quad (4-20)$$

For a $\lesssim .05$, a linear approximation is good to 10 percent, as may be verified from Figure 4-12. For a $\leq .1$, the above quadratic approximation

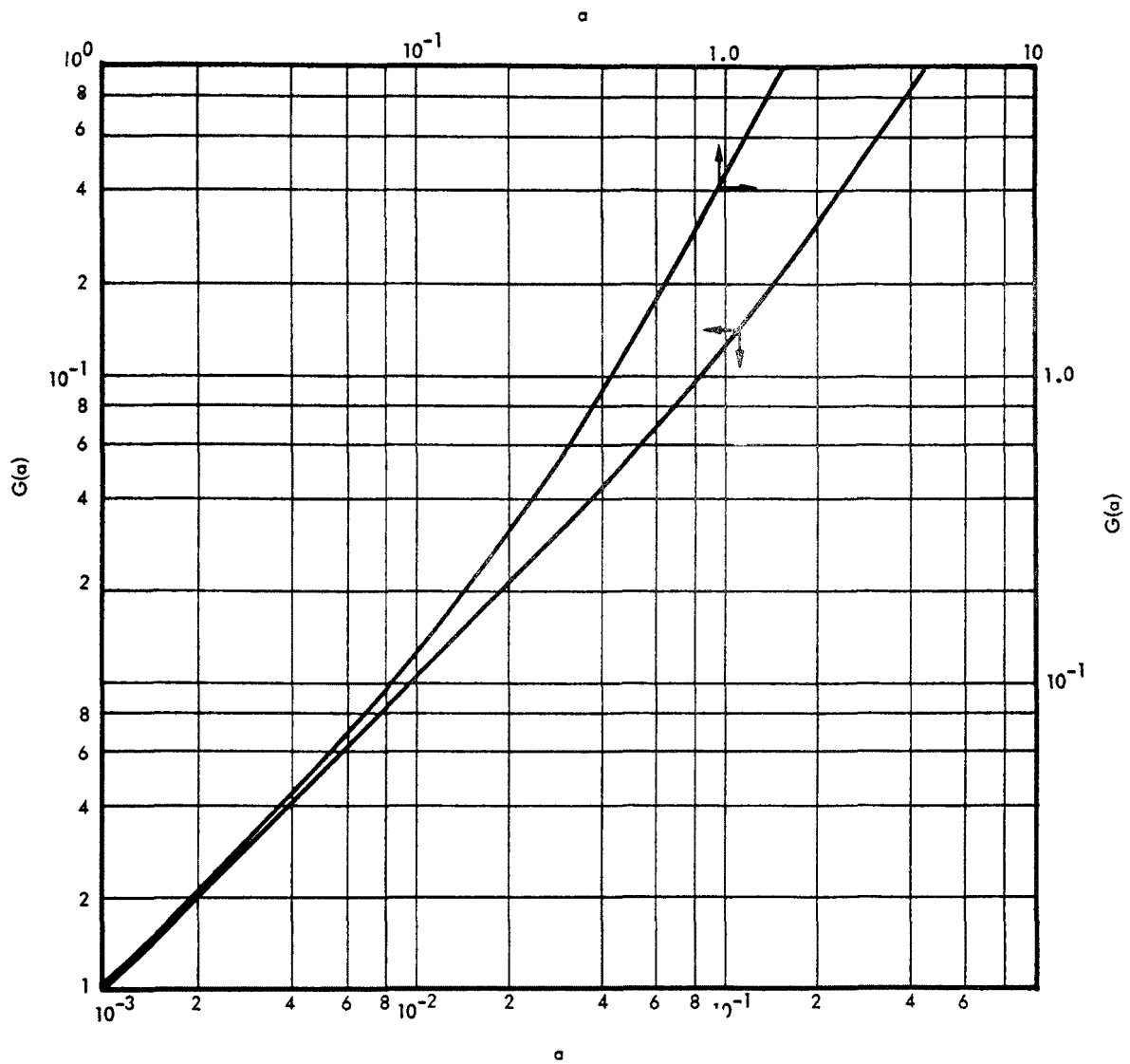


Figure 4-12. PLOT OF EQUATION (4-17) RELATED TO PARTICLE DRIFT TIME

is good to one percent. An approximation for large a which is good to about 3 percent for values of a larger than 10 may also be written.

$$G \simeq \frac{3}{4} a^3 \quad a \gtrsim 10$$

The derivation thus far has assumed that the fraction of charge leaked from the droplet to the particle is small. This charge fraction can be calculated using Equation (4-17). We set an arbitrary upper bound on the charge ratio of b .

$$\frac{q_p}{4\pi\epsilon_0 S^2 E_{oD}} \leq b$$

where b is chosen less than one, and probably less than one tenth. We take the maximum charge that can be impressed upon the particle as that which occurs at $a = R/S$. Assuming that the quadratic form of Equation (4-20) is valid for $G(R/S)$, which it is if R/S is less than 0.1, the above inequality may then be solved to yield a "safe upper bound" for R/S .

$$\frac{R}{S} \leq 1.25 \frac{\epsilon+2}{\epsilon-1} b ; \frac{R}{S} < .1 \quad (4-21)$$

If the particle is to retain the charge q_p , the field strength due to q_p on the surface of the particle must be less than the local corona breakdown field, after correction by Peek's formula. The particle charge obtains a maximum for $d = R$, when particle and droplet touch. Using this maximum, the inequality

$$\frac{q_p}{4\pi\epsilon_0 R^2} < E_B (1 + 0.054/\sqrt{R})$$

must be satisfied. Using Equations (4-17) and (4-20) it was verified that there are no real solutions to the resulting quadratic approximation to the inequality in R/S .

The assumed charging mechanism will be valid only if there is always an inwardly directed charging field on the surface of the particle, directed so as to carry positive charge onto the particle. The field at the particle surface, on the line connecting the particle and droplet centers, was calculated for the assumed charge distribution. It was found to have a zero order term giving a positive charging field of

$$E_{oD} \frac{1}{(1+a)^2} \frac{3\epsilon}{\epsilon+2}$$

which is the field due to the droplet monopole and the particle dipole alone. The remaining terms are of order R/S or smaller, and do not negate the charging field.

Equation (4-19) may now be used as a criterion for an "effective" collision. For a conducting particulate in an average field of 5×10^5 volts/meter, and for a 60 micron radius droplet charged to the Rayleigh limit ($E_{OD} = 2.3 \times 10^7$ v/m), Equation (4-19) gives

$$G(A) = 0.0628 R^2 \frac{\tau_D}{h}$$

with R expressed directly in microns.

A good nominal value for the average drift path length is 0.1 meter. The drift time criterion depends upon how long the particulate is exposed to an ambient precipitating field. In a single stage, the scrubbing volume residence time is about 0.15 second. Depending on scrubber design, however, particulate may spend as long as one second in a strong precipitating field. Particulates passing through a three-stage scrubber will have an average drift time of about 0.5 second, and we will take this as nominal. Then for a particle radius of one micron, a value of $G(a)$ of 0.315 is obtained. The corresponding value of a from Equation (4-17) is 0.205, which in turn gives a d of 12.3 microns. Thus a 2 micron diameter particle must come within 12.3 microns of the droplet in order to effectively collide with it by this criterion. This distance will generally be referred to as D , the distance of farthest approach for an effective collision. And the resulting parameter $A = D/S$ is the interaction impact parameter.

The impact parameter, A , was calculated using Equation (4-19) for a 60 micron droplet radius and for various particulate sizes. An electrical permittivity of 5.0 was assumed for the particulate, so that the results could be compared with the first model, as shown in Figure 4-10 for spherical particles. The results of this calculation are shown in Figure 4-13. Curves are shown for various drift times with a drift path length of 0.1 meter. Other parameters are the same as in the previous example. For small values of impact parameter, the fractional area added to the cross section by induced charging is about twice the impact parameter. For the nominal τ_D , this effect is still about five percent at a particle radius of 0.4 micron.

According to this induced charging model there is a lower limit to the particle radius for which effective induced charging can occur. The smaller the particle, the closer it must approach the droplet. If D , the distance of farthest approach, is equal to a particle radius, then the particle may be considered to collide with the droplet, and induced charging is not an active mechanism. This condition corresponds to a value of $a = R/S$ in Equation (4-19). The equation may then be solved for S to obtain the form

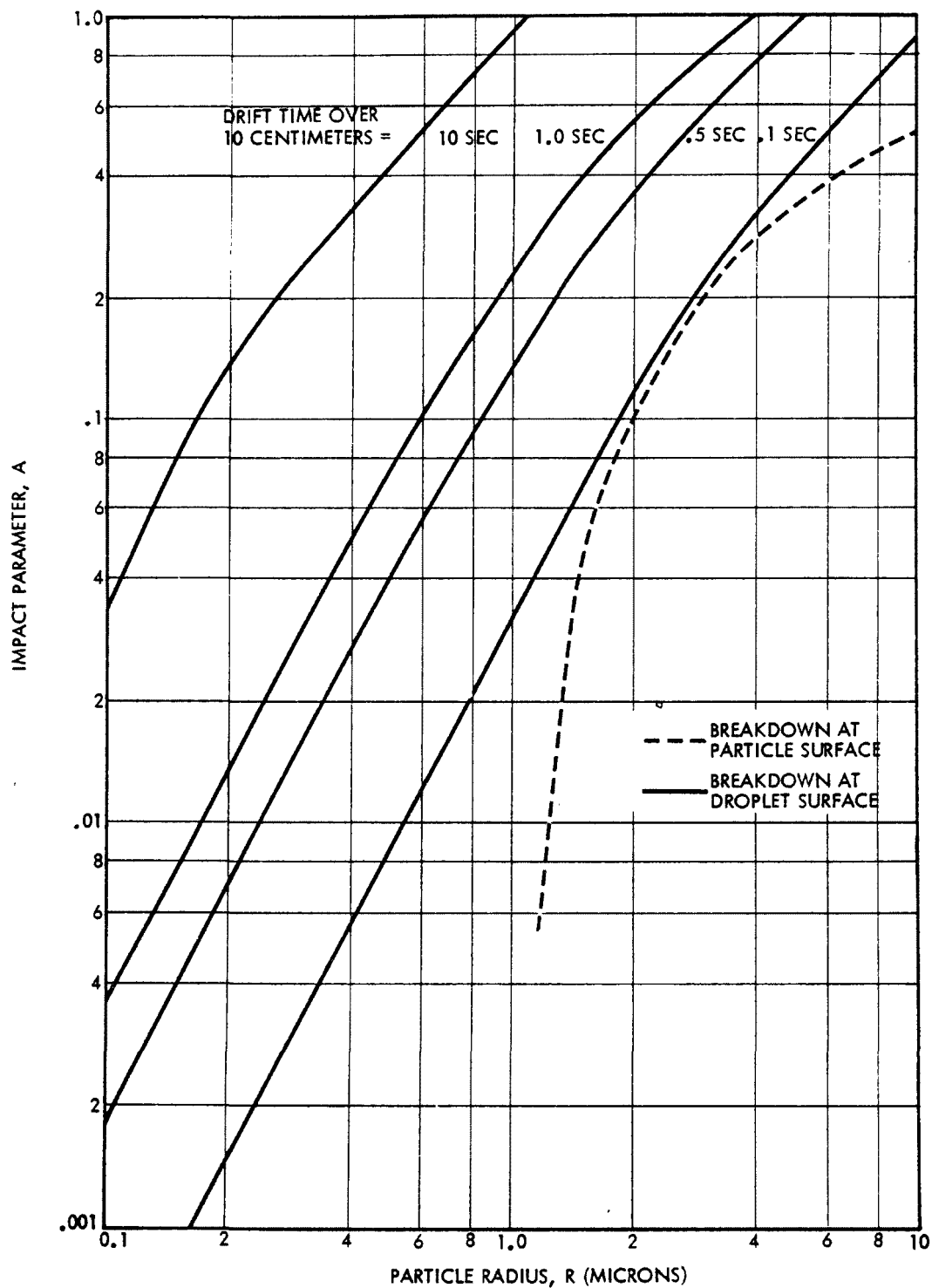


Figure 4-13. INDUCED CHARGING IMPACT PARAMETER FOR THE MODELS OF EQUATIONS (4-13) AND (4-19). A sequence of drift times is plotted. Droplet radius is 60 microns. Particulate is spherical with $\epsilon = 5$. $E_{OD} = 2.3 \times 10^{-7}$ volts/meter. $h = 0.1$ meter.

$$\left[\frac{2}{3} \frac{\epsilon_0}{\mu} \frac{\epsilon-1}{\epsilon+2} \frac{\bar{E}}{h} E_0 D^{\tau_D} \right] S = G (R/S)/(R/S)^2 \quad (4-22)$$

The right hand side of this equation is plotted in Figure 4-14. Using the values of the previous example, a 120 micron diameter droplet will give a value of R/S equal to 0.881×10^{-3} , hence a minimum particle radius of about 0.053 micron can be collected by induced charging.

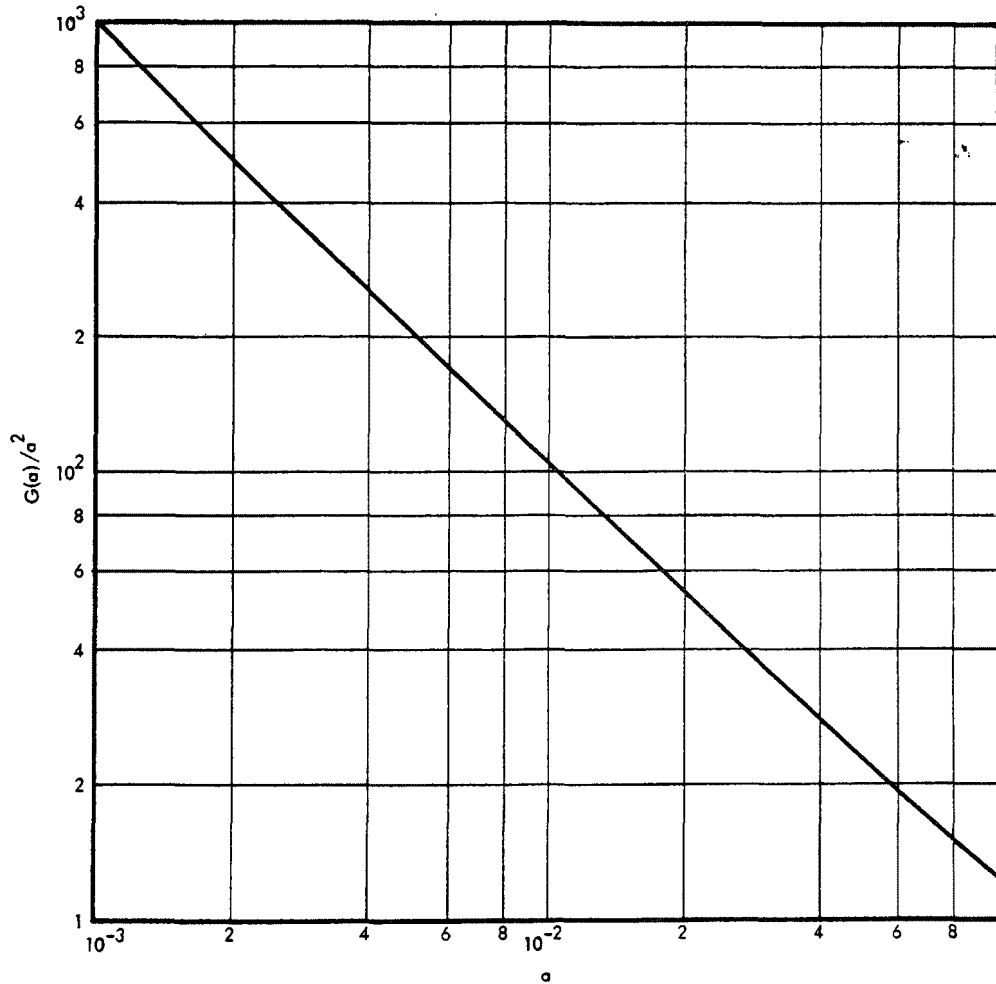


Figure 4-14. PLOT OF EQUATION (4-22) TO OBTAIN MINIMUM PARTICLE SIZE COLLECTIBLE BY INDUCED CHARGING

If R' is the minimum collectible particle radius, and R'/S is small, we may use the Equation (4-20) quadratic approximation in Equation (4-22), and obtain the following asymptotic form for R .

$$R' = R_{\infty} \frac{1}{1 - 2.5 R_{\infty}/S} \quad (4-23)$$

$$R_{\infty} = \frac{3}{2} \frac{\mu}{\epsilon_0} \frac{\epsilon+2}{\epsilon-1} \frac{h}{E} \frac{1}{E_{0D} \tau_D}$$

This demonstrates that as the droplet radius gets arbitrarily large, the maximum collectible particle radius approaches a lower limit, $R' \rightarrow R_{\infty}$. Using the values of the previous example, and remembering that the Rayleigh limited value of E_{0D} is dependent on the square root of droplet radius, we get

$$R_{\infty} = 0.0265 \frac{1}{\tau_D} \sqrt{\frac{S}{60}} \text{ microns}$$

The basic result of this analysis is embodied in Equation (4-19), which shows that the induced charging process can be described entirely in terms of a single dimensionless variable, the impact parameter A . This in effect defines a characteristic drift time τ_D for particle capture. In mapping the effects of induced charging, only the parameter A needs to be directly considered.

The analysis has assumed particle interaction with a droplet that has undergone no charge loss. If E_{0D} is less than critical, an expression for D/S may yet be derived, which contains not one dimensionless parameter, but two. This expression is presented here for completeness, although the problem of droplet charge degradation is too complex to pursue analytically on this program.

$$K_c \frac{E}{h} \tau_D = \frac{G(a)}{1 - \Delta F(a)} \quad ; \quad \Delta F(a) > 1$$

$$= \infty \quad ; \quad \Delta F(a) = 1$$

$$\Delta = \frac{\epsilon+2}{\epsilon-1} \left(\frac{S}{R} \right)^3 \frac{E_{0D} - E_{0C}}{2E_0}$$

$$F(a) = \frac{a^3 (1+a)^5}{a^3 + (1+a)^3}$$

The new parameter, Δ , is a dimensionless form of the difference between the droplet charging field E_{oD} and the critical field E_{oC} .

4.1.4 Collision Effectiveness Probability

The definition of collision effectiveness probability, or collection efficiency, was given in Section 1.3. The method of derivation was also described. The method involves the solution of a set of differential equations defining the motion of a spherical particle in the Stokes law wake of a moving droplet. The vector differential equations of motion are rewritten here from Equation (1-13).

$$M_p \frac{d\bar{u}}{dt} = 6\pi\mu R (\bar{w} - \bar{u}) - q_d \bar{g} \text{rad } \phi \quad (4-24)$$

In this equation, the components of the wake velocity, w , are given by Equations (1-11) and (1-12) in Section 1.3. The droplet charge, q_d , is given by

$$q_d = 4\pi\epsilon_o S^2 E_{oD} \quad (4-25)$$

The expression $\bar{g} \text{rad } \phi$ is the gradient of a potential function given by Equation (1-14). Using Equations (4-15) for the particle dipole and (4-17) for the particle charge, an electrostatic force term of the following form is obtained in Equation (4-24).

$$-q_d \bar{g} \text{rad } \phi = 4\pi\epsilon_o \frac{\epsilon-1}{\epsilon+2} \frac{R^3}{S} \left(\frac{4}{(1+a)^3} - \frac{1}{G(a)} \right) \frac{S^2 E_{oD}^2}{(1+a)^2} \left(\frac{\bar{r}}{r} \right) \quad (4-26)$$

$$a = \frac{r}{S} - 1$$

The function $G(a)$ is as previously defined in Equation (4-17). Equation (4-26) has the property that it vanishes for a given value of a , independently of the values of other parameters. The approximate value of a for which this occurs is 0.29.

In order to obtain the collision effectiveness probability, the differential equations are solved subject to the following set of boundary conditions.

$$\begin{array}{lll} Z = Z^* & \text{at} & t = 0 \\ x = x_0 & \text{at} & t = 0 \\ r = S+D & \text{at} & t = t_f \\ dr/dt = 0 & \text{at} & t = t_f \end{array} \quad (4-27)$$

The collision effectiveness probability is then as given in Equation (1-9).

$$p = \left[\frac{Z^*}{S+D} \right]^2 \quad (4-28)$$

The particle approaches the droplet sphere of aerodynamic and electrostatic influence at time $t = 0$ and some arbitrarily chosen coordinate x_0 . The time t_f is some unknown final time at which the particle experiences a grazing collision and the integration stops. The solution of Equations (4-24) through (4-26) will allow the determination of the unknown value of Z^* .

The collision effectiveness probability is a dimensionless function of Z^* , and thus a dimensionless function of the parameters governing the solution of Equations (4-24) through (4-26). Since the numerical value of p must be dimensionally invariant (independent of the system of units used in its calculation), it follows that p will be a function only of some set of basic dimensionless parameters of the problem. To find what these parameters are, it is convenient to re-cast the equations into a dimensionless form. The resulting dimensionless parameters appearing in the new equations will be those which govern the behavior of p .

Examination of Equation (1-11), for the components of the wake velocity, shows that the parameter S is a natural choice for a characteristic length by which to non-dimensionalize. In equation (4-24):

$$M_p = \frac{4}{3} \pi R^3 \rho \quad (4-29)$$

The resulting coefficient of $\bar{w} - \bar{u}$ suggests a choice for the characteristic time, and the non-dimensional scale is:

$$L_c = S, \quad t_c = \frac{2}{9} \frac{\rho R^2}{\mu} \quad (4-30)$$

Define dimensionless variables

$$t' = t/t_c \quad (4-31)$$

$$u' = \frac{t_c}{L_c} u$$

$$a = \frac{r}{S} - 1$$

The dimensionless form of the velocity \bar{w} is used to define one of the basic parameters as (U/U_c) in the following.

$$\bar{w} \frac{t_c}{L_c} = \left(\frac{U}{U_c} \right) \bar{\alpha} \quad (4-32)$$

The components of $\bar{\alpha}$ are given by

$$\alpha_x = -\frac{1}{2} \frac{1}{1+a} \cos \theta \left(\frac{1}{(1+a)^2} - 3 \right)$$

$$\alpha_z = -\frac{1}{4} \frac{1}{1+a} \sin \theta \left(\frac{1}{(1+a)^2} + 3 \right)$$

and correspond to the components given in Equation (1-11). Substituting Equation (4-26) into Equation (4-24), and using Equation (4-29) through (4-31), a complete set of dimensionless differential equations and boundary conditions is obtained.

$$\frac{d\bar{u}'}{dt'} = \frac{U}{U_c} \bar{\alpha} - \bar{u}' + \frac{E_{oD}}{E_c} \frac{1}{(1+a)^2} \left(\frac{2}{(1+a)^3} - \frac{1}{2G(a)} \right) \left(\frac{\bar{r}}{r} \right) \quad (4-33)$$

$$\frac{Z}{S} = \sqrt{p} (1+A) \quad \text{at} \quad t' = 0$$

$$\frac{x}{S} = \frac{x_0}{S} \quad \text{at} \quad t' = 0$$

$$a = A \quad \text{at} \quad t' = t'_f$$

$$da/dt' = 0 \quad \text{at} \quad t' = t'_f$$

From this analysis it is seen that the solution, p , depends on just three dimensionless parameters. For convenience, these have been expressed as

$$(U/U_c, E_{oD}/E_c, A) \quad (4-34)$$

where U_c and S_c are a characteristic droplet velocity and radius, respectively. The parametric description is completed with the following relations for the characteristic parameters.

$$U_c = \frac{9}{2} \frac{\mu}{\rho} \frac{S}{R^2} \quad (4-35)$$

$$E_c = U_c/K_c$$

The first parameter in Equation (4-34) is U/U_c and is an inertial force parameter, dependent only on fluid mechanics and relative velocity. The second parameter, E_{oD}/E_c , is an electrostatic force parameter depending on particle charge and mobility. The value of K_c in Equation (4-35) is defined in Equation (4-19). The third parameter, A , is the impact parameter and is also defined from Equation (4-19) as satisfying

$$G(A) = K_c \bar{E} (\tau_D/h) \quad (4-36)$$

Equation (4-33) was solved on the computer for a range of values of the three parameters. The method of solution is based on the theoretical approach described in Section 1.3. A discussion of the method of solution and a listing of the Fortran program used is given in Appendix A. The results of the computer analysis are displayed in Figures 4-15 through 4-17.

The results are presented on log-probability scales, and approach straight lines for large U/U_c . Straight-line type behavior would be indicative of an error integral function. The values of each of the three parameters in Equation (4-34) were investigated over about three decades.

The most variation in p appeared with the velocity or inertial parameter. The variability with the other two parameters was relatively slight, increasing for smaller U/U_c . Complete studies were also made for the value $A = 0$, but the values were not appreciably different from those for $A = 0.13$. This latter value was chosen as a nominal, and is shown together with other nominal values in Table 4-1.

Table 4-1. NOMINAL CONDITIONS FOR COLLISION-EFFECTIVENESS-PROBABILITY PARAMETER STUDIES

Physical Parameters	Characteristic Parameters	Dimensionless Parameters
$R = 0.83 \times 10^{-6} \text{ m}$	$\tau_D = 0.5 \text{ sec}$	$A = 0.13$
$S = 60 \times 10^{-6} \text{ m}$	$u_D = 0.2 \text{ m/sec}$	
$U = 30 \text{ m/sec}$	$U_c = 1.277 \text{ m/sec}$	
$E_{OD} = 2.3 \times 10^7 \text{ v/m}$	$q_c = 1.98 \times 10^{-17}$	$U/U_c = 23.5$
$\rho = 5.6 \times 10^3 \text{ kg/m}^3$	$K_c = 0.695 \times 10^{-7} \text{ m}^2/\text{v-sec}$	
$\mu = 1.82 \times 10^{-5} \text{ kg/m-sec}$	$E_c = 1.83 \times 10^7 \text{ v/m}$	$E_{OD}/E_c = 1.25$
$\epsilon = 14$		
$\bar{E} = 5 \times 10^5 \text{ v/m}$		

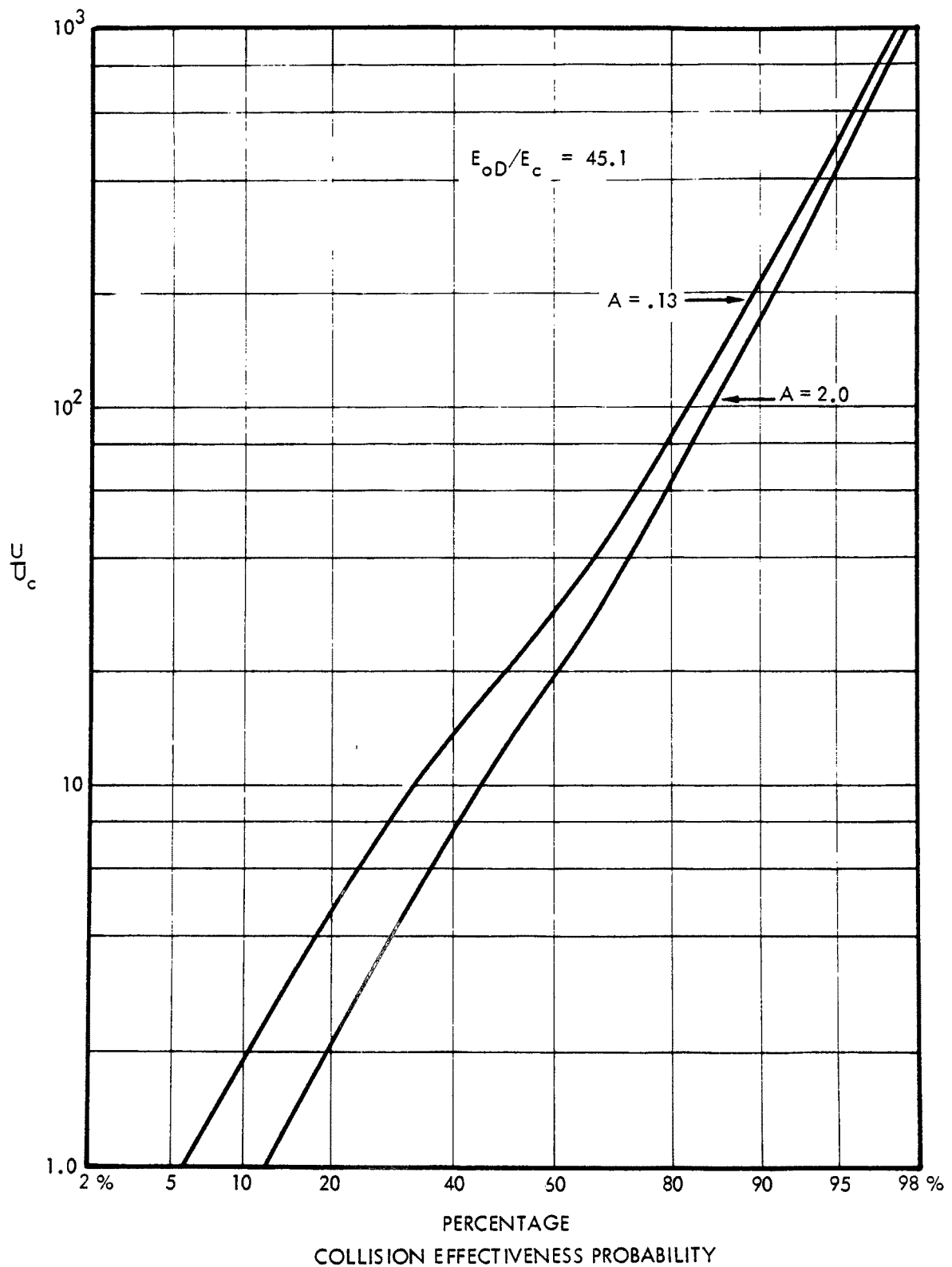


Figure 4-15. PARAMETRIC STUDY OF COLLISION EFFECTIVENESS PROBABILITY FOR $E_{OD}/E_C = 45.1$

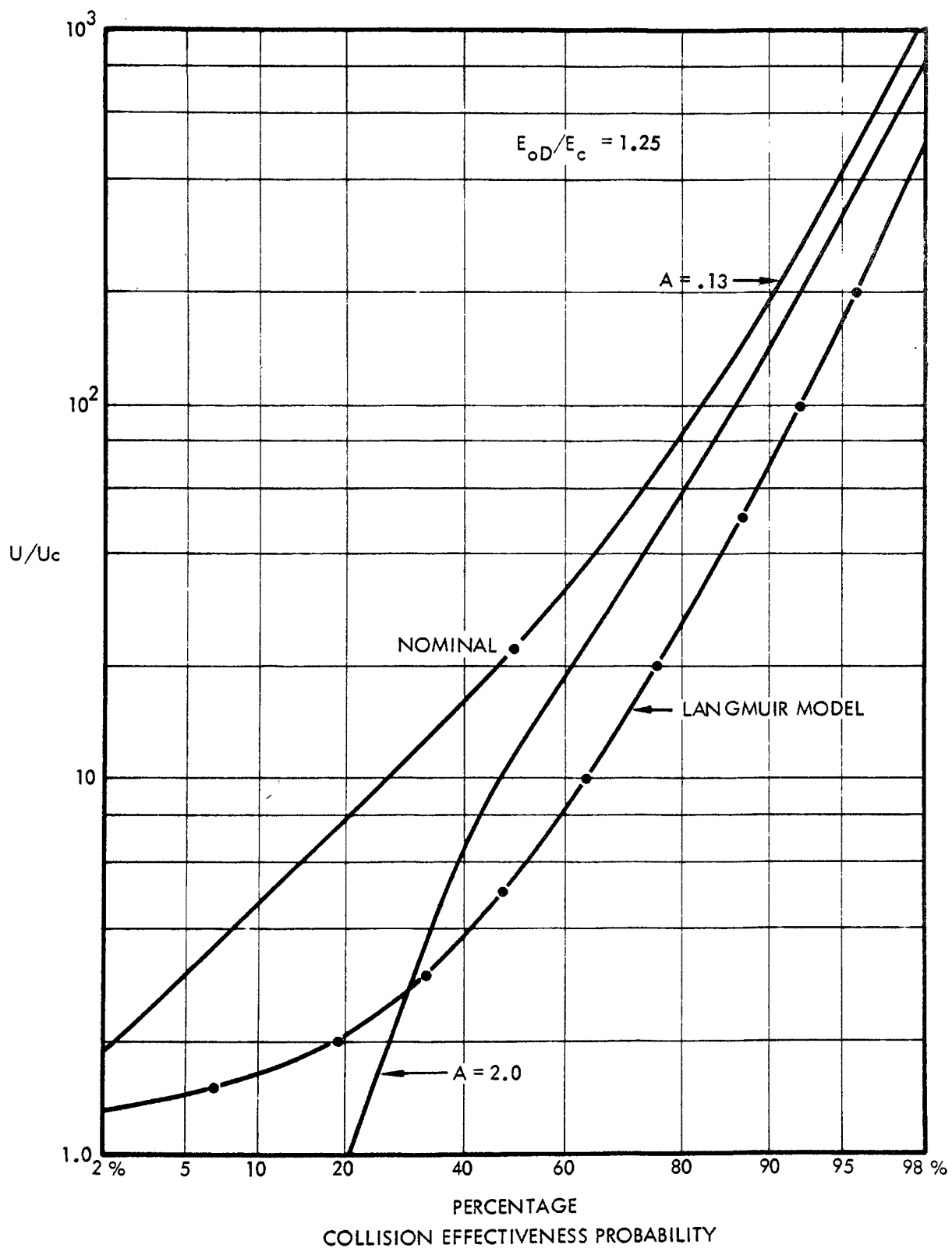


Figure 4-16. PARAMETRIC STUDY OF COLLISION EFFECTIVENESS PROBABILITY FOR $E_{oD}/E_c = 1.25$

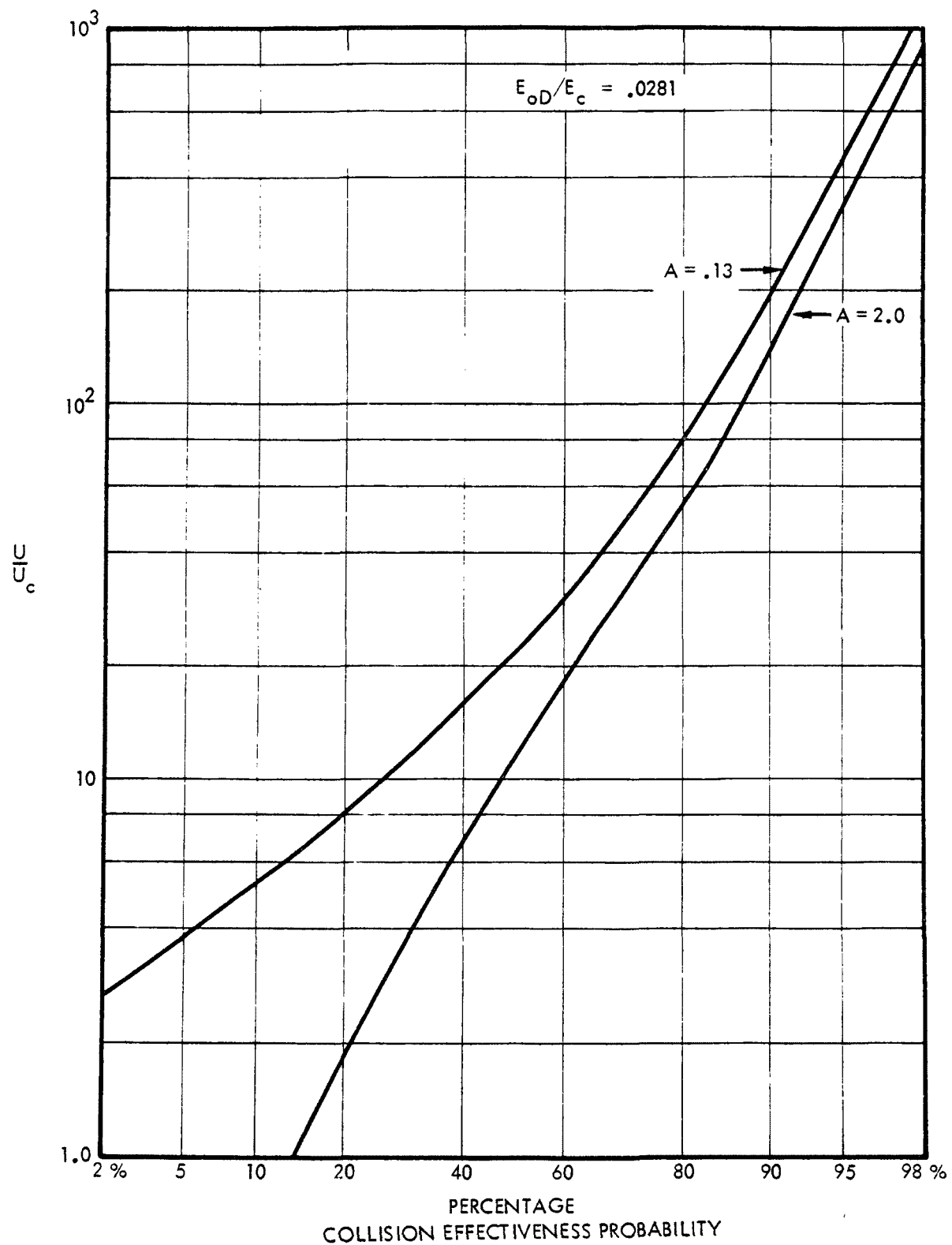


Figure 4-17. PARAMETRIC STUDY OF COLLISION EFFECTIVENESS PROBABILITY FOR $E_{0D}/E_c = 0.0281$

The nominal particulate density and dielectric constant were chosen to approximate a metallic oxide fume, although the nominal particle radius is probably large for such a fume. Parametric studies were made by exploring around these nominal conditions.

The value of $A = 0$ is not physically realizable, but solutions do exist for that value. These solutions correspond to a limiting value of R/S of zero as U/U_c and E_{OD}/E_c each remain finite. Thus very high values of U and E_{OD} may be implied.

The variation of p with the parameter A was explored more fully at various conditions. A plot is shown in Figure 4-18 for the nominal value of E_{OD}/E_c and a small value of U/U_c , where the variation was large. The shape of the curve is typical for any value of U/U_c . There is little change for A between zero and 0.5. Above 0.5 the variation is fairly linear.

In 1947 I. Langmuir¹³ derived an empirical expression for the collision effectiveness probability (collection efficiency) of raindrops in Stokes Law motion. The Langmuir model, applied to the motion of charged droplets in an electric field, is a single parameter model which depends only on the value of U/U_c . In equation form, it appears as follows.

$$p = \left(1 + \frac{3}{4} \frac{\ln 2(U/U_c)}{(U/U_c) - 1.214} \right)^{-2} \quad U/U_c > 1.214 \quad (4-37)$$

$$p = 0 \quad U/U_c < 1.214$$

The Langmuir model has been plotted in Figure 4-16 for comparison.

In order to see the effects of particle radius alone on collision effectiveness probability, the value of R can be varied in Equations (4-30) and (4-31) with all other values held constant. This has been done, and the results are presented in Figure 4-19, using the nominal parameters given in Table 4-1 except for values of R . The value of the impact parameter, A , is also changing along the curve according to the relationship of K_c with R , and a separate scale shows these changes.

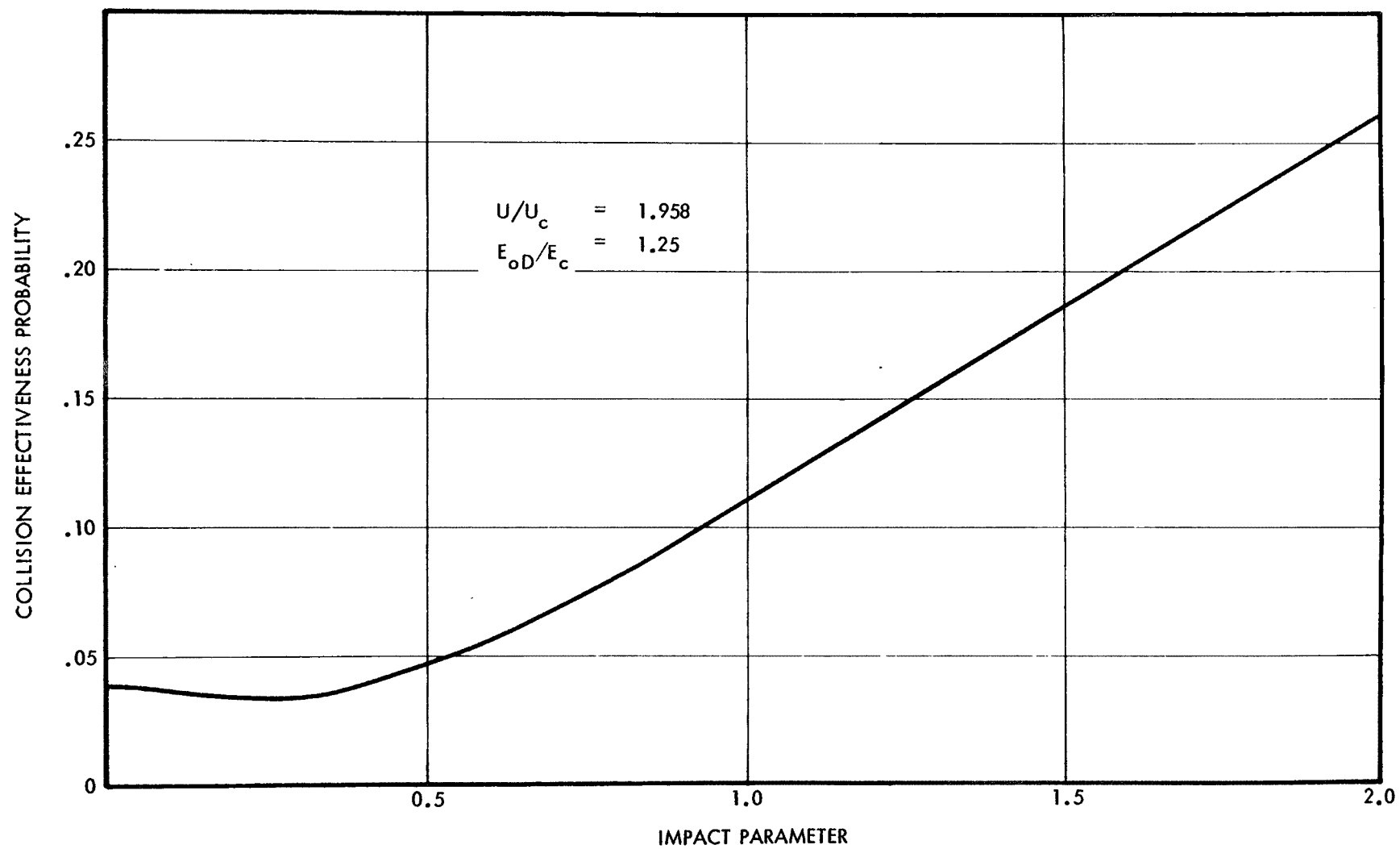


Figure 4-18. FUNCTIONAL DEPENDENCE OF COLLISION EFFECTIVENESS PROBABILITY ON IMPACT PARAMETER, A

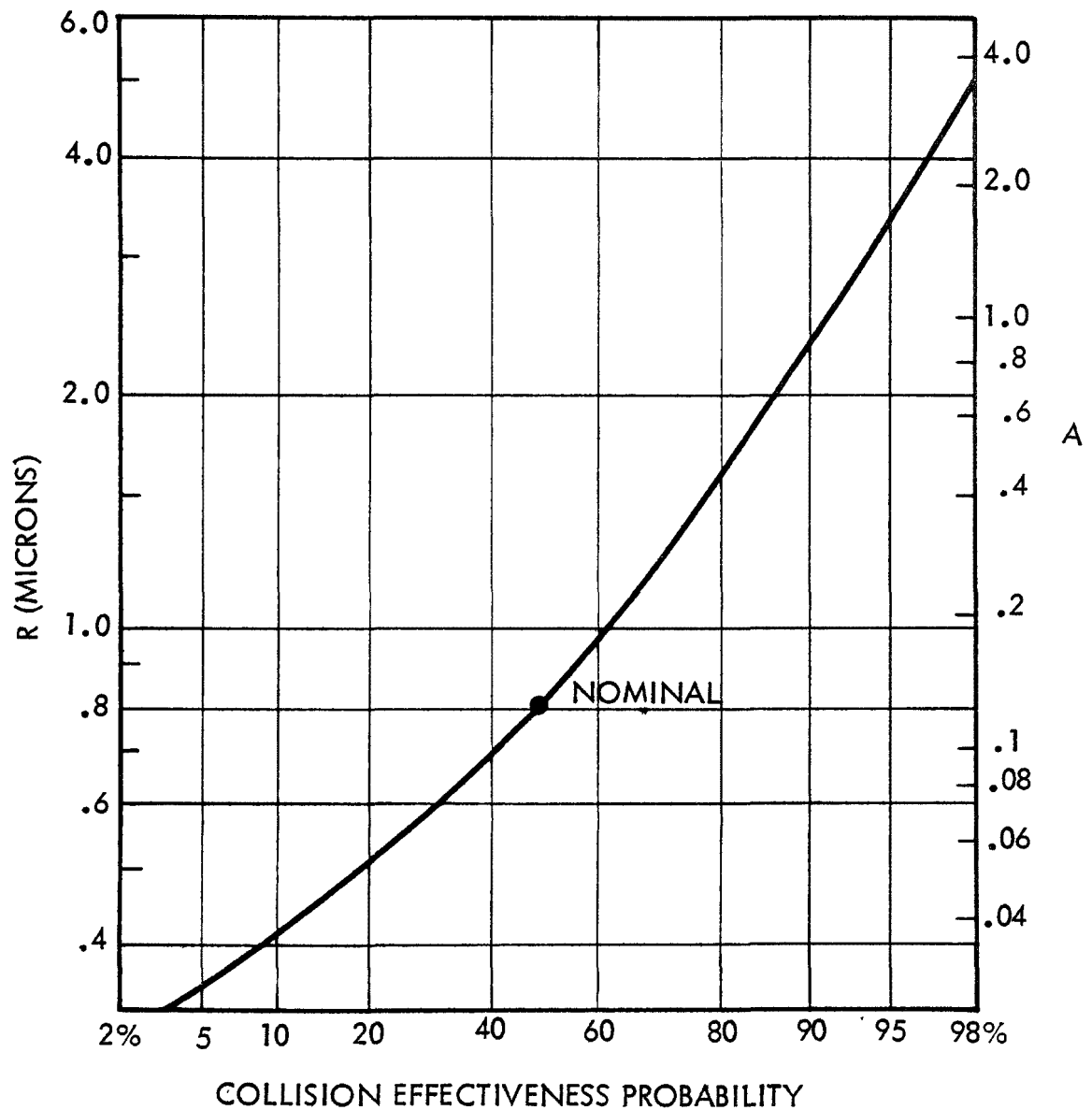


Figure 4-19. FUNCTIONAL DEPENDENCE OF COLLISION EFFECTIVENESS PROBABILITY ON PARTICLE RADIUS

4.2 RESEARCH SCRUBBER MEASUREMENTS

4.2.1 Collector Current

The corona current characteristics of the five-spray-tube electrode were determined. A curve of the corona current as a function of applied voltage is shown in Figure 4-20. The collector plate spacing was 14.3 cm and 18 ga spray tubes were used in the electrode. The current shown in the figure is the total measured from both collectors. There was no water flow during these measurements.

As can be seen from the curve in Figure 4-20, the current-voltage follows the relationship

$$I = A V(V - V_0) \quad (4-38)$$

where A = constant

V_0 = corona onset voltage

This is a typical corona current variation with voltage. The onset voltage for the configuration was approximately 7.0 kv. The typical onset voltage for a 0.050 inch (1.27 mm) diameter wire within the collector plate geometry, with Peek's correction, would be approximately 21 kv. The spray tubes have square tips which are only slightly chamfered. It is in this region where the corona develops. Therefore, the factor of three reduction in corona onset voltage would be expected. The apparent radius of curvature of the spray tube tip is approximately 0.063 mm which is one-tenth that of the tube. The constant, A , has a value of $0.127 \mu\text{amp}/(\text{kv})^2$.

A series of collector current measurements were made using the segmented collector. These data are shown in Figures 4-21 and 4-22. The data shown in most of the figures are averages for several tests. The total scatter in the data is identified on these figures. The horizontal lines on each of the curves represent the current levels on the individual collectors. The curves were faired in as an approximate smoothing of the raw data. The actual water flow rates can be determined from the calibration curves in Figure 4-22.

The measured current is the sum of both the corona ion current and the droplet current. The scrubber is operated at or near a space charge limited condition; therefore, differences in the current noted with and without water flow are due to differences in the mobility of the charge carrying species, i.e., ions and droplets.

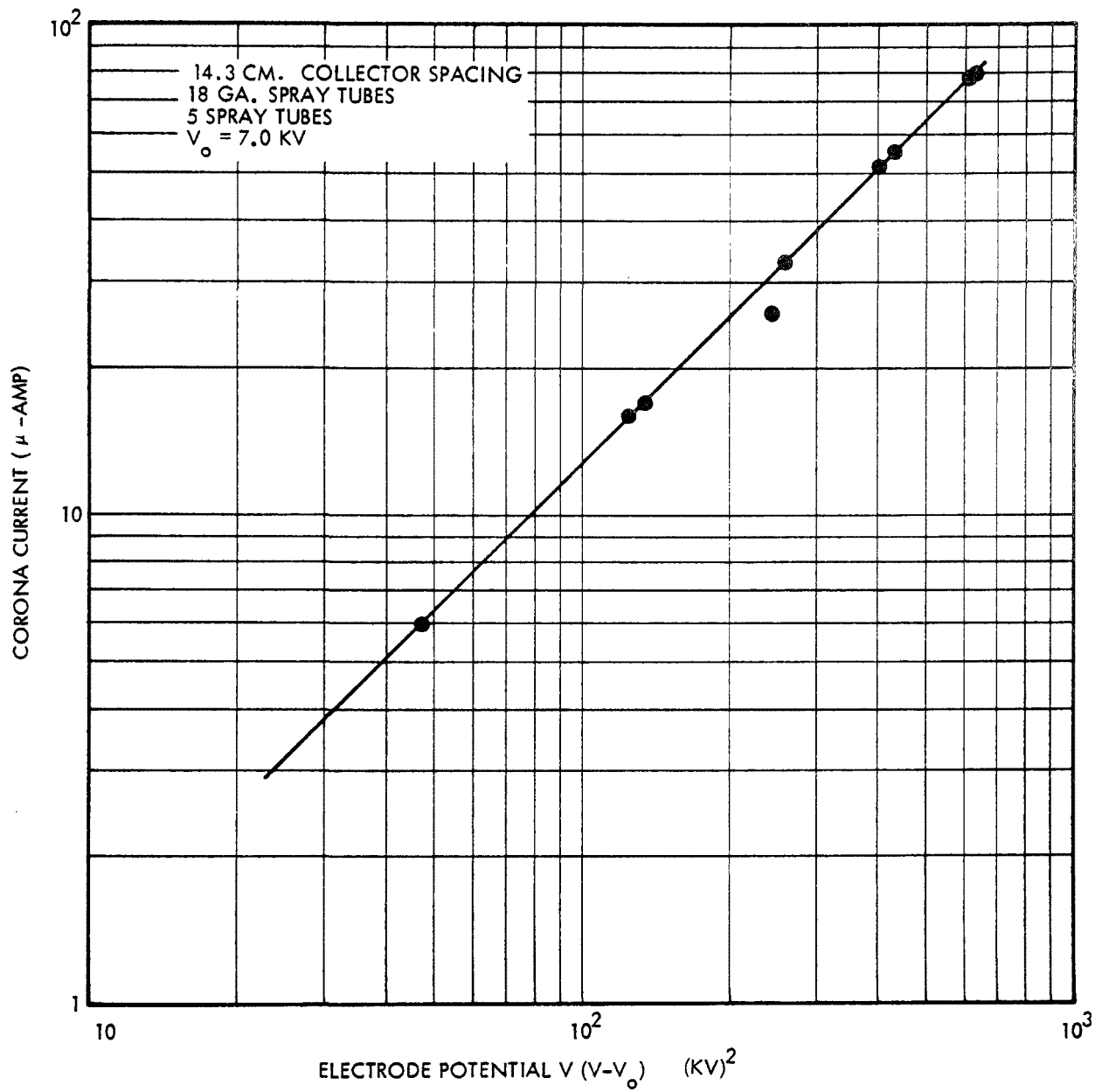
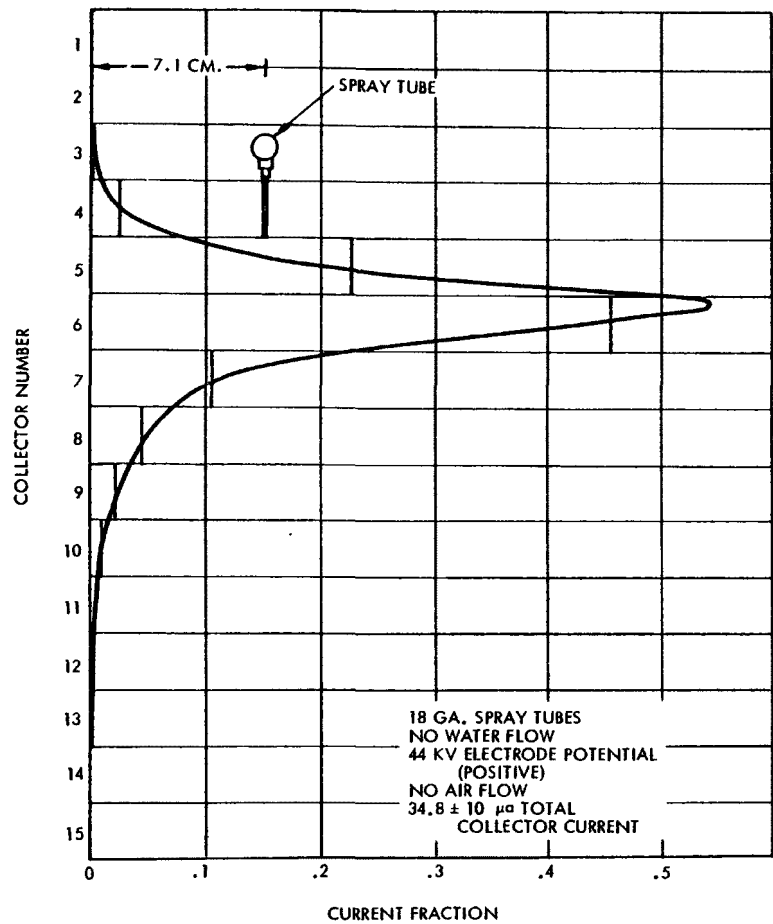
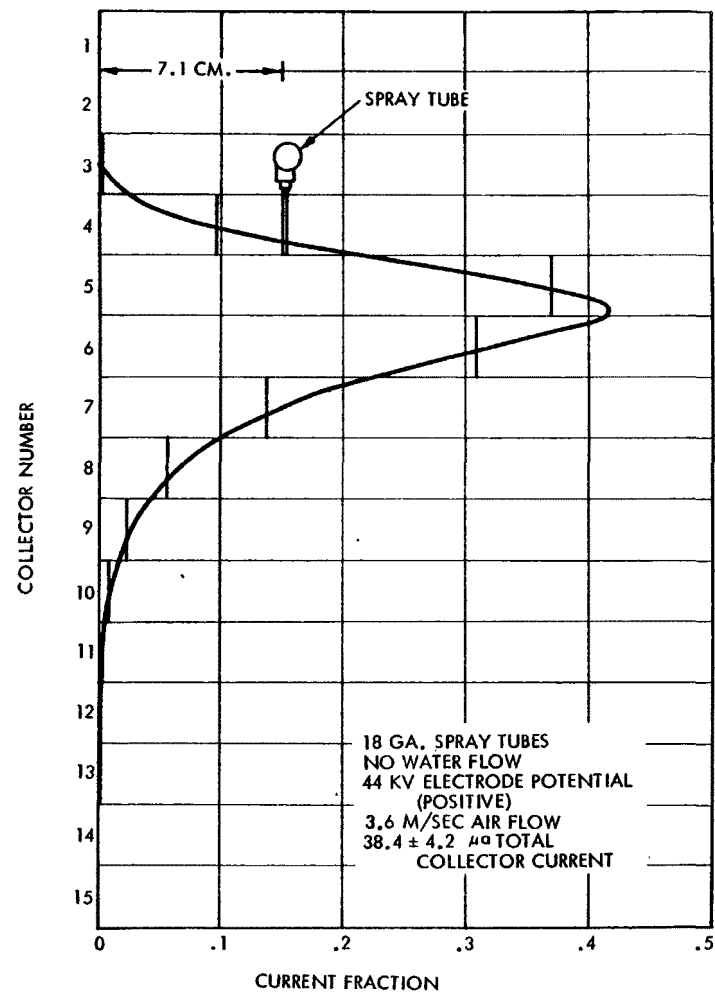


Figure 4-20. CORONA CURRENT VERSUS ELECTRODE VOLTAGE
FOR THE FIVE-TUBE ELECTRODE

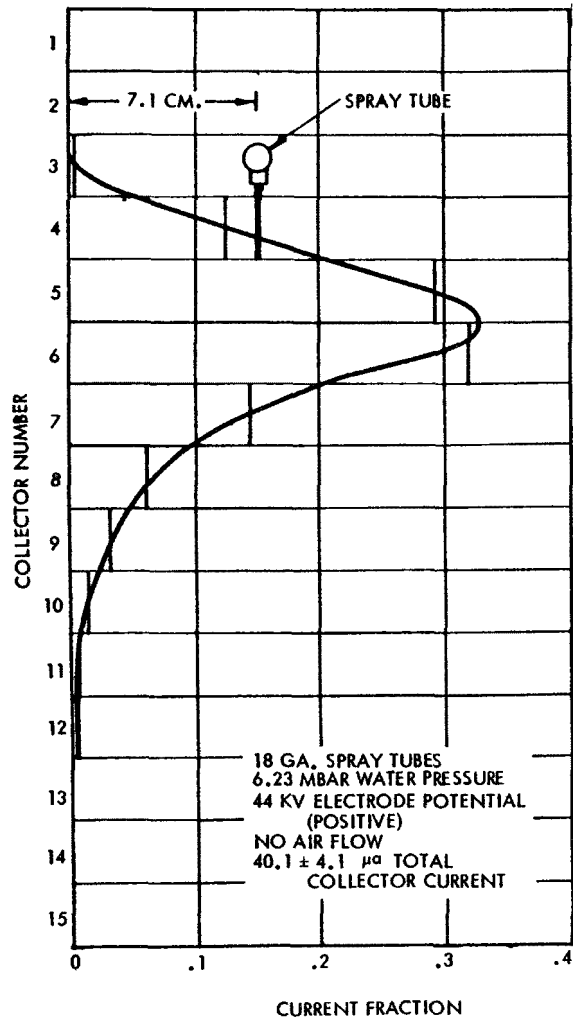


(a) Average of Three Tests

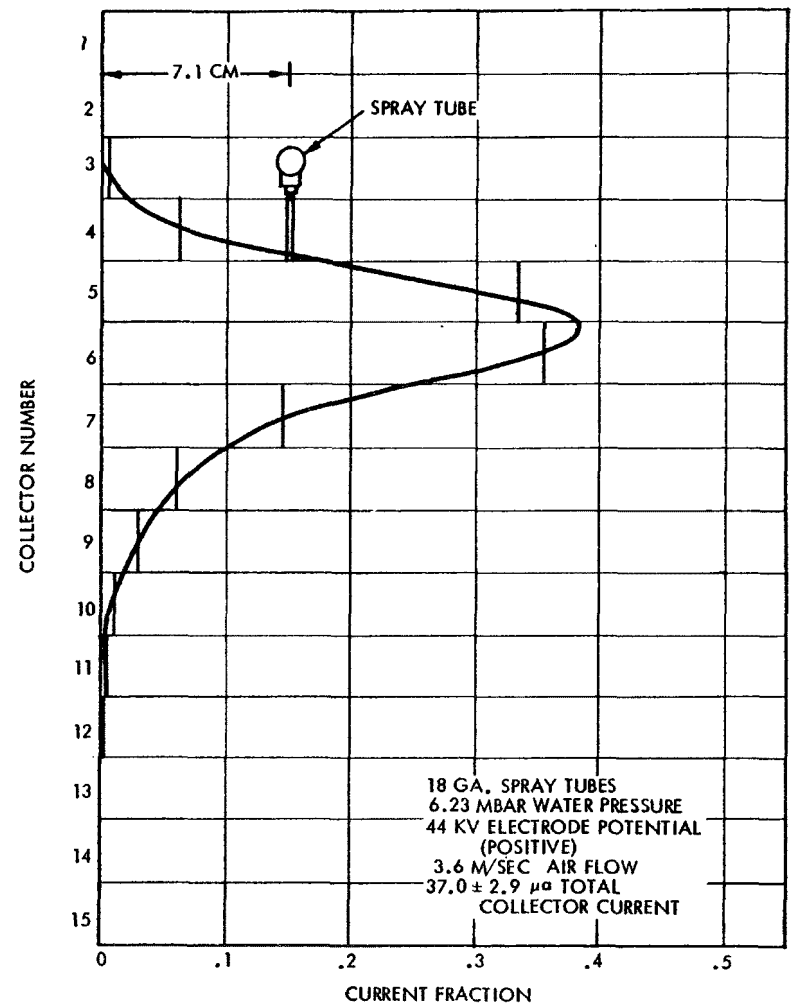


(b) Average of Three Tests

Figure 4-21. COLLECTOR CURRENT DISTRIBUTION FOR 18 GAUGE SPRAY TUBES. WALL-TO-ELECTRODE SPACING IS 7.14 CM. GRID LINES ARE AT CENTER OF COLLECTOR

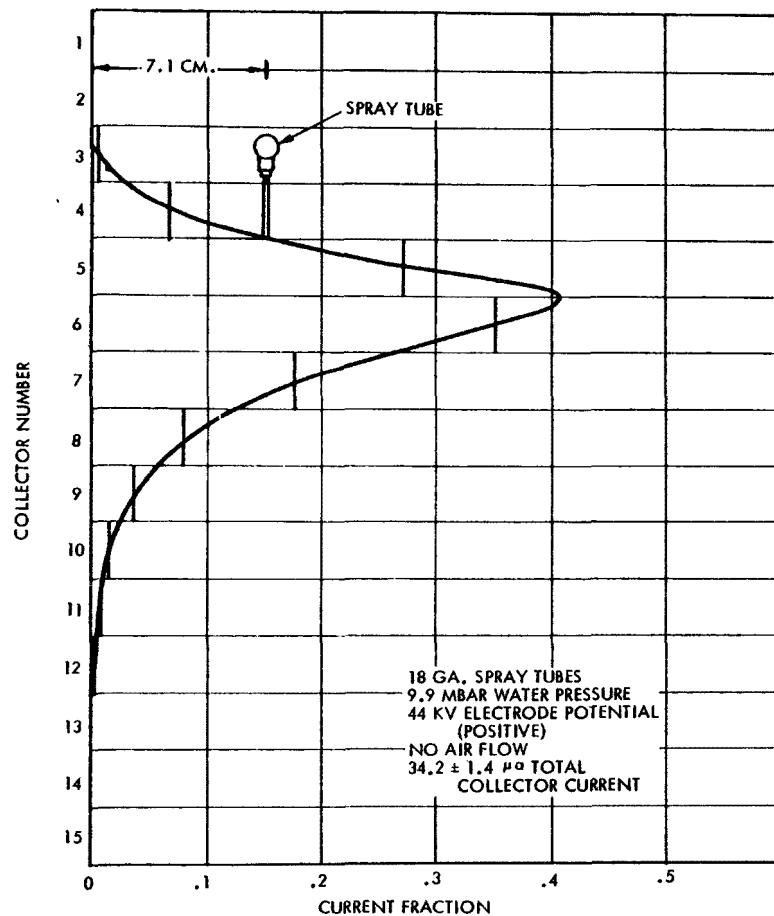


(c) Average of Four Tests

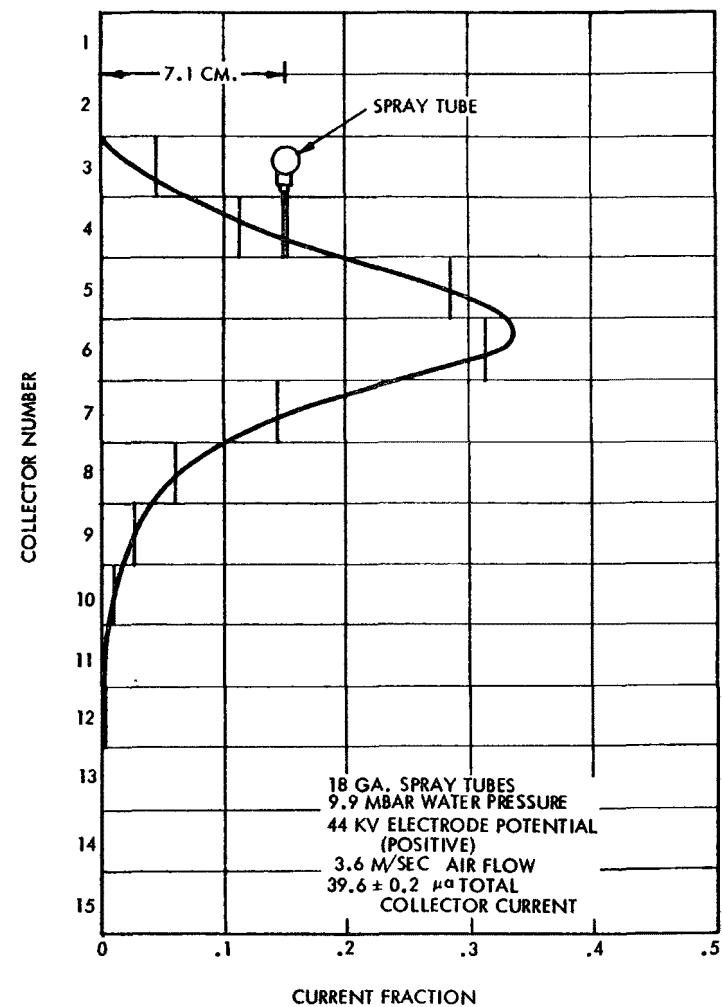


(d) Average of Two Tests

Figure 4-21. COLLECTOR CURRENT DISTRIBUTION FOR 18 GAUGE SPRAY TUBES. WALL-TO-ELECTRODE SPACING IS 7.14 CM. GRID LINES ARE AT CENTER OF COLLECTOR (Continued)

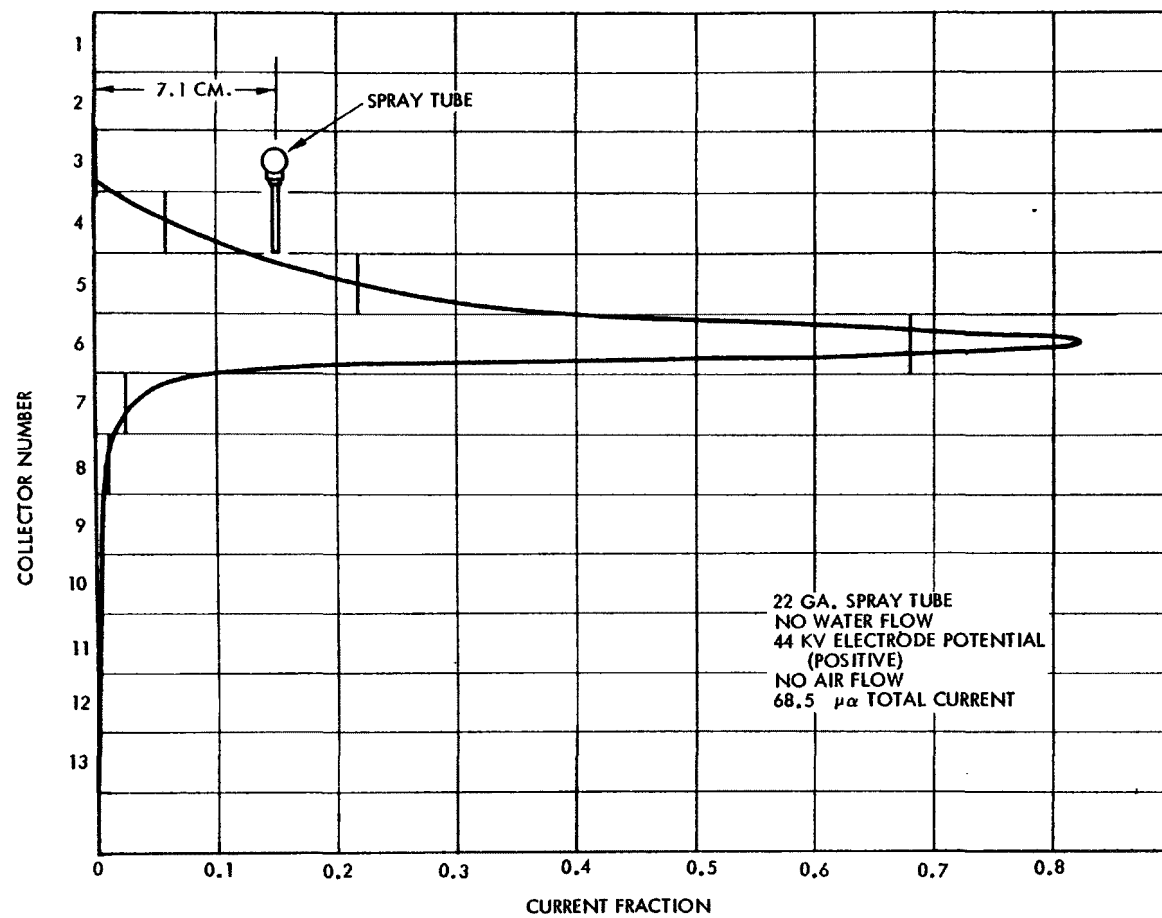


(e) Average of Two Tests



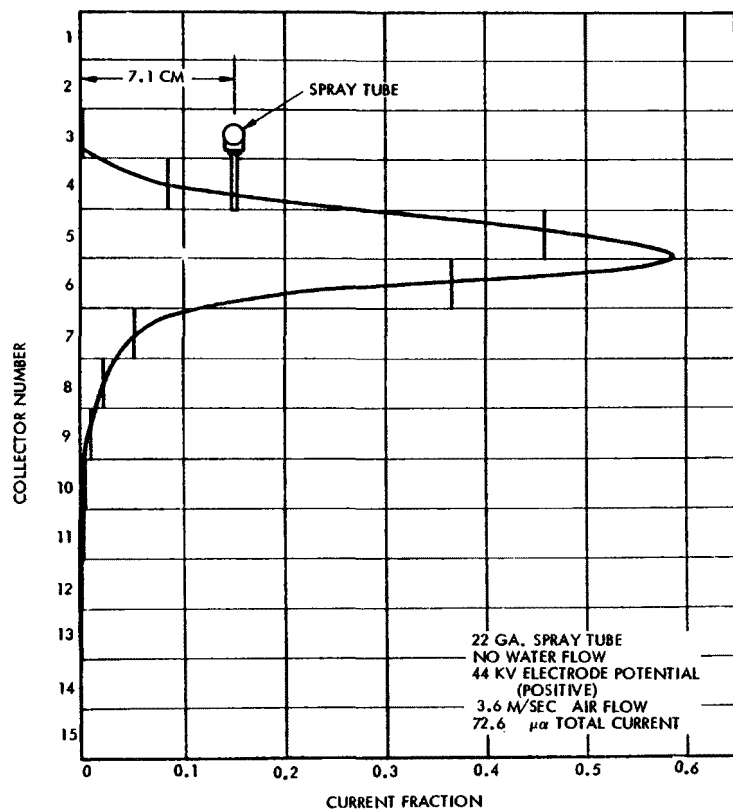
(f) Average of Three Tests

Figure 4-21. COLLECTOR CURRENT DISTRIBUTION FOR 18 GAUGE SPRAY TUBES. WALL-TO-ELECTRODE SPACING IS 7.14 CM. GRID LINES ARE AT CENTER OF COLLECTOR (Continued)

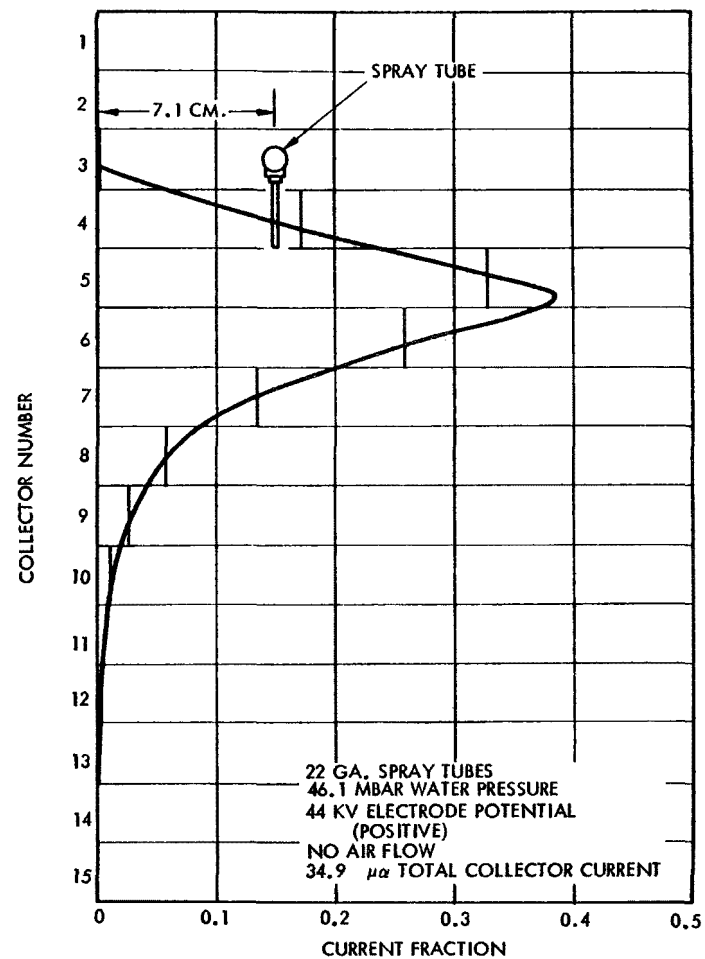


(a) Results of One Run

Figure 4-22. COLLECTOR CURRENT DISTRIBUTION FOR 22 GAUGE SPRAY TUBES. COLLECTOR-TO-ELECTRODE SPACING IS 7.14 CM. GRID LINES ARE CENTERED ON COLLECTORS



(b) Results of One Run



(c) Results of One Run

Figure 4-22. COLLECTOR CURRENT DISTRIBUTION FOR 22 GAUGE SPRAY TUBES. COLLECTOR-TO-ELECTRODE SPACING IS 7.14 CM. GRID LINES ARE CENTERED ON COLLECTORS (Continued)

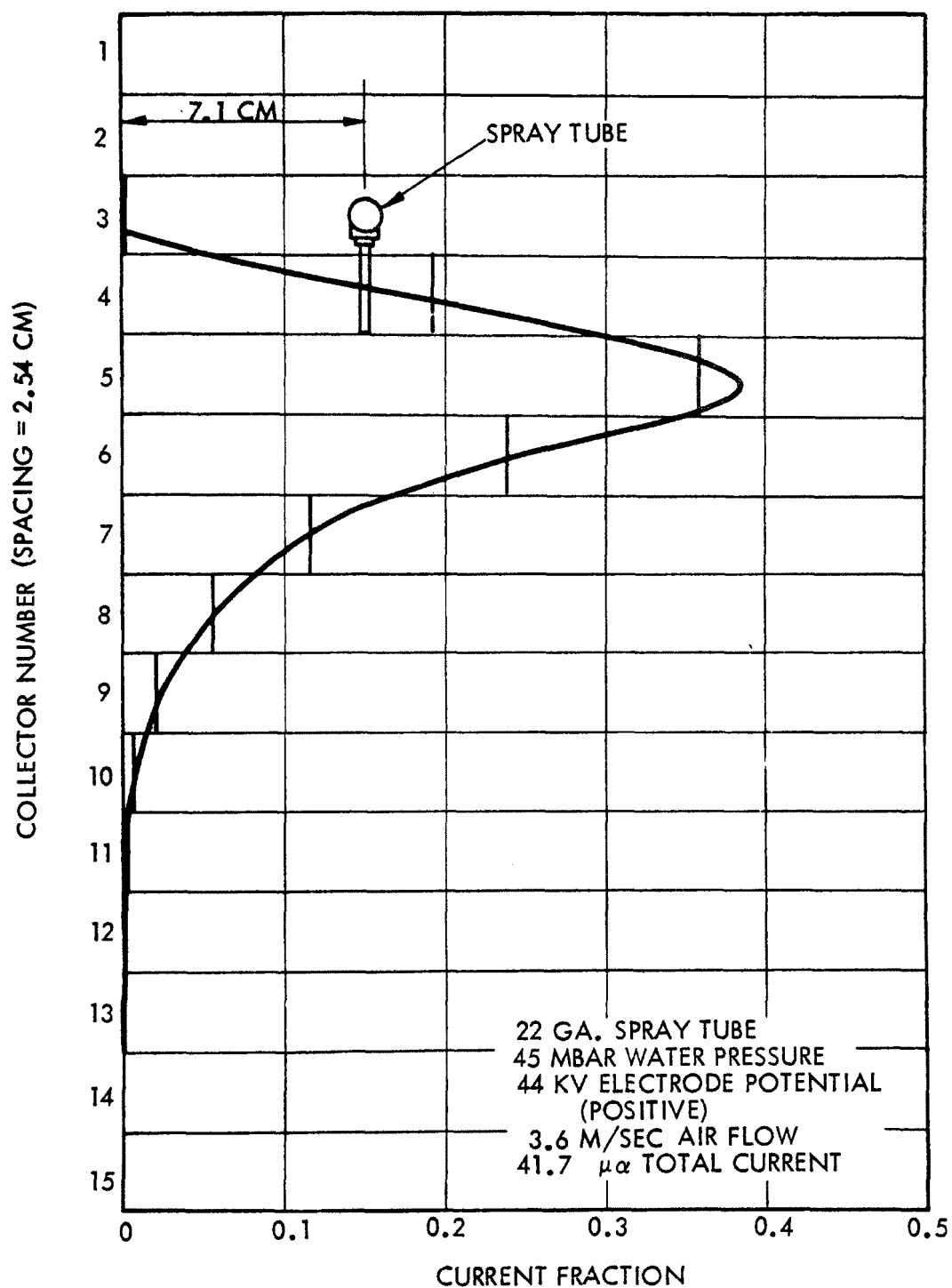


Figure 4-22. COLLECTOR CURRENT DISTRIBUTION FOR 22 GAUGE SPRAY TUBES. COLLECTOR-TO-ELECTRODE SPACING IS 7.14 CM. GRID LINES ARE CENTERED ON COLLECTORS (Continued)

The data from the 18 ga spray tubes, shown in Figure 4-21, indicate that the collected current with and without air flow is approximately the same when droplets are or are not present. The current distribution along the collector plates with droplets is different from that with ions only. This indicates that the presence of space charge associated with the droplets has redistributed the electrostatic field between the electrodes. An effect such as this could mean that there is an increase in space charge in the volume between the electrodes and with equal collector currents. The increase in space charge with droplets would mean that their mobility is smaller than the ions. There are several factors, however, which indicate that the difference in mobility of droplets from 18 ga spray tubes and ions is small. First, the droplets originate from a larger source than the ions as is shown in the photographs of droplet formation in this section. This tends to distribute the current over a large volume. Second, the current for droplets is distributed over only a slightly wider distance relative to the pure ion current, with its peak value depressed approximately 15 percent. The third factor is that the influence on total collected current with air flow is the same with and without droplets. Therefore, to a first approximation, a droplet originating from an 18 ga spray tube has the same mobility as an ion generated in a corona in air.

The current data from the 22 ga spray tubes, shown in Figure 4-22 indicate that the charged droplets originating from these tubes have a lower mobility than the ions. Therefore, droplets originating from a 22 ga tube have a smaller mobility than those from the 18 ga tube. The average droplet size from a 22 ga tube is smaller than that from the 18 ga and is expected to have a smaller mobility. The expected smaller mobility originates from the fact that at steady-state velocity, the accelerating force on a droplet is proportional to its radius squared whereas the drag force is proportional to the radius to a power of one to a value less than two.

The ion current from the 22 ga tubes is larger and more peaked than that from the 18 ga tubes. This is due to the high local field enhancement at the tube tips when operated at the same potential.

The effective length of droplet current to the collector wall is in the range of 2.5 to 3.0 times the distance between the spray tubes and collector wall. The droplet flux to the wall can be approximated by a segment of an ellipse with the centerline located near the spray tube tips. The geometry of the scrubber is near cylindrical close to the spray electrode and approaches planar at the collector walls. This accounts for the elliptical nature of the droplet spray pattern.

The 18 ga spray tube data were taken from multiple tests, so that data scatter could be calculated. As droplet flux increases, the scatter of the current data decreases. This may indicate that the water droplets, which carry a larger fraction of total current with increasing droplet flux, could be more stable in their space charge distribution characteristics than pure corona. The standard deviation of the total current with

four inches (9.9 mbars) of flow pressure is about 10 percent of that for no water flow. Since the pure corona current is about 30 percent variable, and assuming the effect is linear, the ratio of corona-to-droplet space charge at 9.9 mbars of pressure would be the same as the ratio of standard deviations, or about 30 percent. Since droplet and ion mobilities are about the same in this case, this would also be the ratio of corona-to-droplet currents.

4.2.2 Droplet Velocity

Droplet velocities were measured at four locations in the center plane of the research scrubber. The measurements were taken with both the 22 ga and 18 ga spray tubes. The measurement locations are identified by number in Figure 4-23.

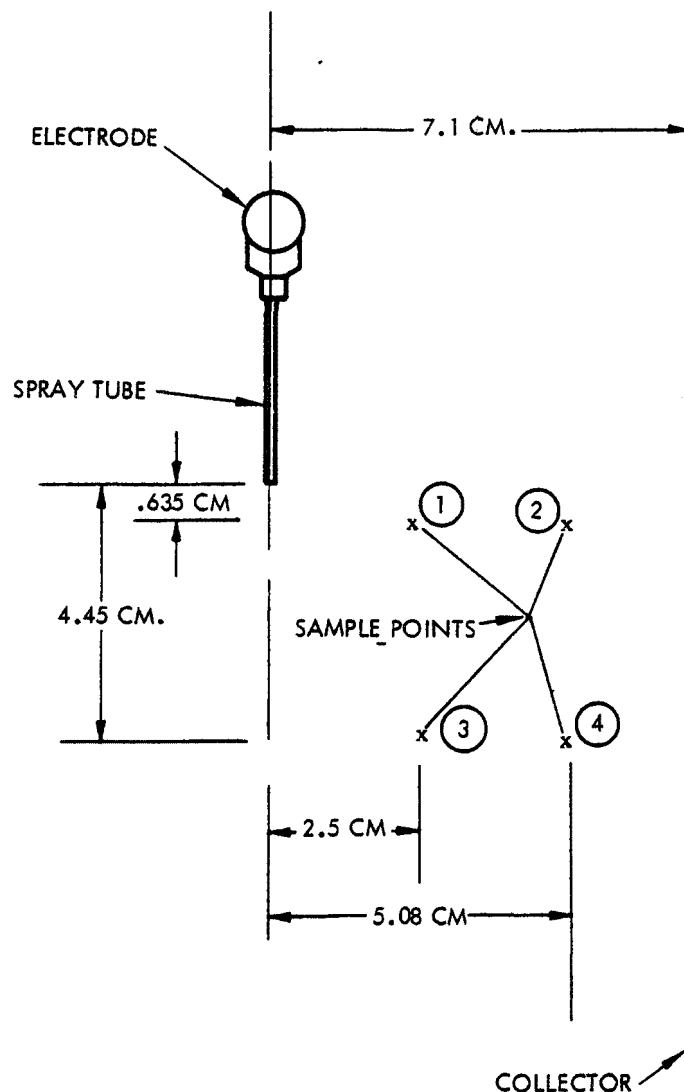


Figure 4-23. VELOCITY MONITORING LOCATIONS

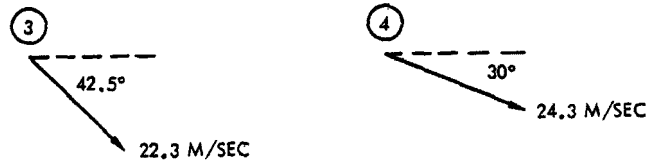
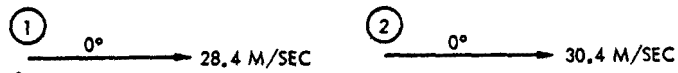
The velocities of the droplets were determined by monitoring the scattered light from individual droplets as described in Section 3. The monitored pulse was used to trigger a memory scope in which the signal was stored. A low frequency cut-off filter was used to prevent scope triggering from background noise. Because of the droplet size distribution and the range of angles out of the vertical plane normal to the collector at which droplets passed through the fringes, a large range of droplet velocities was observed. The maximum measured drift velocities of droplets and their direction relative to the horizontal are shown in Figures 4-24 and 4-25. These velocities were determined from the most prevalent peak frequency measured at each location. Between 200 and 250 traces were examined to identify the droplet velocity and most probable trajectory.

The angle of the droplets relative to the horizontal was determined by first rotating the laser and beam splitter to a position in which no signals would trigger the scope. The most probable trajectory was then found at approximately 90° from this location.

A photograph of a typical high frequency droplet velocity scan is shown on Figure 4-26. The conditions are those shown in Figure 4-25 at sampling location number two. A low frequency sweep of a droplet passing through the fringe volume is shown in Figure 4-27. The effect of the low frequency cut-off filter in the monitoring circuit can be seen in this figure. The entire dc component on the trace has been filtered. As the droplet passes into the grating, the scattering is occurring from an increasingly larger portion of the droplet surface and from an increasing number of fringe lines. This accounts for the increasing amplitude in the signal as the droplet passes into the fringe pattern and the diminishing amplitude as it is moving out. There are 45 visible cycles in the photograph which is essentially the same as the number of fringes in the grating.

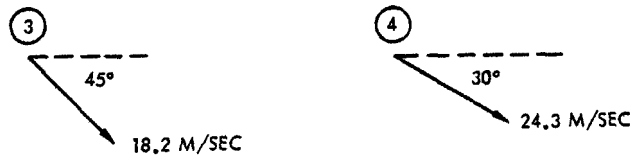
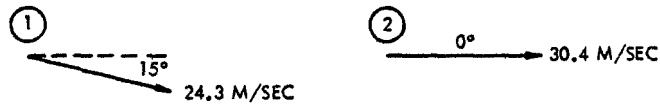
As can be seen in Figures 4-24 and 4-25 the droplets for both spray tube sizes reached the same terminal velocity and had the same relative angle prior to colliding with the collector. At position (1), that closest to the spray tube, there is a difference in both velocity and angle for the droplets from the two spray tubes. This is due to the condition that the droplets are formed closer to the spray tube tip for the 22 ga tube and these droplets are smaller. The electrostatic field lines from the tube tip are more nearly normal to the collector than those passing through regions below the tip. This accounts for the 22 ga tube droplets traveling normal to the collector while the 18 ga tube droplets are at an angle. Since the droplets from the 22 ga tube are smaller, they are accelerated to their terminal velocity faster. Thus, their velocity near the tube will be faster than the 18 ga tube droplets. The same effects also apply at position (3).

An interesting result of the data is that the terminal velocity of droplets from both the 22 ga and 18 ga spray tubes are the same to within



WATER PRESSURE = 46 MBARS
 OPERATING VOLTAGE = 40 KV
 (n) - SAMPLE LOCATION

Figure 4-24. VELOCITY PROFILE - 22 GAUGE SPRAY TUBE



WATER PRESSURE = 8.7 MBARS
 OPERATING VOLTAGE = 40 KV
 (n) - SAMPLE LOCATION

Figure 4-25. VELOCITY PROFILE - 18 GAUGE SPRAY TUBE

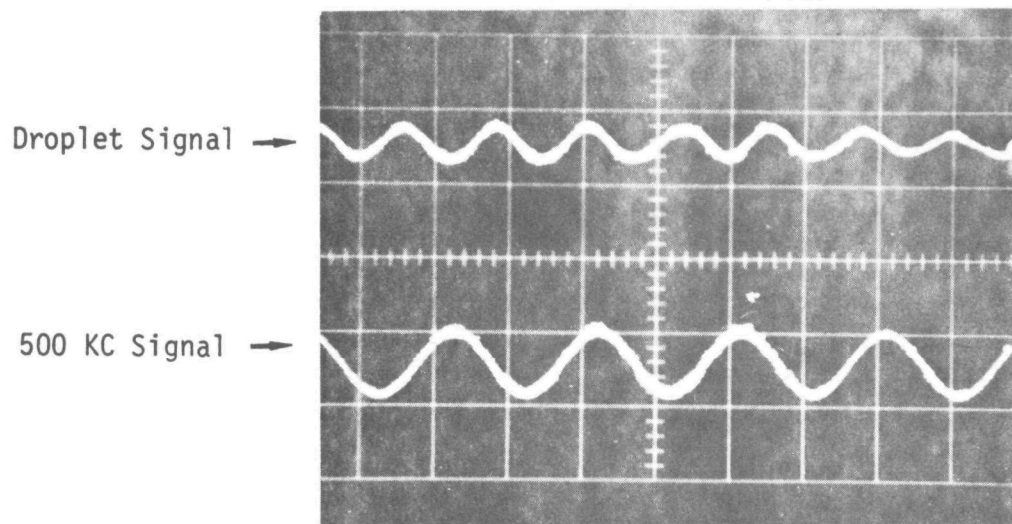


Figure 4-26. HIGH FREQUENCY SWEEP

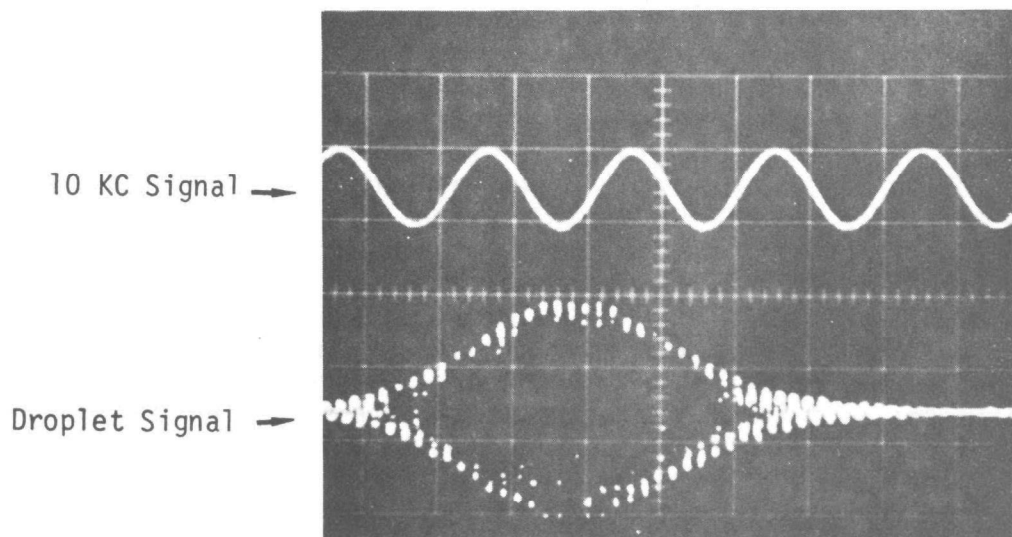


Figure 4-27. LOW FREQUENCY SWEEP

the experimental accuracy. The terminal velocity of a droplet charged to the Rayleigh limit in an ambient electrostatic field is

$$U = \left[\frac{16E}{\delta C_D} \left(\frac{\epsilon_0 \sigma}{S} \right)^{1/2} \right]^{1/2} \quad (4-39)$$

where E = ambient electrostatic field
 δ = density of air
 ϵ_0 = permittivity of free space
 σ = surface tension
 S = radius of the droplet
 C_D = drag coefficient of the droplet in air

and

$$C_D = \frac{F_d}{\frac{\delta U^2}{2} A_p}$$

F_D = drag force

A_p = droplet projected area = πS^2

U = droplet velocity

In the Stokes flow region ($N_{Re} \leq 2$),

$$C_D = \frac{24}{N_{Re}} \quad (4-40)$$

where the Reynolds number (N_{Re}) is

$$N_{Re} = \frac{2S\delta U}{\mu}$$

and μ = viscosity of air

The velocity equation, in the Stokes flow regime, is:

$$U = \frac{4E}{3\mu} (S \epsilon_0 \sigma)^{1/2} \quad (4-41)$$

This indicates that the velocity of a droplet is proportional to the square root of its diameter. The velocimeter data showed a droplet Reynold's number of 224 for a 120 micron diameter droplet, and half this for a 60 micron diameter droplet. This is in the intermediate flow regime.

The drag coefficient in the intermediate flow regime can be approximated by

$$C_D = 18.5/N_{Re}^{0.6} \quad (4-42)$$

The droplet velocity can be expressed, from Equation (4-39), as:

$$U = \left[\frac{1.311 E S^{0.1}}{\delta^{0.4} \mu^{0.6}} (\epsilon_0 \sigma)^{0.5} \right]^{5/7} \quad (4-43)$$

The droplet velocity in the intermediate flow regime is proportional to the droplet diameter to the 0.071 power. This relationship means that a factor of two in droplet diameter results in approximately a 5 percent change in velocity.

The measured velocity of droplets from both size spray tubes was the same at locations (2) and (4). At locations (1) and (3), the measured velocities were lower for droplets from the 18 ga spray tube. Since it is assumed that these droplets are larger than those from the 22 ga tubes, they will accelerate to their terminal velocity at a slower rate. The equation of motion of a charged droplet in an ambient field is:

$$M \frac{dU}{dt} = Eq_D - C_D \frac{\delta U^2}{2} A_p \quad (4-44)$$

where M = mass of the droplet
 q_D = droplet charge

In terms of the droplet properties, and assuming the droplet is charged to the Rayleigh limit, Equation (4-44) can be expressed as:

$$\frac{dU}{dt} = \frac{3}{\rho_D S} \left[\frac{2E (\sigma \epsilon_0)^{1/2}}{S^{1/2}} - \frac{C_D \delta U^2}{8} \right] \quad (4-45)$$

where ρ_D = mass density of the droplet

At low velocities, the acceleration of a droplet is inversely proportional to its radius to a power greater than one. This indicates that a longer time is required for the larger droplets to reach their terminal velocity and accounts for the data at positions (1) and (3).

Equation (4-45) has been integrated numerically over a range of velocities from zero to 30 meter/sec. The corresponding path length range was to about 16 centimeters. The integration has been done for both 60 micron and 120 micron diameter water droplets in an ambient electrostatic field of 5×10^5 volts/meter and moving in ambient air. The results are shown in Figure 4-28. The 60 micron droplet has nearly reached its terminal velocity of 30.5 ft/sec after a path length of 0.1 meter, whereas a 120 micron droplet has not yet reached its terminal velocity of 32.0 m/sec. It would thus appear that those droplets which are nominally sized for effective scrubbing, having diameters of 120 microns or more, do not reach their terminal velocity in a scrubber of 0.1 meter half width. They will, however, closely approach the observed 30 meters per second.

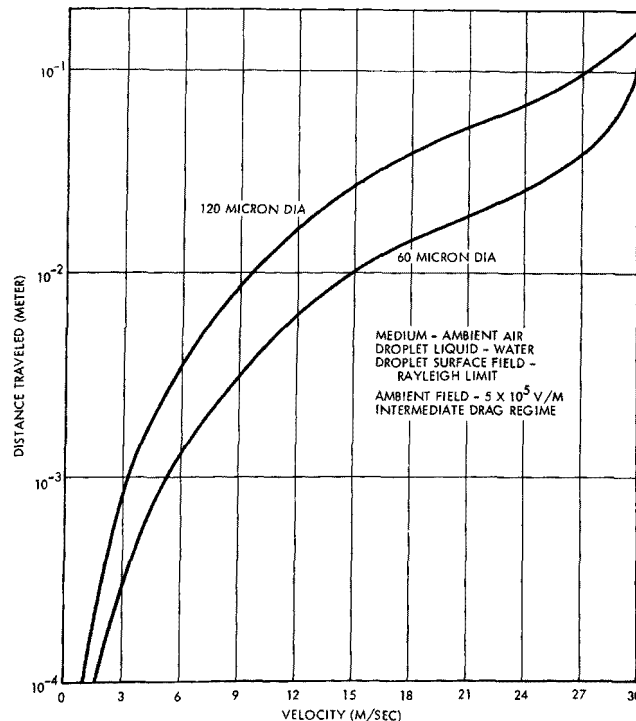


Figure 4-28. VELOCITY PROFILE FOR DROPLETS CHARGED TO THE RAYLEIGH LIMIT

4.2.3 Droplet Formation

Enlarged photographs of the scrubbing volume around a spray tube tip were made in the research scale scrubber, as described in Section 3.2. These photographs gave qualitative information on droplet formation mechanisms, and quantitative information on droplet size distributions and number density distributions.

Of the many photographs taken twelve were selected for study and analysis. Of these, eight were taken with 22 gauge spray tubes and four with 18 gauge spray tubes. The operating parameters for the first eight photographs, with 22 gauge spray tubes, are shown in Table 4-2. The photos themselves are seen in Figures 4-29 through 4-36.

Table 4-2. PARAMETERS FOR 22 GAUGE SPRAY TUBE
PHOTOGRAPHS - FIGURES 4-29 THROUGH 4-36.

Figure Number	Electrode Voltage (KV)	Electrode Spacing (meter)	Feed Water Pressure (m bar)
4-29	28	.092	10
4-30	28	.092	25
4-31	29	.092	30
4-32	28	.092	45
4-33	44	.143	20
4-34	29	.092	36
4-35	29	.092	36
4-36	28	.092	45

The photographs are revealing of the mechanisms by which charged droplets are formed in electrohydrodynamic spraying. The water drops are usually not formed directly at the tube tip, but rather the water is drawn out in a filament from the spray tube under the influence of the electrostatic field. The filament is formed from a meniscus which generally wets the outside of the spray tube. Thus the size of the filament will be determined by the outer diameter of the tube and the water flow rate. The filament is constantly changing position and configuration, as it is driven by fluctuations in local field due to space charge. The movement of the filaments results in bending and breaking, leaving columns of charged liquid moving in space. These charged columns will then break up into droplets which spray off the ends of sharp kinks that may form along its length by means of the action of electrostatic forces. The charge on a filament will concentrate at the locations of these sharp points. As charge and mass are removed from a filament it becomes smaller, thinner and less active. Eventually the residual mass becomes a large droplet. As a filament sprays off droplets,

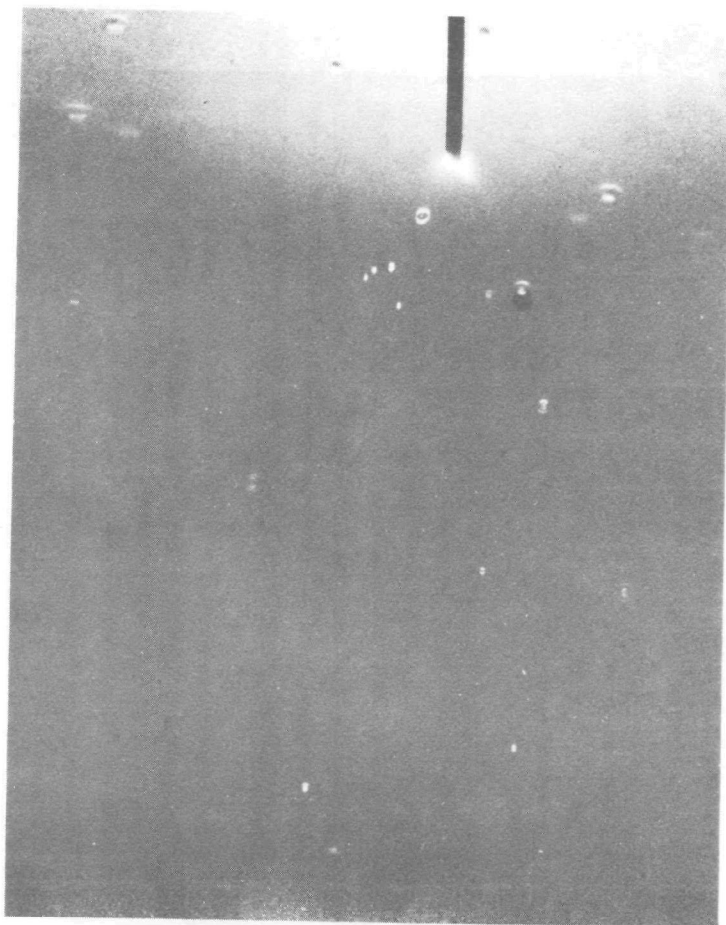


Figure 4-29. END SPRAY TUBE, 22 GAUGE,
4 INCH WATER PRESSURE

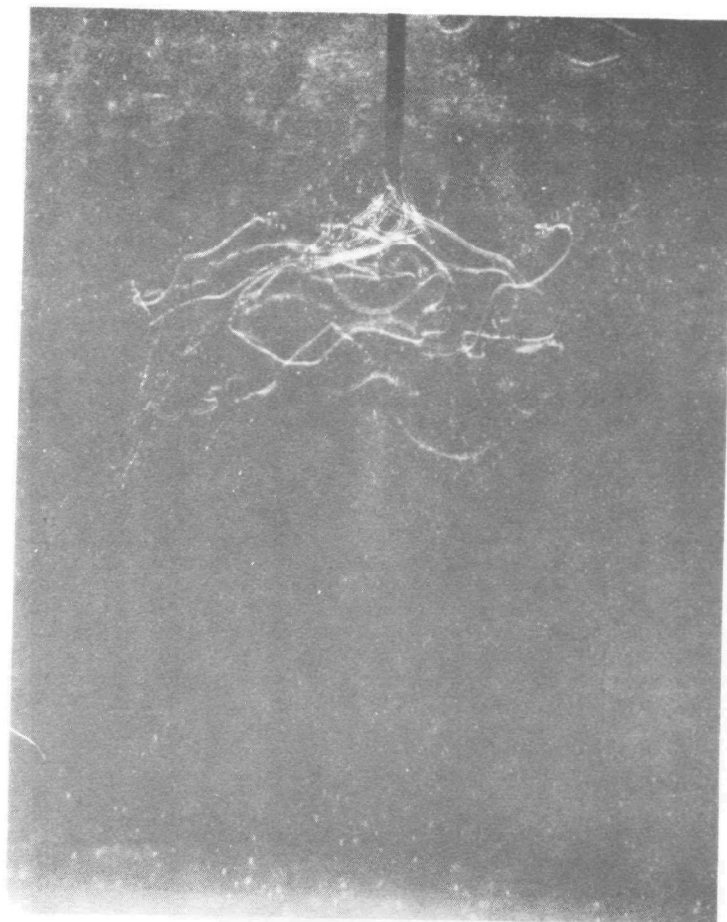
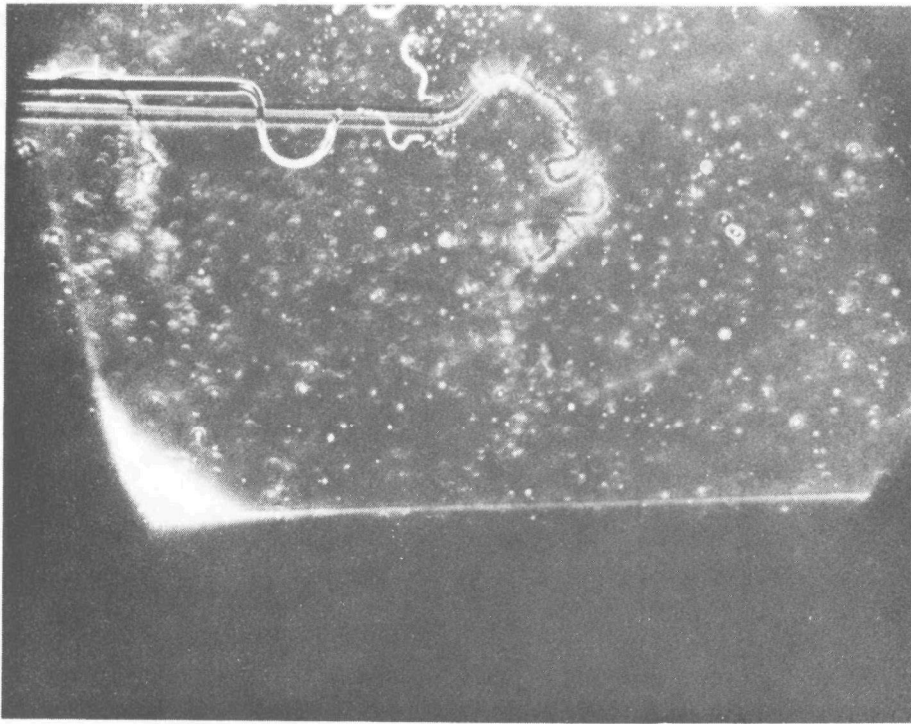


Figure 4-30. END SPRAY TUBE, 22 GAUGE, 10 INCH
WATER PRESSURE, 1/15 SEC EXPOSURE
WITH 70 FLASHES PER SECOND



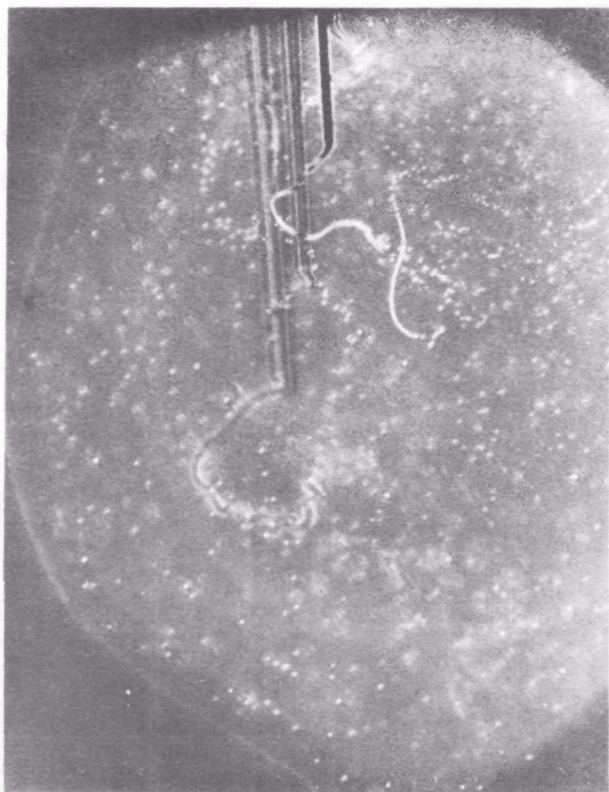


Figure 4-33. END SPRAY TUBE, 22 GAUGE,
8 INCH WATER PRESSURE. 133
DROPLETS COUNTED.

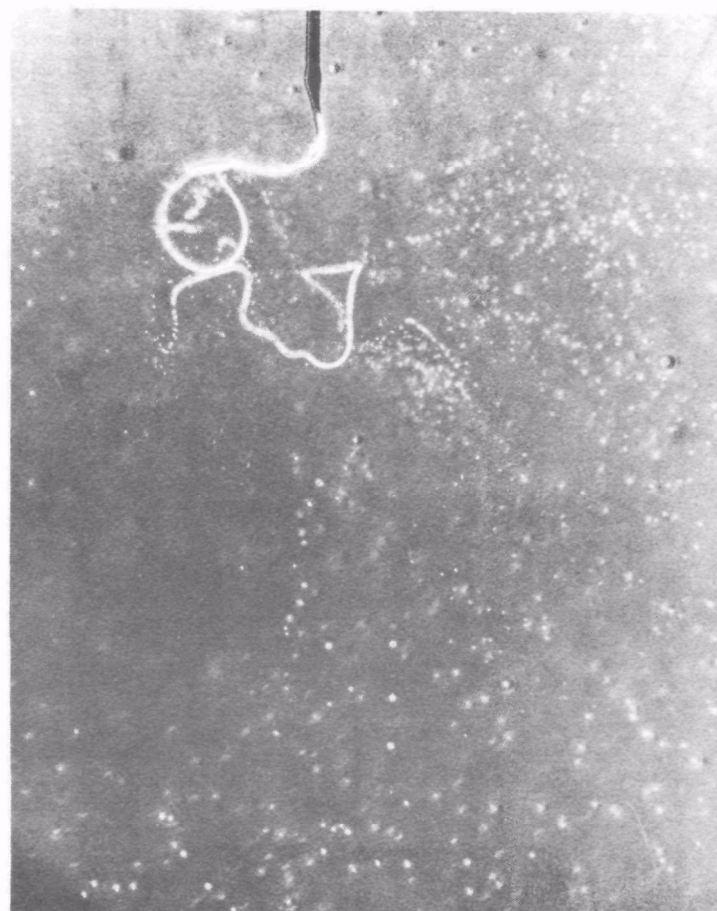


Figure 4-34. END SPRAY TUBE, 22 GAUGE,
14.5 INCH WATER PRESSURE.
159 DROPLETS COUNTED.

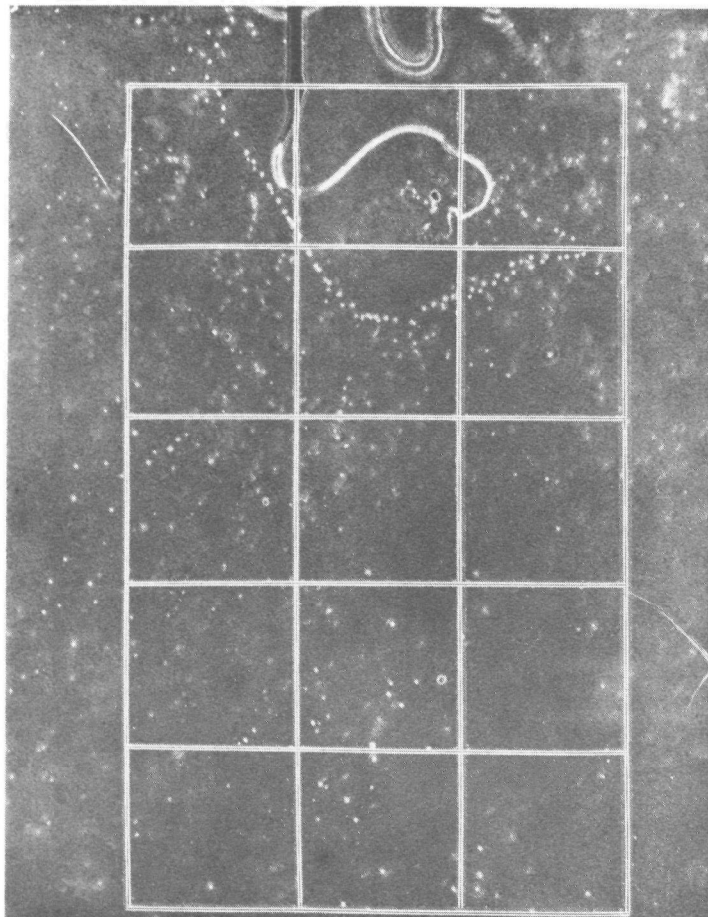


Figure 4-35. END SPRAY TUBE, 22 GAUGE, 14.5 INCHES WATER PRESSURE. GRID OVERLAY FOR COUNTING DROPLETS. 165 DROPLETS COUNTED.

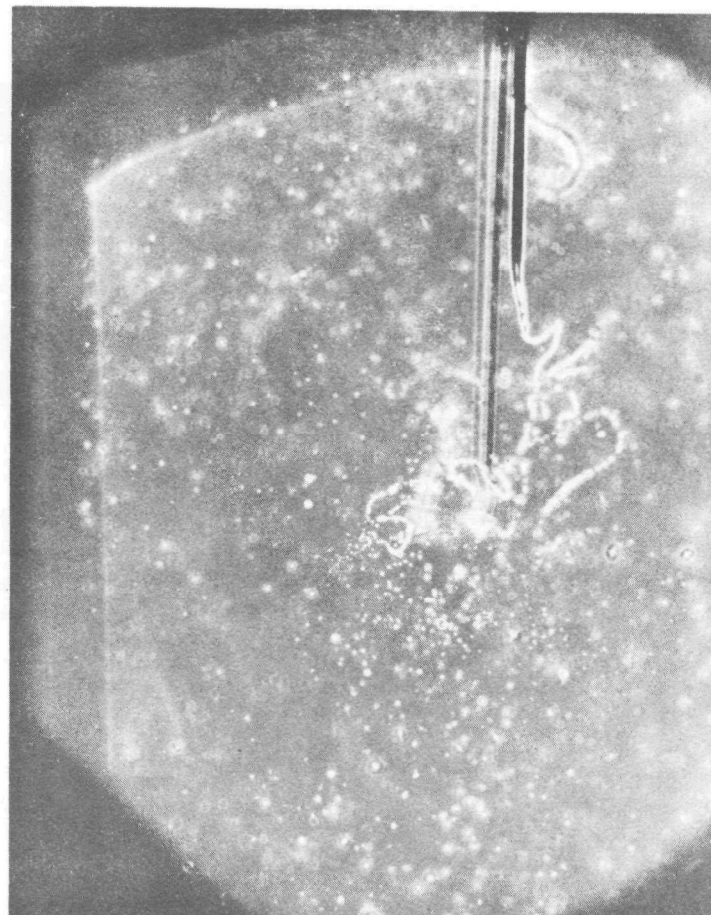


Figure 4-36. SECOND SPRAY TUBE, 22 GAUGE, 18 INCH WATER PRESSURE, WETTING AGENT IN THE WATER. 150 DROPLETS COUNTED.

the space charge produced will modify the local electric field and act to drive the filament away from the area.

The flow tube shown in Figure 4-29 is underfed with liquid. In this case, excessive corona develops at the tube tip. The formation field is reduced by the corona space charge, so that the liquid is extracted from the tip as large droplets rather than as a filament.

Under higher feed pressures, more charge goes into the liquid and less into corona. Droplet formation from filaments is predominant. Figure 4-30 shows how these filaments move about in space under the action of local fields so that droplets are uniformly distributed through space. The figure is a multiple exposure of a liquid filament at the tube tip. The film exposure is 1/15 second with a flash repetition rate of 70 per second.

The photograph shown in Figure 4-31 illustrates the break-up of a section of liquid filament that separated from the main column. The droplets formed in the section are separating in an alternating sequence, indicating that there is a repulsive force between them. The size of the smaller droplets is in the range of 60 to 130 micron diameter, while the larger ones are in the range of 600 to 800 microns. Another break is occurring at a kink in the filament above the droplet forming section. The filament diameter changes abruptly across this kink, indicating a greater liquid flow rate out of the lower portion of the filament.

The exposures shown in Figures 4-32 and 4-36 are for water containing a wetting agent. The water filament break-up is similar to that of Figure 4-31 for water without a wetting agent. However, both the filament and droplet size are larger for the water containing the wetting agent. This condition is predicted from the Rayleigh criterion, Equation (4-5), because of the lower liquid surface tension.

The photographs shown in Figures 4-33 through 4-36 were used in obtaining droplet size distributions and number densities. The photographs in Figures 4-33 and 4-34 illustrate the early stages of the break-up of filament sections. The droplets are just starting to emanate from the ends of the sections.

The exposure in Figure 4-35 shows a liquid column that has disintegrated completely into droplets. This figure also shows the grid overlay that was used in the droplet counts, to obtain number density distribution data.

The operating parameters for the four cases of 18 gauge spray tube performance are shown in Table 4-3. The photographs themselves are shown in Figures 4-37 through 4-40. In each of these the focus is on the center tube of the five tube array.

Table 4-3. PARAMETERS FOR 18 GAUGE SPRAY TUBE
DROPLET PHOTOGRAPHS - FIGURES 4-37
THROUGH 4-40

Figure Number	Electrode Voltage (KV)	Electrode Spacing (meter)	Feed Water Pressure (m bar)
4-37	42	.143	1.25
4-38	42	.143	0.50
4-39	42	.143	3.75
4-40	41	.143	12.50

Figure 4-38 shows several large droplets which illustrate the existence of a large-diameter tail to the droplet size distribution. Also visible are Rayleigh-type instabilities on the surface of the liquid meniscus, which in this case has enveloped all of the visible tube area. While not an important droplet-forming mechanism, these meniscus instabilities do indicate local field strength.

Figure 4-39 shows a multiply kinked filament which has already broken into five equally sized segments. All of the 18 gauge pictures indicate the presence of a large-diameter tail on the droplet distribution, or possibly even a large-diameter mode.

Figures 4-38 through 4-40 were used to obtain droplet size distribution and number density data.

4.2.4 Droplet Size Distribution

During the formation process, droplets are sprayed from the tips or the kinks of liquid filaments of varying sizes, or are formed from the residuals of filaments which have broken up and dropped below critical surface field strength. The sizes of these filaments are not constant, but should be statistically distributed with parameters depending on scrubber configuration and operating parameters. This should also be true of the resulting droplet sizes, and this was verified with an analysis of droplet size classification.

The two electrode voltages used were 29 kv and 44 kv, and were used with collector wall spacings which resulted in an average ambient field strength of about 6 kv/cm. The droplet size distributions obtained were consistent with what is expected for maximum formation field strength (Rayleigh limit).

For a 22 gauge spray tube, the water flow rate condition of Figure 4-35 is the optimum range. This optimum is determined by droplet size, charge



Figure 4-37. CENTER SPRAY TUBE, 18 GAUGE,
0.5 INCH WATER PRESSURE

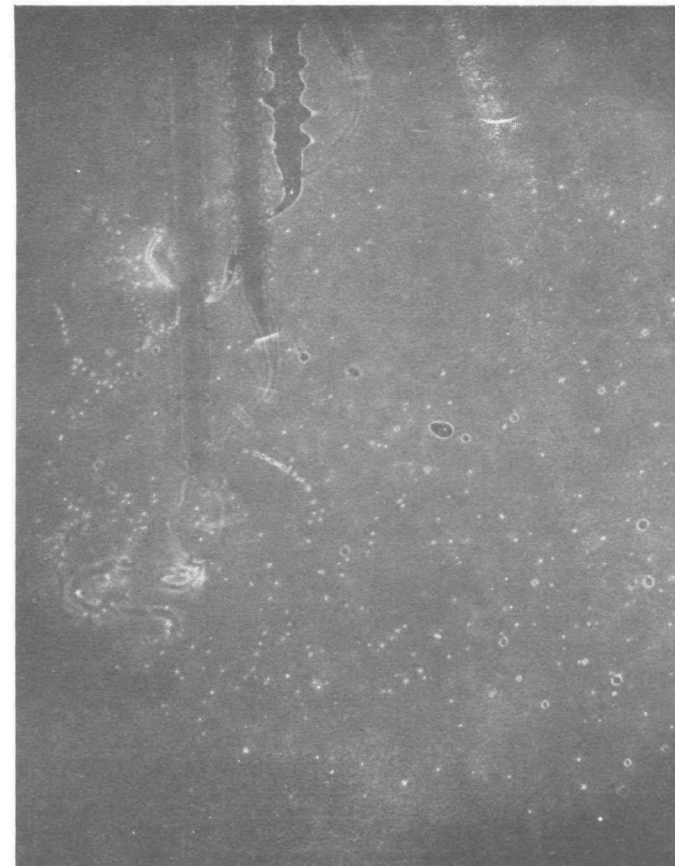


Figure 4-38. CENTER SPRAY TUBE, 18 GAUGE,
0.2 INCH WATER PRESSURE. 150
DROPLETS COUNTED.



Figure 4-39. CENTER SPRAY TUBE, 18 GAUGE,
1.5 INCH WATER PRESSURE.
70 DROPLETS COUNTED.

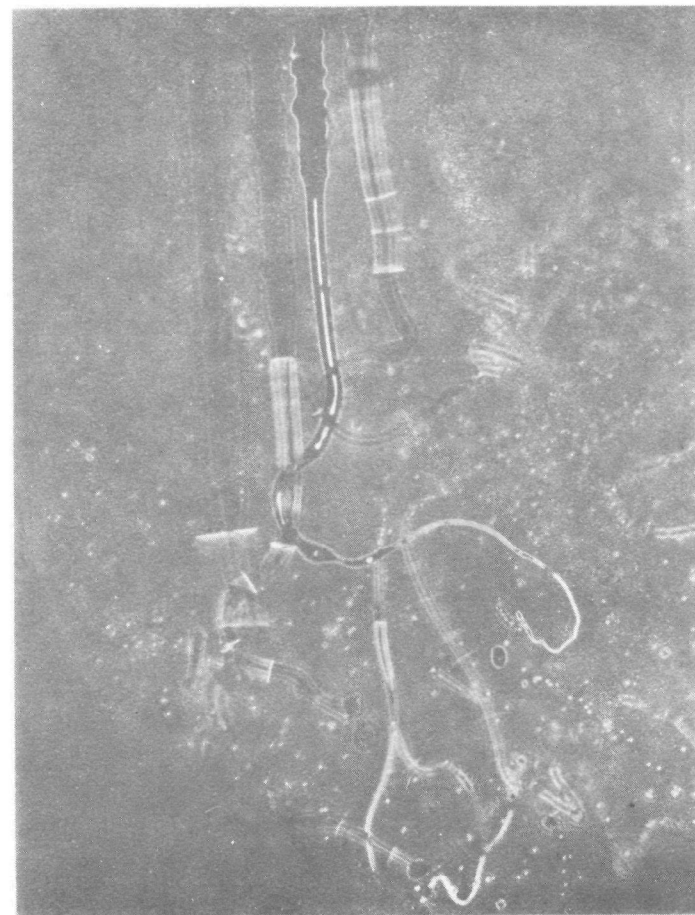


Figure 4-40. CENTER SPRAY TUBE, 18 GAUGE,
5 INCH WATER PRESSURE.
79 DROPLETS COUNTED.

and number density. Figure 4-41 is a histogram plot of the normalized frequency function for droplet radius for this photograph. The normalization was chosen so that the total area under the histogram is unity. The unequal size classifications accentuate the structure of the low end of the distribution. The distribution is possibly bimodal; a supposition which is supported by data from the other photographs. In this case, the smaller mode is around 43 microns. The larger mode is around 57 microns, which is near the optimum droplet diameter. A third mode in the 400-500 range is possible, but has not been confirmed.

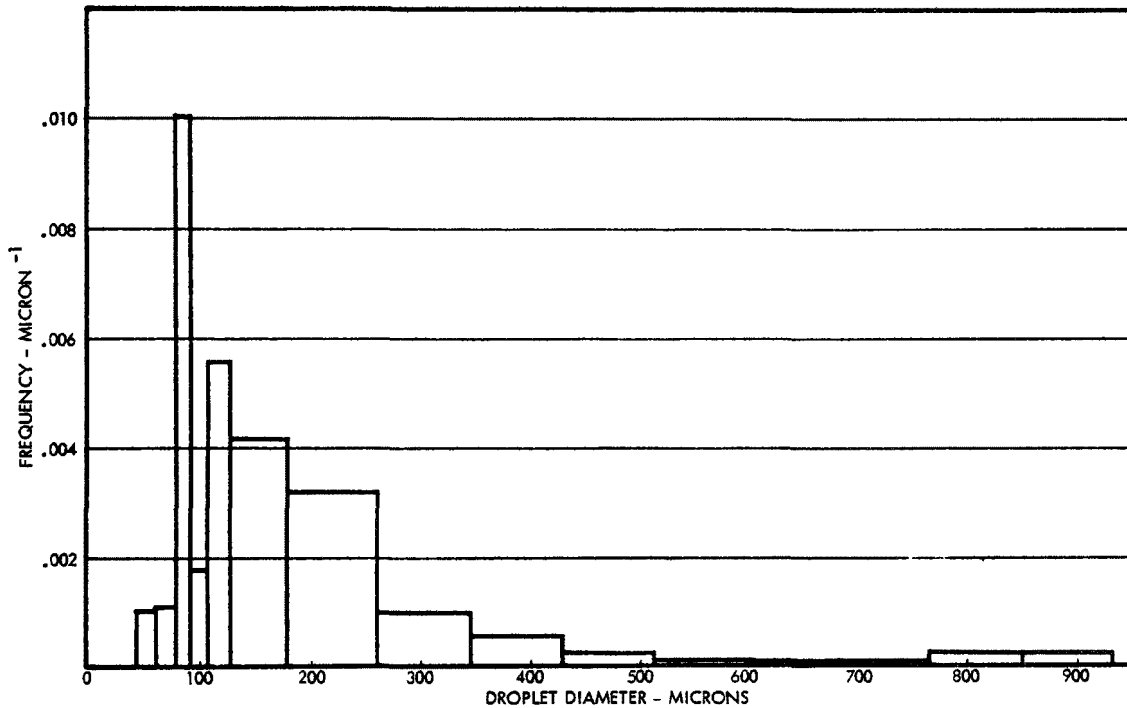


Figure 4-41. HISTOGRAM OF THE NORMALIZED FREQUENCY FUNCTION FOR DROPLET RADIUS. 22 GAUGE SPRAY TUBE, 14.5 INCH WATER PRESSURE, 29 KV ELECTRODE VOLTAGE, 3-5/8 INCH ELECTRODE-WALL SPACING.

Figure 4-42 shows the radius distribution function plotted on log-probability scales. The upper-concaveness of the curve is seen also in distribution plots of some of the other photographs. The distribution is a good fit to a log-normal distribution, represented by a straight line on these scales. The straight line representations for these data were sight-drawn.

The log-normal distribution of droplet radius may be represented as follows:²²

$$\int_0^S f(S') dS' = \text{erf}(t) \quad (4-45)$$

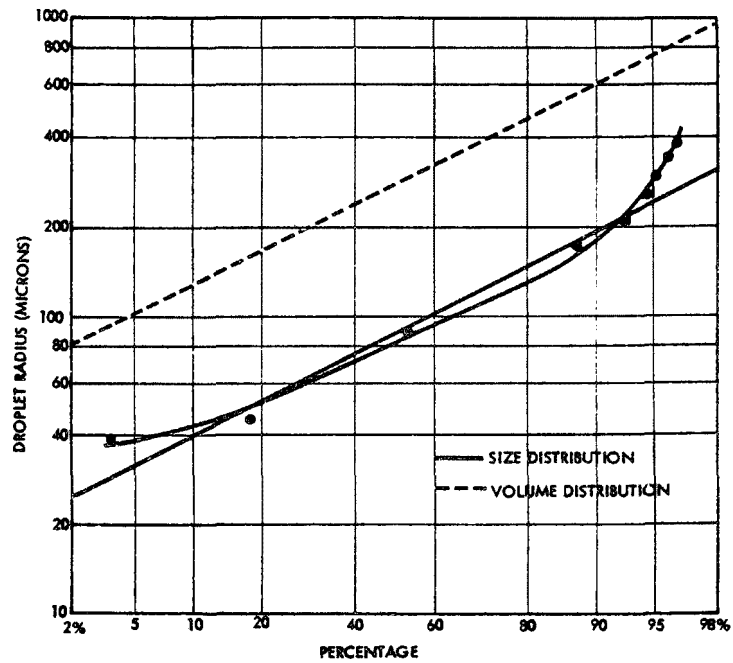


Figure 4-42. PERCENTAGE NUMBER OF DROPLETS LESS THAN A GIVEN RADIUS FROM THE DISTRIBUTION OF FIGURE 4-35. SCALES ARE LOG-PROBABILITY. THE STRAIGHT LINE IS A LOG-NORMAL APPROXIMATION.

$$\begin{aligned}
 S &= \text{droplet radius} \\
 \text{erf} &= \text{error function} \\
 t &= (\ln S - \ln \bar{S}_g) / \ln \sigma_g
 \end{aligned}$$

A volume or mass distribution function for the log-normal radius distribution may be simply expressed as

$$\frac{1}{\bar{S}^3} \int_0^S (S')^3 f(S') dS' = \text{erf}(t - 3 \ln \sigma_g) \quad (4-46)$$

On log-probability scales, this distribution also plots as a straight line, parallel to the corresponding radius distribution and above it by a factor of $\exp(3 \ln^2 \sigma_g)$. For the straight-line approximation of Figure 4-42, the volume distribution shows that 90 percent of the volume contained in the droplets resides in droplets of radius greater than 125 microns. This is one measure of efficiency of water usage, but not as significant as one which is weighted with droplet velocity (Section 1.3).

For an 18 gauge spray tube, the operating conditions of Figure 4-40 are in the optimum range. Figure 4-43 shows the droplet radius distribution for this photo on log-probability scales. Here the data is uniformly scattered about a straight line.

Two parameters are needed to define a log-normal distribution. The standard definitions are in terms of the following.

$$\bar{S}_g = 50\% \text{ value} : \text{geometric mean} \quad (4-47)$$

$$\sigma_g = \frac{84.1\% \text{ value}}{50\% \text{ value}} : \text{geometric standard deviation}$$

Other distribution parameters may then be found as follows:

$$\bar{S} = \bar{S}_g \exp (1/2 \ln^2 \sigma_g) : \text{mean} \quad (4-48)$$

$$\bar{S}_p = \bar{S}_g \exp (-\ln^2 \sigma_g) : \text{mode, or most-probable value}$$

$$(\bar{S}^3)^{1/3} = \bar{S}_g \exp (3/2 \ln \sigma_g) : \text{mass-mean}$$

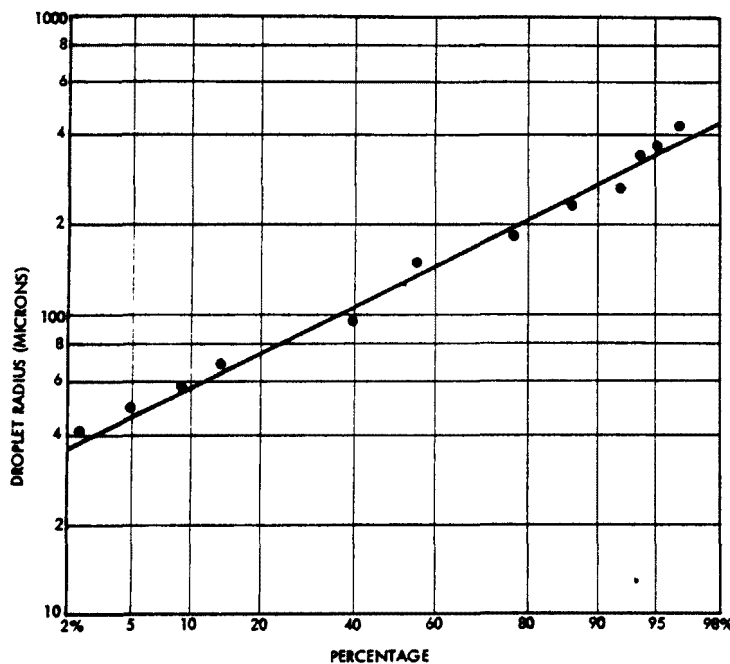


Figure 4-43. PERCENTAGE NUMBER OF DROPLETS LESS THAN A GIVEN RADIUS, FROM THE DISTRIBUTION OF FIGURE 4-40. SCALES ARE LOG-PROBABILITY.

Log-normal distribution parameters were taken from the straight-line fits of Figures 4-42 and 4-43, and are presented in Table 4-4. The most descriptive or useful parameters are the modal value and the mass mean value. These are given for 22 gauge spray tubes in Table 4-5, and 18 gauge spray tubes in Table 4-6. These tables show the best straight-line log-normal fit for each of the photos which were counted.

Table 4-4. DISTRIBUTION PARAMETERS FOR FIGURES 4-35 and 4-40

Figure Number	4-35	4-40
Modal radius (microns)	59	88
Mass-mean radius (microns)	156	212
Geometric mean radius (microns)	88	125
Mean radius (microns)	105	149
Geometric standard deviation	1.86	1.81
Sample size	165	79
Spray tube OD (mm)	.712	1.27
Spray tube ID (mm)	.39	.84

Table 4-5. DISTRIBUTION PARAMETERS FOR 22 GAUGE SPRAY TUBE COUNTS

Figure Number	Sample Size	Modal Radius (micron)	Mass-Mean Radius (micron)
4-33	133	99.7	246
4-34	159	49.7	139
4-35	165	59.0	156
4-36	150	72.1	258

Table 4-6. DISTRIBUTION PARAMETERS FOR 18 GAUGE SPRAY TUBE COUNTS

Figure Number	Sample Size	Modal Radius (micron)	Mass-Mean Radius (micron)
4-38	150	82.9	232
4-39	70	47.6	209
4-40	79	88.0	212

The similarity should be noted between the most probable droplet sizes given in the above tables and the theoretical Rayleigh limit droplet size as calculated from Equation (4-5). The Rayleigh limit is calculated using a field strength corresponding to the local formation field. This is the same as the local breakdown field with Peek's correction for the radius of curvature of the spray tube. The droplet radius should be roughly proportional to the spray tube radius. The expected Rayleigh radius for droplets formed from a 22 gauge spray tube is 40 to 60 microns.

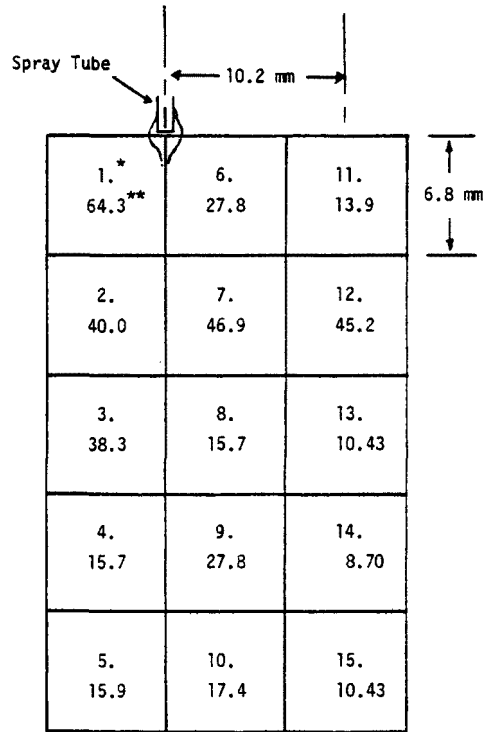
4.2.5 Droplet Flux

Droplet counts from the seven photos listed in Tables 4-2 and 4-3 were also analyzed for droplet number densities. Figure 4-35 shows the spatial grid lines dividing the scene volume into cells used for counting. The cells are .68 cm on a side, and the depth of each cell is the depth-of-field of the camera lens.

The camera was set at F/8 with a 370 mm aperture. The camera objective was about 54 cm from the spray tube tip being photographed. The depth-of-field for the picture under these conditions was calculated to be 1.25 cm.

The average droplet number density, as counted, is based on a spatial average at the given instant of time that the picture was taken. What is really needed for the volume flow rate calculation is a time average density for each point in space. The assumption is made that the spatial average is independent of time, thus introducing some errors of unknown magnitude. These are just errors associated with the time fluctuation of droplet distributions.

The average droplet number density was counted for each cell, and is shown plotted in the grid in Figure 4-44. The average density along



* Cell Number

** Number Density, droplets/cc

Figure 4-44. DROPLET NUMBER DENSITY DISTRIBUTION FOR FIGURE 4-35

the spray tube center plane was calculated from cells 1 through 10 and is 31 droplets/cubic centimeter. The average density in a plane about 1 cm to the right of the spray tube was computed from cells 11 through 15, and is about 18 droplets/cc. Droplet velocities through this plane should be approaching about 3 m/sec, as may be seen in Figure 4-28.

The total volume flow rate of liquid out of a spray tube may be expressed as a volume integral over the droplet flux.

$$\dot{Q} = \int dA \int dS \frac{4}{3} \pi S^3 n(S) U(S) \quad (4-48)$$

where A = an area surrounding the tube tip, containing all the droplet flux.

The total volume flow, \dot{Q} , may be obtained as a function of pressure from flow calibrations given in Section 2.2. For 22 gauge spray tubes at

36 mbar water pressure, the flow rate is 0.66 cc/sec per spray tube.

Let n_{oD} be a position - dependent average number density of droplets, such as in Figure 4-44. Let $f(S)$ be the droplet radius distribution function. Following the approach of Section 1.3, Equation 4-48 may then be rewritten in terms of a volume utilization efficiency, e_3 .

$$\dot{Q} = \frac{4}{3} \pi \overline{S^3} U_p e_3 \left[\int dA n_{oD} \right] \quad (4-49)$$

$$e_3 = \frac{1}{U_p \overline{S^3}} \int dS S^3 U(S) f(S)$$

Values of the area integral in Equation (4-49) may be estimated from the photographs, and values of the mass-mean radius come from the droplet size distribution. It is then possible to obtain estimates for the volume utilization efficiency e_3 , and relate them to the area utilization efficiency, e_2 , derived in Section 1.3.

The ratio e_2/e_3 should be fairly insensitive to mean droplet size, but should depend on the spread of the distribution. Thus, it should be fairly constant. It can be approximated as

$$e_2/e_3 = \overline{S^3}/(\overline{S^2} S_p) = \exp \left[\frac{7}{2} \text{Ln}^2 \sigma_g \right] \quad (4-50)$$

which has a value of about 4.0.

Values of droplet number density in cell locations 11 through 15 of Figure 4-44 were estimated from the photographs. These average values are shown in Table 4-7.

The droplet formation rate at the spray tube tip can be expressed in terms of an average value given by

$$\frac{1}{\tau_{df}} = \frac{\dot{Q}}{4/3 \pi \overline{S^3}}$$

where τ_{df} = average formation time of a droplet.

Table 4-7. DROPLET DENSITY AND FLUX

Tube Gauge	Figure Number	Number Density (cc ⁻¹)	Droplet Flux (sec ⁻¹)	Volume Utilization Efficiency
22	4-33	30	569	.0042
	4-34	88	5,777	.0146
	4-35	18	4,150	.0512
	4-36	30	1,126	.0083
18	4-38	17	899	.0175
	4-39	17	5,884	.0769
	4-40	23	13,784	.1331

This is also equal to the total flux of droplets, integrated over any area surrounding the spray tube. This is also shown in Table 4-7. Finally, assuming all the droplet flux passes through an area of about 15 square centimeters in the photographs, Equation (4-49) was used to calculate a volume utilization efficiency which appears in Table 4-7.

4.3 BENCH SCALE SCRUBBER MEASUREMENTS

Performance parameter measurements were made on an operating, bench scale CDS as described in Section 2.3 and Section 3.4 of this report. The design volume flow rate of the scrubber was 540 m³/hr. The most efficient operation was achieved at volume rates of around 350 m³/hr. Both 22 gauge and 18 gauge spray tube sizes were tested. All tests reported here were run with newly generated zinc oxide fume, which has been characterized as sub-micron (see Section 3.4).

The results sought were overall scrubbing efficiency in terms of volume throughput, power input and water usage. Primary parameters which were controlled and measured were the high voltage, flue velocity, and electrode water inlet pressure. Other parameters which were controlled for each series of tests were spray tube size (choice of two) and collector plate spacing. Fume loading was controlled to a lesser extent by adjustment of the fume generator current, although no calibration was achieved. Other parameters which were measured but not controlled were flue gas temperature, total scrubber current, total collector current, and inlet and outlet grain loading and fume size distribution.

Because of scrubber design and operating conditions, the total scrubber current was in all cases ten to twenty times the actual collector plate current. The balance of the waste current was corona, exterior to the scrubber, which is normally less than five percent of the total. For this reason, the specific powers presented here are based on collector current alone. In addition, specific water flow rates are given in terms of electrode water flow only, since a wall wash spray was not used on this unit. Use of a wall wash will generally result in an extra usage of about 2.2 liters/min. per thousand m³/hr. of gas flow, which is about 3.5 times the electrode flow.

All results are also given for the single stage configuration that was used, rather than the three-stage configuration that has been adopted for pilot work. The water and power consumption would be up a factor of three for the three-stage configuration, but the total penetration would be the cube of the measured single-stage penetration.

All volumetric parameters are given in terms of gas volume flow at flue-gas ambient conditions. In most cases this was the same as surrounding ambient conditions.

Typical of scrubbing efficiencies observed were the 20 to 40 percent per stage measurements at 0.1 micron particle size. Total mass collection efficiencies as high as 98 percent were measured. Projected efficiencies for the one micron size range are 50 to 70 percent. These efficiencies were observed over a wide range of inlet loadings (1-1000 mg/m³), and were fairly independent of loading, except at high loadings where space-charge effects tend to degrade the droplet charging mechanisms.

Changes in scrubbing efficiency are most sensitive to collector plate spacing and specific water flow rates. Under nominal conditions, a change of 30 percent in collector plate spacing was seen to produce a 35 percent change in scrubbing efficiency. Increasing specific water flow a factor of five raised the scrubbing efficiency by about twenty percent. The effects of voltage and flue velocity on the efficiency are less pronounced and less predictable, according to these data.

As discussed in Section 3.4, scrubber efficiency data were obtained using four different sampling methods. These were briefly described as high volume sampling, water entrainment sampling, alcohol entrainment sampling (impingers) and Andersen sampling. These will each be discussed in turn.

The high voltages given are supply voltages. As noted in Section 2, this voltage is separated from the electrode by a water resistance of length 1.9 m and cross section $.75 \text{ cm}^2$. City water was used, typically having conductivity of $475 \text{ } \mu\text{mho/cm}$, hardness of 100 ppm and a pH of 8.0.

4.3.1 High Volume Sampling

A total of seven tests were completed, two of which were with the scrubber off, and four of which have to be interpreted in the light of sampling malfunctions.

The first test, number 4/8-1, was run with 22 gauge spray tubes, a .163 meter collector spacing, a gas velocity of 1.14 m/sec and a gas temperature of 39°C . Other parameters and results are shown in Table 4-8. This test is noteworthy in that it achieved a measured efficiency of 90 percent. The measurement is however a result of nonsimultaneous inlet and outlet sampling, and was never duplicated. It must therefore be discounted. The weight measurements on this run were also uncorrected for filter moisture absorption due to ambient humidity, although such a correction would have been favorable to the efficiency calculation. Subsequent runs were corrected by the amount of the weight decrement in a "master filter", to account for moisture content of the filter.

The remaining six tests were run with 18 gauge spray tubes, and other test parameters constant as shown in Table 4-9. Other results of these tests are also shown in Table 4-8. Sampling and equipment malfunctions occurred in these tests largely as a result of equipment usage shakedown.

During test 4/23-1 the outlet filter pulled away from its seal and partially collapsed. The area effect was under twenty percent. The efficiency estimate is subject to that error.

In test 4/23-2, both filters were saturated (clogged) with fume before the test was over, so the total volume drawn had to be estimated. Conservative estimates give a lower limit on both the inlet loading and the scrubbing efficiency.

Table 4-8. VARIOUS RESULTS OF THE HIGH VOLUME SAMPLER TESTS, NOS. 4/8-1 THROUGH 4/25-4

Test No.	4/8-1	4/23-1	4/23-2	4/25-1	4/25-2	4/25-3	4/25-4
Supply Voltage (kv)	46	32	32	31	0	31	0
Electrode Water Pressure (m bar)	40.8	10	8.8	11.2	0	11.2	0
Specific Water Flow (liter/m ³)	.012	.015	.013	.016	0	.016	0
Inlet Loading (mg/m ³)	65	21	>100	60	124	2.7	14.9
Scrubbing Efficiency (percent)	90*	65	>50	50	<30	67	0

* Result of nonsimultaneous inlet and outlet sampling. Run with 22 gauge spray tubes.

Table 4-9. NON-VARYING PARAMETERS FOR HIGH VOLUME SAMPLER TESTS 4/23-1 THROUGH 4/25-4

Spray Tube (gauge)	18
Collector Spacing (meter)	.114
Gas Temperature (deg. C)	35
Gas Velocity (m/sec)	1.0
Arc Current (amp)	80
Average Collector Current (ma)	.33
Average Specific Power (w/m ³ /hr)	.035

In test 4/25-1, the inlet volume flow rate meter failed, and the total sample volume had to be estimated from nominal operation.

4.3.2 Water Entrainment Sampling

This sampling was done with an aerosol open type sampler as described in Section 3.4. The fume was collected on a 0.2 micron-nominal teflon filter, and was later entrained in a water solution for counting and analysis. The fume quickly formed an agglomerate in solution. Royco size counts were made to obtain a scrubbing efficiency analysis in terms of particle size, but due to the agglomeration this analysis was not meaningful. The efficiency seen in each category reflected the total scrubbing efficiency. The Royco analysis was used to obtain inlet loading estimates, in every test except number 4/22-1, where the catch was weighed directly. This direct measurement was then compared with the Royco analysis to verify its validity.

A total of nine tests were made by this method. Selected results of the testing are summarized in Table 4-10. The two tests not included yielded very little performance information. The first test not shown was number 4/22-1, which was a "scrubber off" run to determine if there was significant fume fall out in the scrubber. The measured penetration on this run was 90 percent. Both catches were weighed directly, and compared with a loading calculation by Royco analysis. The second test not shown in Table 4-10 is number 5/20-1, which failed to scrub due to a fume overloading condition. No data were taken on this run.

The first run recorded in Table 4-10, run number 4/17-1, also failed due to a fume overload condition when the fume generator became too hot. The overloading results in a space charge distribution in the scrubber which degrades droplet charging and results in a "collapsed spray". The data taken on this run include an estimated fume loading (17000 mg/m^3) which is believed to be representative of the threshold loading for spray collapse. The next recorded test, 5/13-1, was run very successfully (95 percent efficiency) with the inlet loading down just about a factor of ten. The larger spray tubes were used, and the high efficiency may be due partly to the high specific water flow.

Tests 5/17-1 and 5/20-2 are two examples of successful runs at low specific power. The low collector current was not a controlled factor in these runs, however, and no apparent cause was found for it.

Comparison of tests 5/15-1 and 5/23-1 show the effect of changing collector plate spacing, which was the largest effect seen in this series of tests. The comparison shows that an approximate 30 percent increase in collector plate spacing results in a 35 percent decrease in efficiency. Comparison of tests 5/15-1 and 5/17-1 show the effect of changing velocity and collector spacing together. The effect of the latter is dominant, and apparently changing velocity alone would have little effect on performance.

Table 4-10. PERFORMANCE RESULTS OF THE WATER ENTRAINMENT SAMPLING TESTS, NOS. 4/17-1 THROUGH 5/23-1

Test No.	4/17-1	5/13-1	5/15-1	5/17-1	5/20-2	5/21-1	5/23-1
Spray Tubes (gauge)	22	18	22	22	18	18	22
Collector Spacing (m)	.114	.114	.114	.164	.164	.164	.164
Gas Velocity (m/sec)	1.83	1.83	1.83	1.14	1.83	1.83	1.83
Supply Voltage (kv)	30	32	32	32	32	48	48
Collector Current (ma)	.30	.40	.25	.10	.08	.30	.30
Inlet Loading (mg/m ³)	17000	1560	250	103	86	119	355
Specific Water Flow (liter/m ³)	.0110	.0719	.0129	.0144	.0499	.0499	.0090
Specific Power (w/m ³ /hr)	.0239	.0340	.0213	.0095	.0047	.0266	.0266
Scrubbing Efficiency (%)	0*	95	85	35	70	65	47

* Scrubbing failure due to fume overload.

A comparison of tests 5/20-2 and 5/21-1 shows the effect of changing scrubber voltage only, other conditions remaining the same. The main effect of this is to change the ambient electric field pulling the droplets through the flue gas. A negligible effect is seen in this comparison.

Comparison of 5/21-1 and 5/23-1 shows the effect of changing spray tubes and specific water flow rate. The larger tube size is generally used where more water flow is desired. The studies discussed in Section 4.2 show that the larger tube also produces a larger average droplet size, but not a larger droplet velocity. The most significant effect

here is probably in increased water flow. A factor of five increase in the flow rate results in a 20 percent improvement of efficiency. Comparison of tests 5/17-1 and 5/20-2 show the effect of increasing both the flue velocity and the specific water flow (by changing spray tubes) and shows that the latter effect is dominant.

All tests except 4/17-1 were run with a fume generator current of 80 amps. Test 4/17-1, which failed because of fume overloading, was run with a 125 amp current. This was subsequently cut back to control the fume.

Flue gas temperatures of 26.5 degrees and 23 degrees centigrade were measured for the first two tests in Table 4-10.

4.3.3 Alcohol Entrainment Sampling

These tests were made with DSR-1 impinger bottles filled with isopropyl alcohol, as described in Section 3. Each test was conducted with one bottle at the outlet and one at the inlet. The inlet bottle had an "umbrella" to protect the sampler from falling water. The impingers were aligned to the best flow, using a Wallach hot-wire anemometer, and sampling was isokinetic. Each impinger was run with a flow rate of 15 SCFH, and each test lasted 30 minutes.

Five tests were run, but the first two were invalid because of a misalignment of inlet vanes causing a non-typical fume loading at the inlet impinger. When this was corrected, three more tests were run.

Table 4-11 shows the constant conditions under which the three tests were run. There were not enough tests run to get a good parameter variation study. Table 4-12 shows the results of the three tests.

Table 4-11. CONSTANT CONDITIONS FOR THE THREE
ALCOHOL IMPINGER TESTS

Spray Tubes (gauge)	22
Collector Spacing (m)	.164
Average Gas Temperature (deg. C)	22.5
Supply Voltage (kv)	48
Average Collector Current (ma)	.3
Fume Generator Current (amp)	80
Specific Power (watt/m ³ /hr)	.0266

Table 4-12. RESULTS OF THE ALCOHOL IMPINGER TESTS

Test No.	7/8-1	7/8-2	7/9-1
Flue Gas Velocity (m/sec)	1.83	1.83	1.27
Inlet Loading (mg/m ³)	1040	1433	819
Specific Water Flow (liter/m ³)	.0079	.0079	0.0
Scrubbing Efficiency (%)	94	98	77

The two 7/8 runs were done under almost identical conditions, with just the inlet loadings being different. The loadings were unexpectedly high, as were the scrubbing efficiencies. No systematic error sources were found, but the area loading distribution in the scrubber may still have been nonuniform. The high efficiencies were characteristic of high loading operation, and should be regarded as about 70 percent confidence level. They could be the result of fume agglomeration in the flue.

The third test, number 7/9-1, was conducted without water flow, but with high voltage, to estimate the effect of corona. The spray tubes were pointed upward and loaded with water so that they were normally conducting. The efficiency was lower, indicating an approximate 75 percent corona effect. This effect would have been enhanced by the lower flue velocity, and probably by the larger particle size, if the fume was agglomerating faster than usual due to the high loading.

Loadings and scrubbing efficiencies were obtained by Royco analysis. The Royco also yielded a fractional distribution of the inlet and outlet catch. As pointed out in Section 3, the fume was well agglomerated in solution, so the fractional efficiencies indicated may be largely reflections of the total efficiency. The measured mass fractions at outlet relative to inlet are shown in Table 4-13.

4.3.4 Andersen Sampling

Three tests were conducted using the Andersen sampler pairs; one with the scrubber off and two with it on. The scrubber operating conditions are shown in Table 4-14. As discussed in Section 3, the tests failed from the standpoint of getting good efficiency measurements, since no

attempt was made to discharge the fume before it entered the sampler. Aerodynamic separation effects were largely overshadowed by electrostatic effects. The tests did give valuable information regarding the fume size distribution and induced charging and corona charging effects.

Table 4-13. ROYCO ANALYSIS OF APPARENT FRACTIONAL EFFICIENCIES, OR NUMBER FRACTION OF OUTLET OVER INLET

Test No.	7/8-1	7/8-2	7/9-1
Diameter Range (microns)	Number Fraction (percent)		
0-2	71	72	66
2-5	86	91	77
5-10	96	98	97
10-25	97	98	85
25-50	96	76	56

Table 4-14. SCRUBBER OPERATING CONDITIONS FOR ANDERSEN SAMPLER TESTS

Spray Tubes (gauge)	22
Collector Spacing (m)	.164
Supply Voltage (kv)	48
Average Collector Current (ma)	0.2
Fume Generator Current (amp)	80

Total efficiency results are given in Table 4-15. The first run, with scrubber off, showed total penetration to within 3 percent. Runs 6/15-2 and -3 differed in flue velocity. Total scrubbing efficiencies were calculated from total material collected on all plates. The higher velocity run showed the higher efficiency, a condition which is probably due to higher specific power.

Table 4-15. ANDERSEN SAMPLING TEST
CONDITIONS AND RESULTS

Test No.	6/15-1	6/15-2	6/15-3
Flue Gas Velocity (m/sec)	1.30	1.30	1.63
Supply Voltage (kv)	0	48	48
Specific Water Flow (liter/m ³)	0	.0094	.0096
Specific Power (w/m ³ /hr)	0	.0025	.0199
Inlet Loading (mg/m ³)	61	72	72
Scrubbing Efficiency (%)	0 (3%)	21	49

The three-stage efficiency corresponding to the 50 percent run 6/15-3 is 86 percent.

The first run was used to gain information about the particulate size distribution, as discussed in Section 3. The two tests with the scrubber on were invalidated by electrostatic effects. The upper plates of the outlet sampler were overloaded due to electrostatic precipitation of fine particulate. This particulate was dry-charged, either by corona from the spray tubes or induced charging from the droplets. The extent of these combined effects could be estimated from the sampler data. This work is summarized in Table 4-16.

The table first shows the inlet and outlet loadings for the two powered runs in each of three aerodynamic size categories - that is, on the upper plates, the lower plates, and the back-up filter. The size categories differed slightly from one sampler to another because of varying temperature. The sizes shown are average, and are good to about 10 percent. The increased loading due to electrostatic effects on the upper plates of the outlet sampler is clearly seen in run 6/15-2. A finer categorization of run 6/15-3 shows the same effect, to a lesser degree.

An "apparent mass efficiency" for the sub-two-micron size category was calculated directly from the plate loadings shown in Table 4-16. If it is arbitrarily assumed that all the outlet particulate, caught by

precipitation or impaction on the plates, was under 2 microns in diameter, an estimated "actual mass efficiency" can be calculated for this size range. This is shown to be less than the apparent efficiency. Finally an estimate was made of the amount of particulate caught in the outlet samples by electrostatic precipitation alone. This is shown as the "dry charge fraction", caught by corona charging or induced charging. If this is further reduced by the ratio of droplet space charge to corona space charge in the scrubber it is indicative of the probability of induced charging in this size range.

Table 4-16. EFFECTS OF DRY CHARGING ON
ANDERSEN SAMPLER RESULTS

Test No.	6/15-2		6/15-3	
Loading (mg/m ³)	Inlet	Outlet	Inlet	Outlet
>2 micron	4.83	9.77	8.99	6.29
2-.25 micron	8.16	14.68	13.78	8.76
<.25 micron	59.21	32.94	48.92	21.86
Total	72.20	57.39	71.69	36.91
Apparent Mass Efficiency, <2 micron	.29		.51	
Actual Mass Efficiency, <2 micron	.15		.41	
Dry Charge Fraction	.28		.16	

4.4 SCRUBBER PERFORMANCE

The bench scale CDS was operated over a range of variables which included:

- Fume loading
- Gas stream velocities
- Collector plate spacing
- Water flow rate
- Electrode voltage

The main parameters tabulated for the operating runs, in addition to the operating variables, were the particle removal efficiencies, specific water flow rates and specific power. Several attempts were made to determine fractional particle removal efficiencies, and the results from two runs were reported. The data as reported is in a form which allows comparison with other particle removing devices. The data in this form is limited for the purpose of size extrapolation and determining optimum operating conditions for the CDS.

The easiest method of arriving at CDS performance is to characterize the operating variables and parameters in terms of unit electrode length and then convert to specific values for a particular application. The current between the electrode and collector is space charge limited. The maximum current in the scrubber, as a result of this space charge limitation, is approximately 0.8 ma per meter of electrode. This value is that determined during the experimental runs when the scrubber was operated at its maximum voltage. Any appreciable concentration of small particle material that is induced or corona charged will have a low mobility relative to the droplets and ions and will reduce the current flow. Therefore, the maximum nominal specific power would be based on a current of 0.8 ma per meter.

The water flow rate, likewise, can be specified as unit volume per unit time-meter of electrode. There is a flow rate band over which each spray tube will exhibit stable operation. The low end of this band is the point at which the momentum of the flowing stream from the nozzles is insufficient to overcome the surface tension force of the liquid on the spray tube. Under this condition, droplets will form on the spray tube and will be extracted from the tube tip under both the influence of gravity and the electrostatic field. These droplets will be large, ineffective scrubbers and will be accompanied by large corona currents. This type of break-up is seen in Figure 4-29. If the flow rate is too large, the droplet break-up will occur a large distance from the spray tube in a lower electrostatic field region. Both electrostatic and aerodynamic forces influence the break-up. The droplets will also be large, have a low charge density and be ineffective scrubbers. When the kinetic energy of the stream flowing from a spray tube is equated to the surface tension energy of the liquid at the spray tube tip in the absence of an electrostatic field, the volumetric flow rate, \dot{Q} , is:

$$\dot{Q} = \pi \left(\frac{d_o^3 \sigma}{2\rho} \right)^{1/2}$$

when: d_o = spray tube external diameter

σ = surface tension

ρ = liquid density

The corresponding flow rates for the 22 and 18 gauge spray tubes are 1.572 and 3.071 liters/hour, respectively. The spacing used in the bench scale scrubber was 2.54 cm or 40 per meter. This spray tube spacing would correspond to flow rates for the 22 and 18 gauge tubes of 62.9 and 122.8 liters/hour-meter of electrode, respectively. Previous experiments with 18 gauge spray tubes have indicated that 4.32 cm spacing is adequate which would correspond to 72.2 liters per hour-meter of electrode. Because of the charge on the liquid stream leaving the flow tubes, a portion of the surface tension force is negated by electrostatic forces. Therefore, the flow rate necessary to insure that a stream and not drops is issuing from the spray tube and have droplet break-up is in the range of 10 to 15 percent of the no field value. The flow rates of the tests with the bench scale scrubber using the 22 gauge spray tubes were in this range. The tests using the 18 gauge tubes were either at 100 percent of the no field minimum flow or below the threshold for constant droplet break-up with field. From the flow criteria for a spray tube, the CDS flow rates should be in the range of 6.3 to 18.4 liters/hour-meter of electrode, depending on spray tube size and spacing.

There was some indication, although not definite because of the limited number of data points, that the narrower of the two collector spacings may have resulted in higher collection efficiency. The droplet velocity profile data from Section 4.22 indicate that the narrower collector spacing (0.114 meter) was probably the minimum at which full utilization of the droplets could be achieved. If the spacing was less, either no improvement or a decrease in collection efficiency would result because the droplets would still be accelerating. A nominal collector plate spacing should be 0.125 meters.

The bench scale experiments were performed over a gas stream velocity range of 1.0 to 1.83 meters/second. This range is characteristic for a single stage scrubber; however, a lower velocity may be necessary for a multistage scrubber operating with high, submicron particle loadings. The gas stream velocity range of the scrubber will be between 0.9 and 1.8 meters/second.

The specific water flow rate, using these flow rates, collector plate spacing and gas stream velocity, will be in the range of 1.0 to 5.0×10^{-2} l/m³. A CDS with 0.125 meter collector separation will operate in the range of 38 to 40 kv. The specific power under these operating conditions will be in the range of 3.8 to 7.9×10^{-2} watts/m³.

Although the specific power is essentially proportional to the inverse of the gas stream velocity, the specific water flow rate is not only an inverse function of the velocity but also a function of the spray tube size. Therefore, the specific water flow rate is strongly dependent on the process stream conditions which will determine the most effective tube size.

Another specific parameter used to characterize performance is the collection area necessary for particle removal. This collection area is dependent on the drift time of a particle moving out of the gas stream. Those particles removed by inertial impact with the droplets will have the same drift times as the droplets. Particles charged by induced charging from the droplets will drift toward the collector under the influence of the electrostatic field. The drift time in the absence of turbulence will be approximately 0.5 second for a 0.1 micron particle in a scrubber with 0.125 meter collector spacing. The time is approximately inversely proportional to the particle size. The length of collector required is in the range of 0.5 to 1.0 meter. If more than one electrode stage is required to accomplish the particulate material removal, the separation between stages will also be in this same range to insure that charged particles from one stage do not influence the space charge in the subsequent stage. A single electrode will have between 1 and 2 square meters of collecting surface per meter of electrode length. When multiple flow channels formed by collectors are used, one collector will serve adjacent channels. Therefore, there will be $(n + 1)$ collectors for n flow channels. Where n is larger, the actual collector area per meter of electrode will be between 0.5 and 1.0 square meters per meter of electrode. The corresponding specific collection area is $1.2 \times 10^{-3} \text{ m}^2/\text{m}^3/\text{hr}$.

Overall collection efficiencies were in the range of 21 to 98 percent. A large portion of this range is due to operating the scrubber at non-optimum conditions. Some was due to sampling difficulties. The fractional efficiency data is limited and is subject to considerable error due to particle agglomeration and effects of residual particle charge. The data reported in Section 4.3 indicate that the cleaning efficiency increased with increasing particle loading. The limit of this increase was the level at which the high particle concentration upsets the normal space charge distribution around the electrode. The experimental data³ indicated that the scrubber would perform with loadings up to $1560 \text{ mg}/\text{m}^3$. The next data point where operating difficulties were encountered was at a loading over ten times this value; therefore, the actual upper limit was not established. The particle size distribution data indicated that there was a mean size increase as the particulate material concentration increased. This effect may be responsible for the increase in removal efficiency with increasing particle concentration. The bench scale data indicate that under optimum conditions, the single stage scrubber removal efficiencies would be 40% for 0.1 micron particles and 70% for 1 micron zinc oxide particles. These values are characteristic at a flow rate of 1.0 m/sec.

A summary of the optimum CDS operating and performance characteristics are shown in Table 4.17. The area utilization efficiency based on the experimental data for those experiments performed near optimum conditions is 0.33. This value is higher than those determined from the droplet photographs. A portion of the higher area utilization efficiency is due both to the corona current and the space charge due to charged particulate material.

Table 4.17. CDS PERFORMANCE FOR SUB-MICRON PARTICLE REMOVAL⁽¹⁾

<u>Number of Stages</u>	<u>Specific Power (watt/m³/hr)</u>	<u>Specific Water Flow Rate (liter/m³)</u>	<u>Collection Area (m²/m³/hr)</u>	<u>Cleaning Efficiency</u>	
				<u>Particle Size</u> <u>0.1 Micron</u>	<u>1.0 Micron</u>
1	7.9×10^{-2}	2.7×10^{-2}	1.2×10^{-3}	40%	70%
2	1.58×10^{-1}	5.4×10^{-2}	2.4×10^{-3}	64%	91%
3	2.37×10^{-1}	8.1×10^{-2}	3.6×10^{-3}	78%	97%
4	3.16×10^{-1}	1.08×10^{-1}	4.8×10^{-3}	87%	99%

(1) For 0.125 meter collector spacing, a gas stream velocity of 1.0 m/sec and particle loadings in the range of 50 to 1600 mg/m³.

4.5 PERFORMANCE COMPARISON

The performance comparison of the CDS with a high efficiency electrostatic precipitator (EP) is shown in Table 4.18. The power requirement for the CDS is lower than that for an electrostatic precipitator because of the charged water droplets in the CDS. These droplets constitute a fraction of the current carriers in the CDS in addition to the ions. The droplets have a lower mobility than ions which results in a lower electrode current.

The major items relative to the comparison of the CDS and electrostatic precipitators are the collection area and volume. The CDS is able to perform a comparable air cleaning operation with a lower collecting area and consequently smaller volume than an electrostatic precipitator. This smaller volume results from the higher charge density that the scrubber is able to impart to fine particulate material in a shorter time period than in an EP. The particles are then able to drift out of the gas stream in a shorter distance. The vehicle for imparting the high charge density is the highly charged droplets.

Table 4.18. PERFORMANCE COMPARISON¹

<u>Parameter</u>	<u>CDS (3 Stages)</u>	<u>High Performance Electrostatic Precipitator</u>
Specific Water (liter/m ³)	0.081 ²	N/A
Specific Power (watts/m ³ /hr)	0.24	0.35
Collection Area (m ² /m ³ /hr)	0.0032	0.033
Residence Time (m ³ /m ³ /hr)	0.0003	0.003

¹Removal Efficiency - approx. 78% less than .5 micron
 - approx. 95% overall

²Electrode flow only. Total water requirement is approximately 2.5 times this value for continuous wall wash.

5. CONCLUSIONS

The program of research described in this report concludes a feasibility study on the application of charged droplet scrubbing for fine particle control. Positive results have been obtained with a particular type of charged droplet control device, the TRW/CDS, which indicate that the method is indeed feasible, and applicable over a wide range of conditions. The principal results leading to these conclusions will now be reviewed.

(1) Mass removal efficiencies of order 20 to 40 percent per stage have been demonstrated for 0.1 micron nominal diameter zinc oxide fume. In a three-stage device, this leads to efficiencies as high as 80 percent. Particulate agglomeration in the flue improves this. Total three-stage efficiencies ranging from 70 to 90 percent have been measured for particulate of order 1.0 micron geometric mean diameter.

(2) Induced charging or dry charging of particulate by charge transfer from droplets is an effective and major collection mechanism in the fine particulate size range. This mechanism may account for up to 80 percent of the droplet collision probability in that size range. The most effective and critical scrubber parameter is precipitation time (collector spacing) for dry-charged particulate of this type.

(3) The data indicates a higher volume utilization efficiency for the droplets, or a higher droplet-particle interaction cross section, than is predicted by theory. This could be due to corona current in the scrubber, which is an appreciable fraction of the total. But this has not yet been verified.

(4) Other parameters being equal in equal situations, the TRW/CDS shows a lower specific volume and lower specific power than other control devices. Where water usage or flue pressure drop is a basis of comparison, the CDS shows definite competitiveness.

(5) Under conditions of normal humidity and standard temperature and pressure, droplet evaporation in the scrubber is not a significant problem for sizes above 50 microns. For smaller droplets, or for extremely high temperature, low humidity flue gas, droplet evaporation will degrade performance.

(6) The droplet distribution within the CDS is log-normal. The most effective scrubbing droplet is the most frequently occurring. It is 100-200 microns in diameter, charged to the Rayleigh limit, and travels through the flue gas at about 30 m/sec. This velocity is lower than predicted by Stoke's Law. The effectiveness of this droplet distribution bears out the assertion that large droplets (100 micron) give better performance characteristics than small (10 micron) droplets.

It can be concluded from these results that charged droplet scrubbing devices have unusual effectiveness in the fine particulate size range compared to conventional methods of electrostatic precipitation or wet scrubbing. The "fines" size range, one to one-tenth micron diameter, is too small, on the one hand, for effective impact scrubbing by neutral water droplets or for effective field-charging by corona space charge fields. On the other hand, this size range is too large for effective diffusion mass transfer to take place. The mechanism of charge transfer from charged scrubbing droplets, allowing high surface charge densities, makes the difference in this size range.

The performance and efficiency of a charged droplet scrubber depend greatly on the type of device and the mechanisms it uses. In general, the requirements for high efficiency at low or nominal grain loading of fines are maximum possible droplet charge and maximum relative velocity between droplet and particulate. These requirements may be met economically in the TRW/CDS, or similar applied field electrical impact scrubbers. The major mechanism is then charge transfer from the droplets. At higher grain loading, mechanisms of agglomeration through droplet impact and precipitation through diffusion charging become more important. The requirements tend toward higher droplet densities and weaker droplet charges, and the advantages of short residence times and low water usage are sacrificed. The operating conditions tend toward those of the electrical agglomerator.

6. RECOMMENDATIONS

There are really two parallel programs which need to be undertaken in continuation of this project. Most importantly, charged droplet scrubbing is now ready for a pilot scale field demonstration. Such a demonstration is needed to show applicability of the method to an important source of industrial fine particulate. This does not mean, however, that the need for further research and development is over. Feasibility has been proven, but further research should be directed toward concept improvement and development of design criteria for efficiency and reliability.

6.1 PILOT DEMONSTRATION PROGRAM

Recommendations for a Charged Droplet Scrubber pilot demonstration program have already been discussed in Reference 23. The program consists of installing and field testing a 51,000 m³/hr (30,000 ACFM) commercial design Charged Droplet Scrubber. The installation will be equivalent to roughly half of a commercial, operational unit and so represents a very good approximation to real operating conditions in the field.

The test has been negotiated on a coke oven effluent stack at Kaiser Steel in Fontana, California. Kaiser-Fontana has seven such stacks, and they represent a critical air pollution problem in the area. The particulate in the stack effluent is a condensed hydrocarbon, tarry in nature, and about 40 percent submicron by weight. It is similar to an oil smoke, and reaches loadings as high as .2 gm/m³ (.1 grain/ft³). Several attempts have already been made to control this emission and have been for the most part unsuccessful. These include conventional electrostatic precipitation, wet scrubbing, and a less conventional incineration method.

The Kaiser environment also offers a severe test in terms of elevated temperatures and low humidities; 400°F (204°C) and a 15% moisture content at the stack base. Charged droplet scrubbers can be designed to cope with these conditions where regular scrubbers fail. The droplet charging mechanism in the CDS is a means of droplet size control. Droplet evaporation in a conventional scrubber results only in loss of efficiency. In a CDS it is a charge release mechanism, and therefore a collection mechanism.

The recommended test program includes a study of the effects of selected operating parameters in terms of performance. Performance can be characterized principally by scrubbing efficiency, power usage and water usage per volume rate of treated gas. The scrubber control parameters whose effects should be explored will include the following:

- Electrode polarity
- Electrode voltage

- Electrode water flow rate
- Electrode water hardness, being given a choice between fresh water and plant water
- Collector plate irrigation water flow rate
- Pre-cooling water flow, sprayed into the gas at the inlet
- Particulate inlet loading, being given a choice between nominal or plant upset conditions
- Flue velocity

The test program will also include an evaluation of long term performance through a moderate duration endurance test. This test will be conducted at nominal plant operating conditions.

Table 6-1 shows the nominal design conditions for the TRW/CDS, per 1700 m³/hr (1000 CFM). Quantities which scale directly with volume flow are the duct cross section, electrode length, operating current and water flow rates. The leakage resistance scales inversely with gas volume flow. The design parameters were chosen based on data gathered on the program and on previous experience with simulated pilot scale tests.

The recommended scrubber structural arrangement is shown in Figure 6-1. The depicted scrubber has twenty modules, each having a three meter active electrode length. The nominal scrubbing volume cross section, for all modules, is 8.5 ft by 10.5 ft (2.6 m by 3.2 m).

The lower section of the scrubber is the gas distribution section, shown in Figure 6-2. It contains a series of flow turning vanes, and optional diffuser baffles, or flow straighteners at the entrance to the upper section. The upper section contains the electrodes and collector plate assemblies, and is shown in Figure 6-3. The electrode support insulators are housed in compartments at the corners of the scrubber. The electrodes of each stage are fed from and suspended from a header pipe that is supported from two insulators. The electrode header is supplied with water from insulating pipe of polyvinyl chloride, or other suitable material, which acts as a resistance between the electrode and high voltage. Water is supplied from ground to high voltage through an insulating "pipe nest", consisting of sequentially connected runs of pipe. The collector plates are stiffened at top and bottom, and clipped down the sides.

Table 6-1. DESIGN PARAMETERS FOR TRW/CDS

Number of Stages	3
Volume Flow	1000 ACFM (1700 m ³ /hr)
Flue Velocity	5 ft/sec (1.5 m/sec)
Duct Cross Section	3.6 sq ft (0.33 m ²)
Spray Nozzle Spacing	1.75 inch (4.5 cm)
Active Electrode Length	128 inch (3.25 m)
Electrode-to-Wall Spacing	2.5 inch (6.4 cm)
Spray Nozzle O.D.	0.050 inch (1.25 mm)
Operating Voltage	40 kv
Operating Current	6 milliamp
Electrode Inlet Pressure	4 inch H ₂ O (1000 n/m ²)
Scrubbing Water Flow	0.4 gpm (1.5 liter/min)
Wall Wash Flow	1.2 gpm (4.5 liter/min)
Water Conductivity	400-700 μ mho/cm
Leakage Resistance	>10 megohm

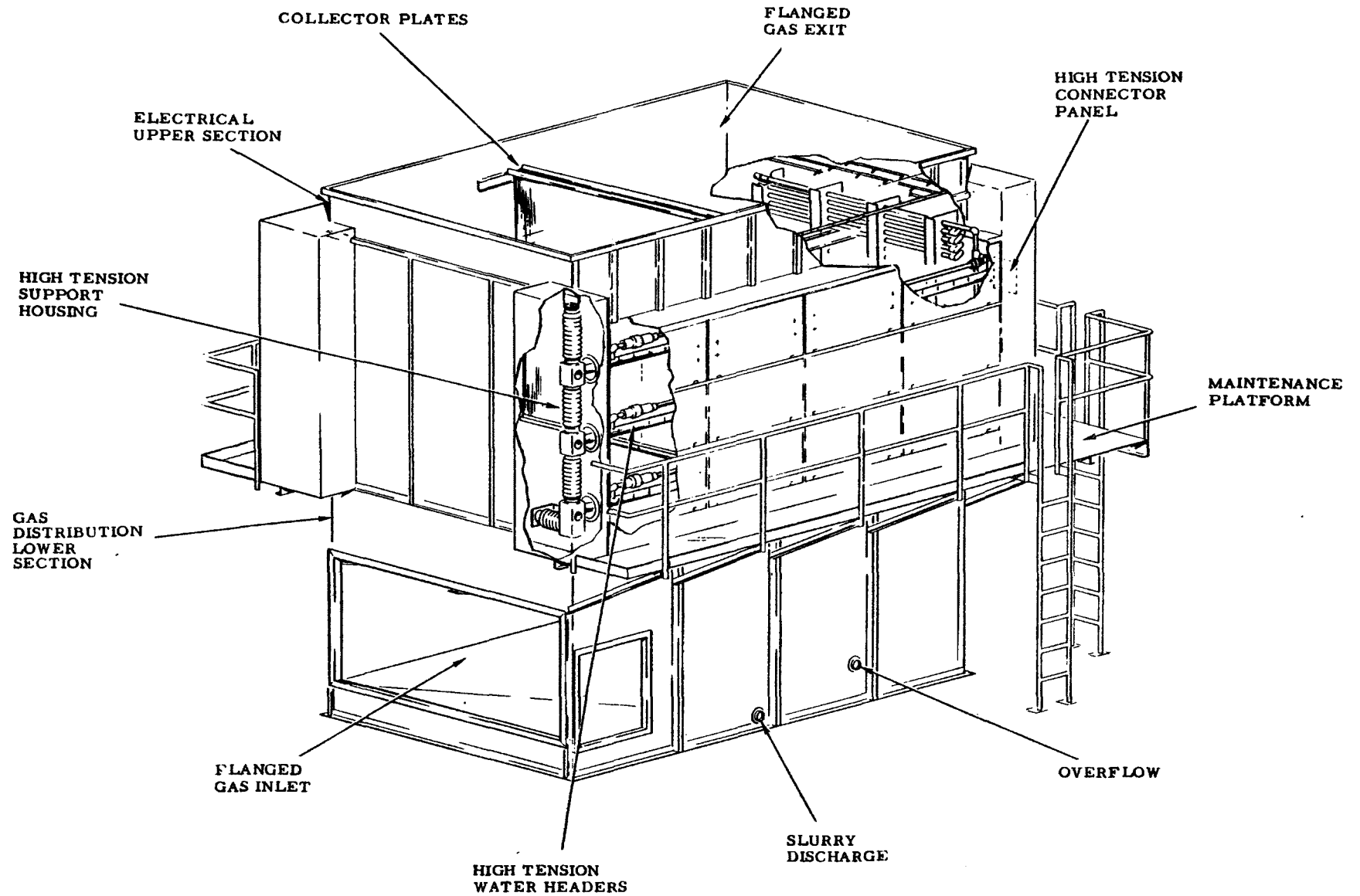


Figure 6-1. Structural Arrangement of Recommended 50,000 M³/hr CDS Pilot Plant

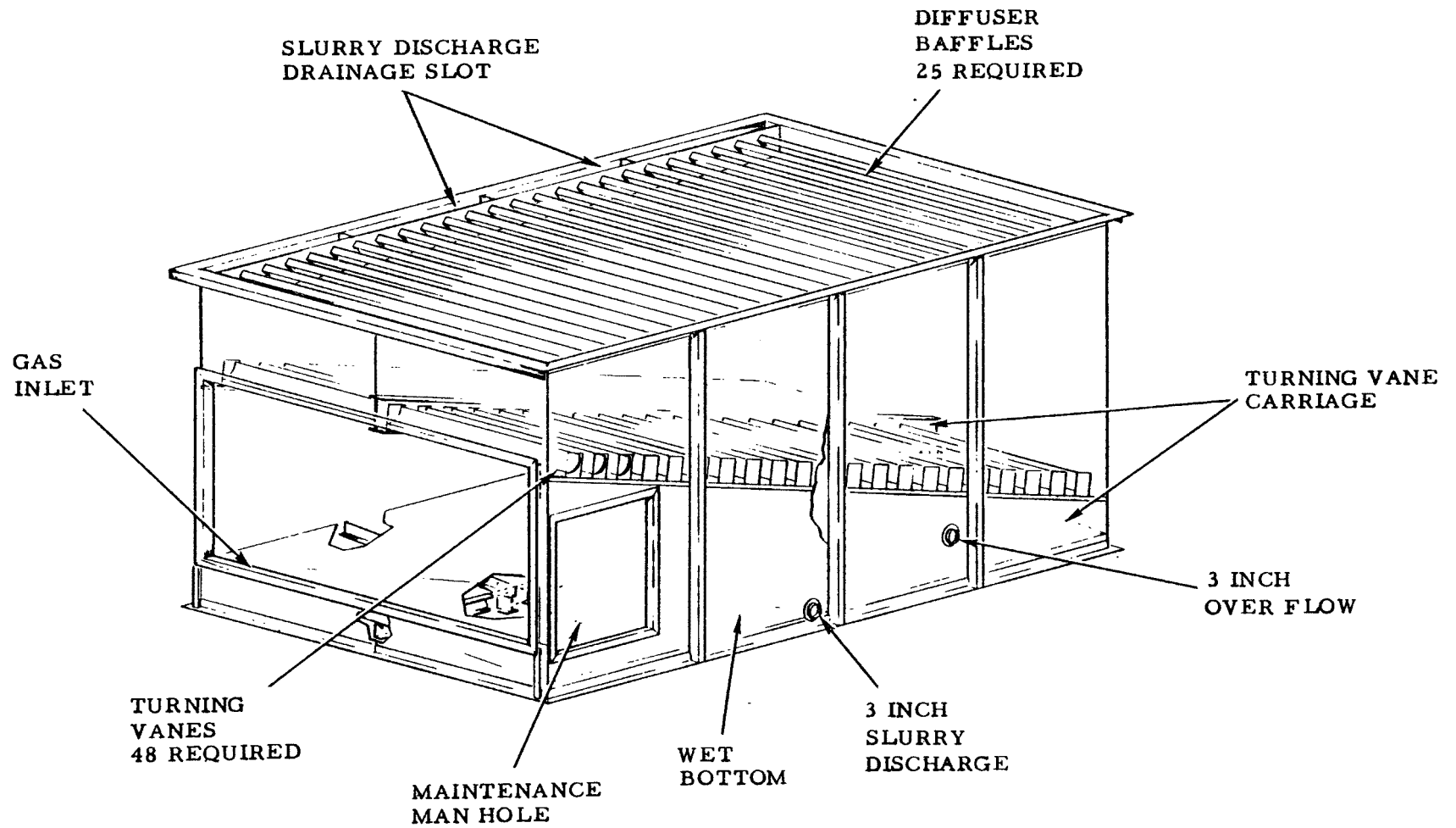


Figure 6-2. CDS Lower Section Assembly

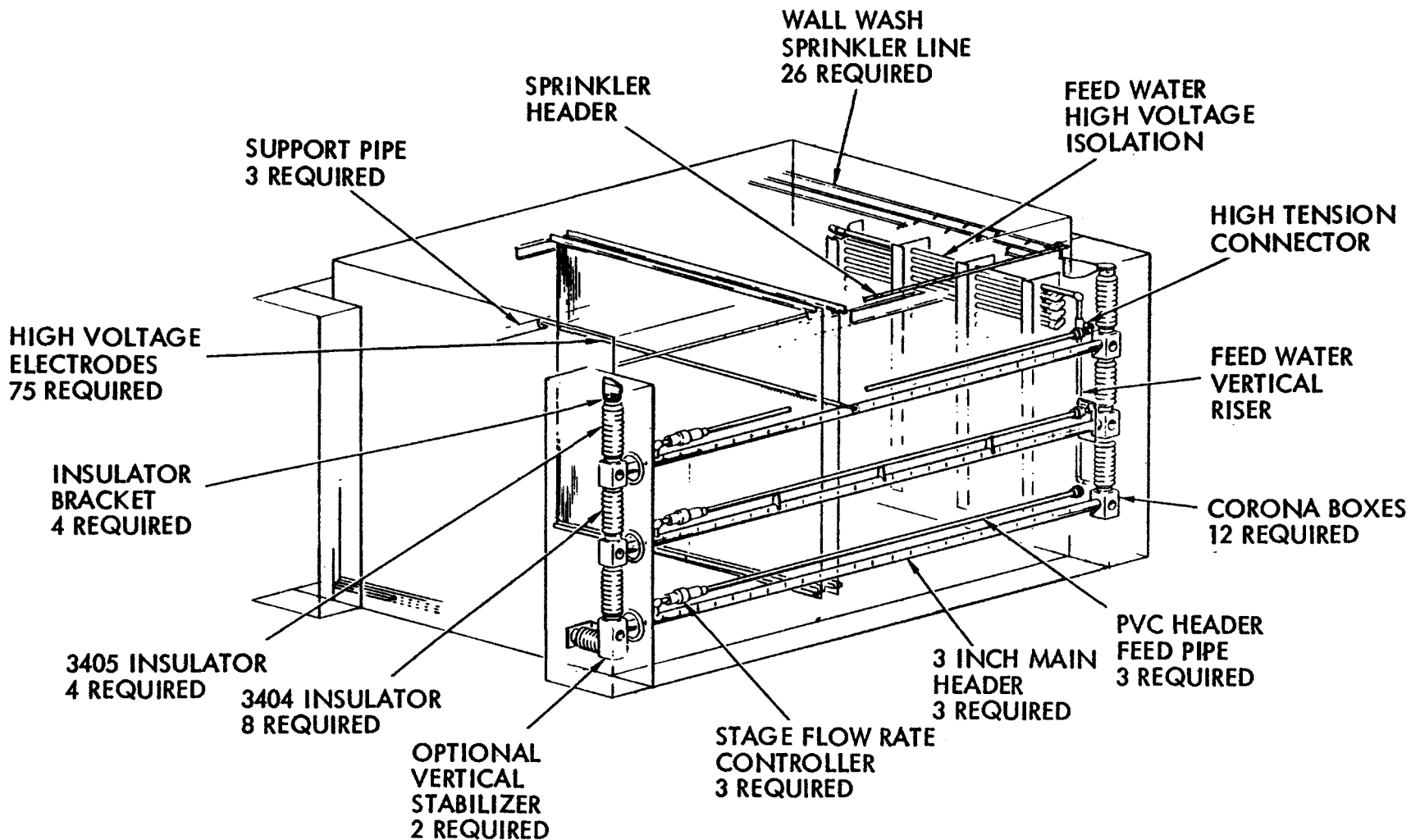


Figure 6-3. CDS Electrode and Collector Plate Assemblies

6.2 CONTINUED RESEARCH AND DEVELOPMENT

There are a number of problems which immediately suggest themselves as topics for continuing research and development. One such problem is a further quantitative verification of the induced charging of particulate. In the present program, we have established that induced charging is an important mechanism for particle collection. Calculations were made of fractional loading of dry-charged particulate, and rough comparisons were made with the data. Drift times of inductively charged particulate were also calculated, but these were not measured. Drift time is a parameter that influences the design of collector plate spacing and total scrubber length.

Drift times could be measured, and induced charging probability could be remeasured, with an experimental apparatus such as is shown in Figure 6-4. This is a cross section of a modified experimental CDS.

The point P can be monitored for current density as well as particle flux and size distribution. The inlet loading is known. The collection areas remain dry and the particulate sticks to the walls. The outer walls are held at a negative potential to maintain the drift field. The point P sees particle trajectories from a narrow range of angle, θ , which may be controlled by raising or lowering the inner walls.

The center plate in Figure 6-4 provides a high, uniform precipitation field everywhere in the scrubber. It is a non-discharging, low current type of electrode. If it were installed after the last stage of an operational CDS, it would be an economical and effective way to enhance scrubber efficiency. The enhanced precipitation field would take out more of the dry-charged particulate with slow drift velocities. Configurational studies of precipitation field enhancement could be a fruitful line for development.

Another challenging problem is the potential use of condensation scrubbing in the CDS. A hot, moist gas entering the CDS is cooled almost immediately, because of the presence of wall wash and irrigation water. The gas may become supersaturated, and charged particulates make good condensation nuclei. The upper stages of the CDS would then act as a demister.

Other potential applications for the CDS include demister operation in backing up a large wet scrubber of conventional design, and various SO_2 scrubbing operations. The CDS in its present conceptual form is not an efficient gas scrubber. However, there are SO_2 recovery schemes which suffer from the disadvantage of heavy fuming. Again the CDS would act as a back-up to remove residual fumes.

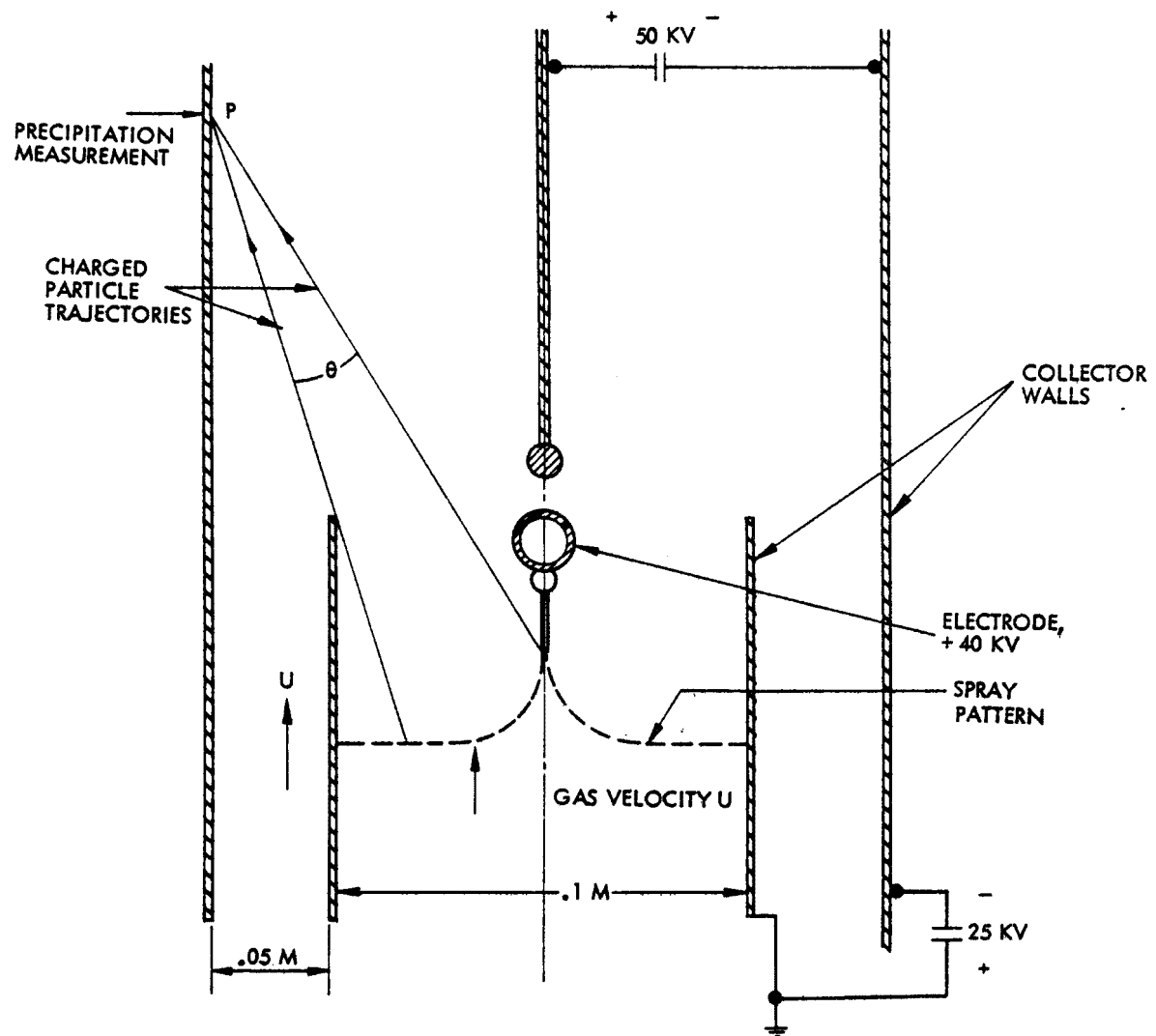


Figure 6-4. Experimental Device for Measuring Induced Charging Drift Times. The particulate is charged in the spray, then drifts to the walls under the influence of a uniform field.

7. REFERENCES

1. Melcher, J. R., and Sachar, K. S., "Charged Droplet Technology for Removal of Particulates from Industrial Gases," Final Report, EPA Contract No. 68-002-0018, August 1, 1971.
2. Joubert, J., Private communication.
3. Eyraud, C., Joubert, J., Henry, C., and Morel, R., "Étude des Trajectoires des Particules Sub-microniques dans les Champs Ionisés," Le J. de Phys. Appliqués, Supplement An. #3, Tome 25 (1964), pp. 67A-72A.
4. Wuerker, R. F., "Research on Electrostatic Charged Droplet Streams," Air Force Aerospace Research Laboratories, Report No. ARL 67-0211, Oct. 1967.
5. Huberman, M. N. et al, "Present Status of Colloid Microthruster Technology," Journal of Spacecraft and Rockets, 3, 11 (Nov. 1968).
6. Huberman, M. N., "Measurement of the Energy Dissipated in the Electrostatic Spraying Process," JAP 41, No. 2, pp. 578-584, Feb. 1970.
7. Krieve, W. F., "Charged Droplet Scrubber Development Program," Final Report, TRW Systems Independent Research and Development Program, 1 July 1971.
8. Dudley, G. L., "Charged Droplet Scrubber Development Program," Phase II Report, TRW Systems CDS Development Program, Dec. 1972.
9. Krieve, W. F., "Charged Droplet Scrubber Design Manual," Phase III Report, TRW Systems CDS Development Program, Feb. 1973.
10. Fuchs, N. A., The Mechanics of Aerosols, Pergamon Press and Mac Millan Company, N.Y., 1964.
11. Calvert, S., Goldschmid, J., Leith, D., and Jhaveri, N., "Feasibility of Flux Force Condensation Scrubbing for Fine Particulate Collection," EPA Report 650/2-73-036, October 1973.
12. Robertson, J. H., "Interactions Between a Highly Charged Aerosol Droplet and the Surrounding Gas," University of Illinois, Department of Electrical Engineering, Ph.D Thesis (1969).
13. Suits, C., Guy, Ed, The Collected Works of Irving Langmuir, (Vol. II, Cloud Nucleation) Pergamon Press Inc., New York (1962).
14. Happel, J., and Brenner, H., Low Reynolds Hydrodynamics, Prentice Hall, Inc., pp 96-123 (1965).

REFERENCES, Continued

15. Peek, F. W. Jr., Dielectric Phenomena in High-Voltage Engineering, Chapter IV, McGraw-Hill Book Co., 3rd Edition, 1929.
16. Farmer, W. M., "Measurement of Particle Size, Number Density and Velocity Using a Laser Interferometer," App. Opt. Vol. II(II), November, 1972.
17. Perry, J., and Perry, R., Engineering Manual, McGraw-Hill, 1959, pp 5-57.
18. Frenkel, J., Kinetic Theory of Liquids, Dover, New York, pp 412-413, 1955.
19. Fletcher, N. H., The Physics of Rainclouds, Cambridge University Press, pp 122-127, 1962.
20. Shahin, M. M., "Mass Spectrometric Studies of Ion-Molecular Reactions in Gas Discharges," Ion-Molecular Reactions in The Gas-Phase, R. F. Gould, Ed., Am. Chem. Soc., pp 315-332, 1966.
21. Jackson, J. D., Classical Electrodynamics, John Wiley and Sons, 1962.
22. White, H. J., Industrial Electrostatic Precipitation, Addison-Wesley Publishing Co., Inc., Reading, Mass., p. 165, 1963.
23. TRW Systems, Proposal No. 24800.1, "Proposal for Charged Droplet Scrubber Pilot Demonstration for Fine Particle Control," 28 May 1974.

APPENDIX

The enclosed appendix is the coding of the Fortran 4 program used to compute the collision effectiveness probabilities given in this report.

PROGRAM KK(INPUT,OUTPUT,TAPE2=INPUT,TAPE3=OUTPUT)

* UNITS--MKS
* RHO:=PARTICLE DENSITY
* VAR(1):=X POSITION OF PARTICLE

* VAR(2):=Z POSITION OF PARTICLE
* VAR(3):=X VELOCITY OF PARTICLE
* VAR(4):=Z VELOCITY OF PARTICLE

* DER(1):=VAR(3), DER(2):=VAR(4)
* DER(3):=X ACCELERATION
* DER(4):=Z ACCELERATION

* E0:=EPSILON-ZERO
* E1:=LOCAL FIELD
* E2:=FORMATION FIELD

* S:=DROPLET RADIUS
* R:=PARTICLE RADIUS
* XMU:=MU (VISCOSITY OF AIR)

* TC:=DIMENSIONLESS DRIFT TIME
* A:= INDUCED CHARGING IMPACT PARAMETER
* VC:= DIMENSIONLESS DROPLET VELOCITY

* QC:= DIMENSIONLESS ELECTROSTATIC FORCE
* IC:=ITERATION COUNTER
EXTERNAL HB

DIMENSION EU(4),EL(4),SCR(8,4)
COMMON VAR(4),DER(4),U,Q,Q1,C(2),RAD,ES
NAMELIST/INP/RHO,VAR,E0,E1,E2,S,R,XMU,X0,DT,EPS,EU,EL,TMX,EPSP,A,

* IPRNT
DATA RHO,E0,E1,E2,S,R,XMU,X0,TMX,EPSP/
* 2.15E3,8.854E-12,5.E5,2.3E7,6.E-5,1.E-6,1.82E-5,1.E-2,7.,1.E5/

DATA PI/3.1415926535898/
CALL NMLEOF
DT=5.E-7 \$ EPS=5.E-8

IPRNT=1
A=R/S
EU(1)=1.E-5

EU(2)=1.E-9
EU(3)=.01
EU(4)=1.E-4

EL(1)=1.E-7
EL(2)=1.E-11
EL(3)=1.E-4

EL(4)=1.E-6
HMAX=1.E-5

```

      HMIN=1.E-7
      CALL SECOND(TOM)
C   BEGIN NEW CASE
      4   READ (2,INP)
      IF (EOF,2) 73,1
      1   ES=S
          RR=1.+A
          R1=RR*RR*RR
          R2=R1*RR
          R3=RR+.5*A
          TC=A*R2*R3/(A*A*A+R1)
          QQ=(EPSP-1.)/(EPSP+2.)
          U=2*E0*E1*E2*S/3./XMU
          VC=2.*U*RHO*R*R/S/XMU/9.
          QC=2.*VC*QQ*E2*R*R/E1/S/S
          QC=SQRT(1./QC)
          D=ES*A
          ZMX=SR=S+D
          ZMN=0.
          AM=4./3.*PI*R*R*R*RHO
          C(1)=6.*PI*R*XMU/AM
          C(2)=6.*E0*E2*E2*QQ/ES/RHO
          DISPLAY *  U= *,U,*  PART. MASS =*,AM
          IC=0
          IF (IPRNT) 2,2,3
      3   WRITE(3,105)
      2   Z0=.5*(ZMN+ZMX)
          IF (ZMX-ZMN.LT.EPS) GO TO 40
C   BEGIN TRAJECTORY CALCULATION
          T=0. $ DT=5.E-7
          VAR(1)=X0
          VAR(2)=Z0
          VAR(3)=-U
          VAR(4)=0.
          CALL HB
          ICNT=0
      11  IF (VAR(2).GT.SR) GO TO 12
          IF (RAD.LT.SR) GO TO 13
          IF ((VAR(1).LT.0.).OR.VAR(1).GT.X0) GO TO 14
          IF (VAR(1).LT.DT*ABS(VAR(3))) 8,9
      8   DT=ABS(VAR(1)/VAR(3))
          ICNT=0

```

```

9  CALL RKAMS(T,DT,VAR,DER,HB,4,0,EU,EL,HMAX,HMIN,ICNT,SCR,NH)
   GO TO 11
12  K=-1 $ GO TO 15
13  K=0  $ GO TO 15
14  K=1
15  IC=IC+1
   IF(IPRNT) 5,5,6
6   WRITE(3,110)IC,Z0,VAR(1),VAR(2),T,K
C   END TRAJECTORY CALCULATION
5   CALL SECOND(TIM)
   SEC=TIM-TOM
   IF(SEC.LT.TMX)GO TO 17
   WRITE (3,131)
   GO TO 40
17  IF(K)10,20,30
*   MISS
10  ZMX=Z0
   GO TO 2
*   HIT
20  ZMN=Z0
   GO TO 2
*   SHOULD NOT HAPPEN
30  WRITE(3,130)VAR(1)
40  P=Z0*Z0/SR/SR
   CS=Z0/S
   TOM=TIM
   WRITE(3,100)ZMX,ZMN,IC,P,CS,TC,VC,QC,SEC
   GO TO 4
73  STOP
100 FORMAT(* Z0 BETWEEN*E12.4* AND*E12.4,
** IC=*I5* P =*F8.5/** Z0/S = *E10.3* TC = *
*E10.3/* EA/EC = *E10.3* S/SC = *E10.3
**//2X,F10.3* CPU SEC*/1H1)
105 FORMAT(3X*IC*6X*Z0*11X*X*11X*Z*11X*T*8X*K*/)
110 FORMAT(I5,4E12.4,I5)
130 FORMAT(* X OUT OF BOUNDS AT*,E12.4)
131 FORMAT(* TIME LIMIT FOR THIS CASE*)
END
SUBROUTINE HB
*   CALCULATES FLOW FIELD INFLUENCE ON PARTICLE TRAJECTORY
*   PER HAPPEL AND BRENNER.
COMMON VAR(4),DER(4),U,Q,Q1,C(2),RAD,ES

```

```
1 RAD=SQRT(VAR(1)*VAR(1)+VAR(2)*VAR(2))
```

```
Q=ES/RAD
```

```
Q1=Q*Q
```

```
DER(1)=VAR(3)
```

```
DER(2)=VAR(4)
```

```
VX=VAR(3)+U
```

```
SNT=VAR(2)/RAD
```

```
CST=VAR(1)/RAD
```

```
10 RR=1./Q
```

```
A=RR-1.
```

```
R1=RR*RR*RR
```

```
R2=R1*RR
```

```
R3=RR+.5*A
```

```
G=A*R2*R3/(A*A*A+R1)
```

```
WR=-.5*U*CST*(Q1-3.)*Q
```

```
WT=-.25*U*SNT*(Q1+3.)*Q
```

```
WX=WR*CST+WT*SNT
```

```
WZ=WR*SNT-WT*CST
```

```
Q2=Q1
```

```
Q1=(2.*Q2*Q2*Q2-.5/G)*Q2*Q2
```

```
DER(3)=C(1)*(WX-VX)+C(2)*Q1*CST
```

```
DER(4)=C(1)*(WZ-VAR(4))+C(2)*Q1*SNT
```

```
2 RETURN
```

```
END
```

TECHNICAL REPORT DATA

(Please read instructions on the reverse before completing)

1. REPORT NO. EPA-600/2-76-249a		2.	3. RECIPIENT'S ACCESSION NO.	
4. TITLE AND SUBTITLE CHARGED DROPLET SCRUBBER FOR FINE PARTICLE CONTROL: LABORATORY STUDY			5. REPORT DATE September 1976	
			6. PERFORMING ORGANIZATION CODE	
7. AUTHOR(S) C. W. Lear			8. PERFORMING ORGANIZATION REPORT NO.	
9. PERFORMING ORGANIZATION NAME AND ADDRESS TRW Systems Group One Space Park Redondo Beach, California 90278			10. PROGRAM ELEMENT NO. 1AB012; ROAP 21ADL-043	
			11. CONTRACT/GRANT NO. 68-02-1345	
12. SPONSORING AGENCY NAME AND ADDRESS EPA, Office of Research and Development Industrial Environmental Research Laboratory Research Triangle Park, NC 27711			13. TYPE OF REPORT AND PERIOD COVERED Phase Final; 6/73-6/75	
			14. SPONSORING AGENCY CODE EPA-ORD	
15. SUPPLEMENTARY NOTES IERL-RTP project officer for this report is D. L. Harmon, Mail Drop 61, 919/549-8411 Ext 2925.				
16. ABSTRACT <p>The report gives results of a feasibility study of the application of charged droplet scrubbing for fine particle control. Results, using the TRW charged droplet scrubber, indicated that the method is feasible and applicable over a wide range of conditions. In the charged droplet scrubber the electrical interaction mechanisms exist in addition to the normal impact and diffusional scrubbing mechanisms. Electrical interaction is strong in the 0.1 to 1.0 micron particulate size range where the normal mechanisms lack effectiveness. Collection efficiencies as high as 80% for 0.1 micron and 90% for 1 micron particles were demonstrated in a three-stage unit. Induced charging or dry charging of particulate by charge transfer from droplets is an effective and major collection mechanism in the fine particulate size range. Large (100 micron) droplets give better performance characteristics than small (10 micron) droplets.</p>				
17. KEY WORDS AND DOCUMENT ANALYSIS				
a. DESCRIPTORS		b. IDENTIFIERS/OPEN ENDED TERMS		c. COSATI Field/Group
Air Pollution Dust Scrubbers Drops (Liquids) Electrostatic Charge Tests		Air Pollution Control Stationary Sources Particulate Charged Droplets Laboratory Studies Electrical Interaction		13B 11G 07A 07D 20C 14B
18. DISTRIBUTION STATEMENT Unlimited		19. SECURITY CLASS (This Report) Unclassified		21. NO. OF PAGES 181
		20. SECURITY CLASS (This page) Unclassified		22. PRICE